1-1-2017

A Reconciled Estimation of the State of Cryospheric Components in the Southern Andes and California Using Geospatial Techniques

Pushkar Inamdar

A reconciled estimation of the state of cryospheric components in the Southern Andes and California using geospatial techniques

By

Pushkar Inamdar

A Dissertation
Submitted to the Faculty of
Mississippi State University
in Partial Fulfillment of the Requirements
for the Degree of Doctor of Philosophy
in Earth and Atmospheric Sciences
in the Department of Geosciences

Mississippi State, Mississippi

December 2017

A reconciled estimation of the state of cryospheric components in the Southern Andes and California using geospatial techniques

By

Pushkar Inamdar

Approved:

_____

Shrinidhi S. Ambinakudige
(Major Professor)

_____

Darrel W. Schmitz
(Committee Member)

_____

Qingmin Meng
(Committee Member)

_____

Padmanava Dash
(Committee Member)

_____

Renee M. Clary
(Graduate Coordinator)

_____

Rick Travis
Dean
College of Arts & Sciences

Name: Pushkar Inamdar

Date of Degree: December 8, 2017

Institution: Mississippi State University

Major Field: Earth and Atmospheric Sciences

Major Professor: Shrinidhi Ambinakudige

Title of Study: A reconciled estimation of the state of cryospheric components in the Southern Andes and California using geospatial techniques

Pages in Study 110

Candidate for Degree of Doctor of Philosophy

Glaciers are the essential source of fresh water not only to human sustenance, but it is also vital for all lifeforms on earth. Glaciers are also key components in understanding rapid changes in climate. This makes understanding of glacier mass, extent, and overall state essential. In this dissertation, the objective was to analyze the state of snow and ice masses in the mid (California) and low latitude (Chile/Argentina) western American regions using geospatial technology. This study also analyzed the effects of anomalies in snow mass on the regional agricultural practices in California's Central Valley.

In the Southern Andes, the digital elevation models from Shuttle Radar Topographic Mission (SRTM) (the year 2000) were compared with the elevation footprints from the Geoscience Laser Altimeter System (GLAS) campaign for the years 2004 through 2008. Generally, in all sub-regions, in glaciers, the elevation values were lower than the elevation for the year 2000, which demarcates continuous recession of ice mass in the Andean region. Also, this study quantified snow cover extent and mass balance variations in the Sierra Nevada and Mt. Shasta regions in California. To unearth anomalies in snow mass, study used digital elevation models generated from the Advanced Spaceborne

Thermal Emission and Reflection Radiometer (ASTER) between the year 2000 and 2015. A remarkable reduction in snow cover extent of about 80% was observed in the studied watersheds of California. Lastly, the impacts of snow mass anomalies on the total water storage (TWS) and agriculture land cover in the California's Central Valley were quantified and geovisualized. The study noticed the change in the land cover area of about 20% (6993 sq.km) due to the alteration of Agriculture land to impervious land covers. Most of the change in the agriculture land cover of about 4402 sq.km occurred in the San Joaquin and Tulare Basins of southern Central Valley region.

This dissertation concludes that the increased temperature in the Andes and California has adversely impacted Cryosphere components in the region in the past decade. Besides, it provides valuable insights into the changing state of cryosphere components and highlight impacts of anomalies in TWS on a billion-dollar agricultural industry.

DEDICATION

This dissertation is dedicated to the memory of my mother and grandparents. Also, dedicated to my beloved father Dr. Pradeep Inamdar, my sister Mrs. Pallavi Bawaskar, brother-in-law Mr. Swapnil Bawaskar, other family members and friends who supported me.

ACKNOWLEDGEMENTS

I would like to sincerely thank my supervisor, Dr. Shrinidhi Ambinakudige for his guidance and support throughout this study, and especially for his confidence in me. I learned from his insight a lot and I believed I learned from the best.

I would also like to thank Dr. Schmitz, Dr. Meng and Dr. Dash for serving as committee members on my dissertation and for their constructive criticism that significantly improved the quality of this dissertation. I would like to thank Dr. Schmitz. His comments and questions were very beneficial in completion of my research work. I thank Dr. Meng who always assured me with his encouraging words. To Dr. Dash, I was grateful for the discussion and interpretation of some of the results presented in this dissertation.

I express my thanks to Dr. Ronald Cossman, Associate Research Professor and Research Fellow, SSRC, for providing research assistantship in the first semester. I thank the entire faculty and staff that helped me complete this journey. Also, I am thankful to all my colleagues and friends at the Department of Geosciences, especially Mary Grace Chambers, Sauree Silwal, Aynaz Lotfata, Shatrughan Singh, Madhur Devkota, and Tianyu Li. I could not have reached this goal without their support and encouragement. I will always be indebted to the Department of Geosciences, Mississippi State University for supporting my research through a financial assistantship without which this dissertation would have never been possible.

TABLE OF CONTENTS

DEDICATION ii

ACKNOWLEDGEMENTS iii

LIST OF TABLES vi

LIST OF FIGURES i

CHAPTER

I. INTRODUCTION 1

1.1 Background 1
1.2 Why study glaciers in Southern Andes and California? 6
1.3 Overview of glacier mass balance measurements techniques 8
1.3.1 Glaciological or direct measurement 8
1.3.2 Hydrological method 9
1.3.3 Geodetic method 9
1.4 Glacier mass balance calculation 10
1.5 Study objectives 13
1.5.1 Spatial Patterns of glacier mass change in the southern Andes (Chapter-II) 13
1.5.2 Spatiotemporal analysis of snow cover extent and mass anomalies in California (Chapter III) 14
1.5.3 Effects of snow mass anomalies on the total water storage and agricultural yield in the California's Central Valley between 2003 and 2005 (Chapter IV) 15

II. SPATIAL PATTERNS OF GLACIER MASS CHANGE IN THE SOUTHERN ANDES 17

2.1 Abstract 17
2.2 Introduction 17
2.2.1 Status of glaciers in the Andes 18
2.3 Study Area 24
2.4 Data 27
2.5 Methods 29
2.6 Results and Discussions 33
2.7 Conclusions 36

III. SPATIOTEMPORAL ANALYSIS OF SNOW COVER EXTENT AND MASS ANOMALIES IN CALIFORNIA 39

3.1 Abstract 39
3.2 Introduction 40
3.3 Study Area 44
3.4 Data 45
3.5 Methods 48
3.5.1 Snow cover change 49
3.5.2 Snow mass difference 50
3.5.3 Uncertainty assessment 51
3.5.4 Climate data analysis 52
3.6 Result and discussion 53
3.6.1 Extent of snow cover change in California 53
3.6.2 Snow mass change 2000-2015 57
3.6.3 Climate data analysis 61
3.7 Conclusions 64

IV. EFFECTS OF SNOW MASS ANOMALIES ON THE TOTAL WATER STORAGE AND AGRICULTURAL YIELD IN THE CALIFORNIA'S CENTRAL VALLEY BETWEEN 2003 AND 2015 67

4.1 Abstract 67
4.2 Introduction 68
4.2.1 Water depletion in the Central Valley 69
4.2.2 Effects of climate change on the Central Valley agriculture 70
4.3 Study Area 73
4.4 Data used 74
4.5 Methods 75
4.5.1 Hybrid classification 76
4.5.2 GRACE data analysis 78
4.6 Results and Discussion 79
4.6.1 Change detection analysis 79
4.6.2 Total Water Storage (TWS) 82
4.6.3 Statistical Analysis 86
4.7 Conclusion 92

V. CONCLUSIONS 94

5.1 Discussions on the overall outcomes and scope for the future research 94

VI. REFERENCES 100

LIST OF TABLES

2.1 List of Landsat (ETM+) scenes used in this study 28

2.2 Average elevation differences and trends between ICESat and SRTM data from 2004 through 2008 35

3.1 List of Landsat scenes used in this study. 46

3.2 List of 7.5-minute series (1:24000) quadrangle maps used in this study. 48

3.3 Snow mass anomalies in watersheds of Sierra Nevada. Base year: 2000 59

3.4 Snow mass anomalies in named glaciers of Sierra Nevada. Base year: 2000 60

3.5 Snow mass anomalies in named glaciers of Mt. Shasta. Base year: 2000 61

4.1 Rate of change for TWS and Temperature between 2003 and 2015 87

4.2 Statistical analysis based on the sub regions in the Central Valley using NDVI, TWS and Temperature for the dry season months between 2003 and 2015 90

4.3 Statistical analysis: Regression between TWS, NDVI and Temperature 91

LIST OF FIGURES

1.1 Illustration of study sites 6

2.1 Current State of three glaciers in Southern Andes 21

2.2 Illustration of the study area in South America.....24

2.3 Flowchart summarizes the methodology.....29

2.4 Trends of standard deviation of elevation difference from randomly selected points over clean ice 32

2.5 Average elevation differences per annum and linear trends between ICESat and SRTM data from 2004 through 2008 on clean ice in four regions 34

3.1 Illustration of the study area in California.....44

3.2 Flowchart summarizes the methodology.....48

3.3 Percent snow cover extent in major glaciers in Mt. Shasta.....54

3.4 Percent snow cover extent in major glaciers in the Sierra Nevada 55

3.5 Percent snow cover extent change in major watersheds in Sierra Nevada California.....56

3.6 Average snow mass anomalies (megaton) and linier trends between reference ASTER 2000 and ASTER data through 2002-2015.....58

3.7 Average monthly mean temperature from 1996 through 2015 during dry and wet seasons. 62

3.8 Average monthly mean snowfall from 1991 through 2015 during the wet season.....63

4.1 Illustration of the study area in California.....74

4.2 Hybrid classified images for the year 2003 and 2015 80

4.3 Illustration of change detection analysis:2003-2015 82

4.4 GRACE data anomalies (equivalent water height) monthly and annually 83

4.5 Association between snow mass anomalies in the snow elevation difference in the Sierra Nevada and total water storage in the Central Valley. 85

4.6 Monthly graphical representation of TWS between 2003 and 2015 in the California's Central Valley 86

4.7 Linear trend fitted through Temperature, TWS, and NDVI through 2003 to 2015 for the four sub regions. 87

4.8 Monthly graphical representation of Temperature (°C) between 2003 and 2015 in the California's Central Valley 88

4.9 Sub-region wise Total water storage anomaly 89

4.10 Monthly graphical representation of crop yield (NDVI) between 2003 and 2015 in the California's Central Valley 91

CHAPTER I

INTRODUCTION

1.1 Background

Water is significant for all life forms on earth. The importance of water in the life of earth's history can be only recognized entirely from analysis of its role in the human and environmental sustenance. About 75 percent of earth's surface is covered with water, of which, about 3% is fresh water. Almost 85% of the fresh water is locked in the glaciers and acts as a major contributor to this 3% (Kaser et al., 2003; Singh, 2001). In recent years, water enclosed in the frozen reserves are depleting at a rapid rate. Because glaciers, snowpacks and ice caps are sensitive to minute changes in temperature, they are the essential markers of the climate forcing. Slight variations in the temperature affect the equilibrium state of a glacier and its overall mass budget. In the past century, glaciers observed to be melting at an incremental rate primarily because of the increased temperature (Ambinakudige and Joshi, 2015; Basagic and Fountain, 2011). This dissertation, aimed to understand the state of snow and ice masses in the mid and low latitude western American regions using Geographic Information System (GIS) and Remote Sensing. This research also quantified the rate of change of these frozen fresh water reserves and its possible effects. The dissertation provides a precise temporal assessment of glacial extents and mass budgets which will contribute to the understanding of global impacts of climate forcing.

Glaciers are also known as slow-moving rivers of ice, where a huge mass of ice drifts due to its weight and under the influence of gravity (Singh, 2001). The river of ice begins forming in places where snow deposition exceeds the rate of ablation. Each year snow piles up and starts to compress (Singh, 2001). This compression slowly changes light snow crystals to dense and tightly packed ice. Principally, glaciers are composed of snow (low density), firn (medium density) and ice (high density). The sensitivity of glaciers to the increased temperature directly related to the density of glacier components. This makes monitoring and thorough understanding of the state of the different glacier components and varied effects of temperature on it essential.

In the last quarter of the past century, the researchers observed increased temperature around the globe (Hansen et al., 2006), leading to frequent ENSO occurrence, anomalies in precipitation and incremental rates of other catastrophic events (Vuille and Bradley, 2000). A global surface temperature study (Hansen et al., 2006) used more than 100 years of data collected by Goddard Institute of Space analysis and reported an increase in the global surface temperature with a gradient of 0.2°C per decade during the past 30 years. The steady increasing temperature causes a flux in the Eastern Equatorial Pacific and Western Equatorial Pacific regions, which leads to the frequent ENSO events around the globe (Hansen et al., 2006). Similarly, many other studies on climate reported an uninterrupted rise in the temperature around the world specifically after the industrial revolution (Hansen et al., 2006; Rahmstorf et al., 2017; Vuille and Bradley, 2000). The years 2014 through 2016 observed new global heat records. Another study (Rahmstorf et al., 2017) finds that this increase in temperature aligned with a consistent worldwide temperature alteration since 1970 and predicts to follow incremental warming trend.

Constantly increasing global temperature is impacting regional and microclimatic conditions. In the tropical Andes, the temperature has increased by 0.10°–0.11°C per decade since 1939 (Vuille and Bradley, 2000). The rate of warming of mean annual temperature has found triplicated over the last three decades by about 0.32°–0.34°C per decade (Vuille and Bradley, 2000). Also Vuille and Bradley (2000) observed increasing frequency of warmest El Niño events in the recent decade in the Southern Andes. While Villalba et al., (2003) examined anomalies in the temperature across the southern Andes (37–55° S) using a blend of long-term tree-ring records and instruments and noticed a definite warming trend around southern Andeans region ~ 46°S with incremental warming rates in the higher altitudes. Similar to the Southern Andes, over the past century California has also experienced increased warming rates. California has a history of severe, prolonged dry events, including recent droughts between 2012 and 2014 (Griffin and Anchukaitis, 2014; Swain et al., 2014). Bonfils et al. (2007) analyzed nine different observational datasets and found increased temperature of about 2°C with higher rates in winter. Importantly Bonfils et al. (2007) attributed increased warming in California to anthropogenic activities. Besides, Howat and Tulaczyk (2005) analyzed historical climate data using a multivariate model and found that impact of the warming is considerably reliant on coexisting precipitation variation and watershed topography in the Sierra Nevada.

Many recent studies suggest that the climate is changing mainly due to anthropogenic activities. These slight variations in climate directly impact the glacier mass balance cycle. While the steady increase in temperature after the industrial revolution and associated fluctuations in snowfall with the negative trend forces glaciers to melt faster

than they are restocked. This results in the disequilibrium state with shrinkage of glaciers globally. World glacier monitoring service (2009) reported about 90% of the glaciers are retreating. Johnson et al. (2013) in their laser altimeter analysis in the Glacier Bay region of Southeast Alaska, USA, and British Columbia, Canada observed massive retreat with a mass loss rate of 3.93±0.89 Gt a^{-1}. Similarly, most of the glacier in Himalaya are melting at a high rate (Bolch et al., 2012). Kääb et al. (2012) in their study observed contrasting patterns of glacier mass change between 2000- 2008 in the Hindu Kush-Karakoram-Himalaya region and reported mass loss rate of -0.21 ± 0.05 m w.e. yr^{-1}. A recent time series analysis of glacier mass in the Italian Alps observed increasing mass loss rates between -1788 to -763 mm w.e. yr^{-1} (Carturan et al., 2015). While the study (Scheuchl et al., 2016) in Western Antarctica using Sentinel-1a (C- band satellite radar interferometry data) with Progressive Scans mode noticed continuous retreat Pope, Smith, and Kohler glaciers, in West Antarctica, for the years 2014–2016. Further, reconciled estimate of ice sheet mass balance between 1992 and 2011 of Greenland, East Antarctica, West Antarctica, and the Antarctic Peninsula reported change in mass by $–142 \pm 49$, $+14 \pm 43$, $–65 \pm 26$, and $–20 \pm 14$ Gt a^{-1}, respectively (Shepherd et al., 2012). In the Andes, several studies have observed retreat and mass loss of glaciers in the last few decades (Gardner et al., 2013; Rabatel et al., 2011; Rignot et al., 2003).

Masiokas et al., (2009) reviewed glacial fluctuations in the last 1000 years and found that in the Central Andes, glaciers have retreated throughout the 20th century. A gravimetric analysis using Gravity Recovery and Climate Experiment (GRACE) data from 2002 through 2006 in the Patagonian Icefields reported a mass loss rate as 24.3 ± 4.3 $km3yr^{-1}$ (Chen et al., 2007). Likewise, similar recession patterns were observed in the North

America. After examining remotely sensed and climate data (McCabe and Fountain, 2013) found considerable spatiotemporal variability in Western United States glaciers occurred between 1900 to 2000 mainly due to warming and fluctuations in rainfall in high elevation areas.

In essence, it is essential to study the state of glaciers, to understand impacts of anthropogenic activities, to understand changing climatic conditions, and to comprehend depleting total water storage. Multi-decadal evaluation of mass balance variations provides chronological information about changing climate events (Singh, 2001). Mountain glaciers are sensitive to minute changes in local and global climate, and they act as pointers towards climate forcing (Ambinakudige and Joshi, 2015; H. Basagic and Fountain, 2011). It is important to monitor components of the cryosphere because, in general, these frozen fractions of water play a substantial role as a water reserve, its contribution to sea level rise, its role in global energy budget, hydrological cycle, Agricultural yield, Dairy industry and much more.

The dissertation is structured as a series of chapters. The first chapter covers background, includes, the significance of study sites, different techniques of mass balance measurements, goals and brief overview of the methodology used. Chapter-II comprises findings of the glacier mass balance study in the South Andean cryosphere. Chapter-III covers findings of mass and extent analysis of snowfields in the Sierra Nevada and Mt. Shasta regions in California. Chapter-IV is an extension of chapter-III. In which study analyzed possible effects of changing snow patterns in the agricultural fields in the Central Valley California. The results of Chapter-IV were achieved by analyzing temperature, Total Water Storage (TWS) and Normalized Difference Vegetation Index

(NDVI). Conclusively, the last Chapter-V covers brief discussion about the overall outcomes and scope for the future research.

1.2 Why study glaciers in Southern Andes and California?

Figure 1.1 Illustration of study sites

Southern Andean and California regions lack comprehensive quantitative documentation of glacier measurements. Due to the inaccessible terrain and absence of data, the mass balance of the South American cryosphere has not been documented extensively over the years. On the other hand, in California and other western states, many small perennial snow and ice covered regions exist over a vast area. Because of this scattered distribution pattern, the California region lacks in the complete historical records of glacier extent and mass wastage before the development of recent topographic maps (Krimmel, 2002). As a result, the both regions has suffered from the absence of a systematic, long-term and

validated mass balance program (Bamber and Rivera, 2007; H. Basagic and Fountain, 2011; Dyurgerov and Meier, 1997; Krimmel, 2002).

In addition, Sothern Andes (low latitude) and California (mid-latitude) are chosen for the analysis because of their geolocations (Figure 1.1). Southern Andes extends up to the polar region, and contrariwise California is situated near the equator. As a result, they represent entirely different climatic conditions and topography resulting in diverse glacier morphology. As glaciers in Southern Andes are larger in size, on the other hand, small scattered snow masses are situated in California. Analysis of these study sites aided understanding questions, as, how melting patterns differs in both the regions? Is there latitudinal and longitudinal variation in glacier recession?

Glaciers in Southern Andes and California are primarily situated on high mountains and nourishes water to many rivers. In the Western United States, Sothern Andes and several other parts of the world rivers originated from glaciers are perennial and act as a primary source of fresh water, and also irrigates one-third of the land (Singh, 2001). The glaciers of Chile serve as a valuable source of fresh water, as its summer runoff contributes in many river basins. It is important support of water to the populated and ecoregions of the Chile (Rivera et al., 2006). During the twentieth century, melting glaciers of the Andes contributed about 10 percent of the water that caused the sea level rise (Bamber and Rivera, 2007; Rignot et al., 2003; Rivera et al., 2002). Similarly, in the state of California, snow mass plays a significant role as natural water reservoirs. Because of the Mediterranean climatic conditions, the region gets most of its precipitation in winter. It makes snow mass as a primary source of freshwater for the rest of the year. Typically, snowmelt provides one-third of the water utilized in California's urban areas and ranches

every year (Chou, 2014). Over the past century, California has experienced severe prolonged dry events, including those during 1976–1977 and late 1980s droughts, and recent drought during 2012-2014 (Griffin and Anchukaitis, 2014; Swain et al., 2014). Thus bearing in mind the role of Andean glaciers in sea level rise and water scarcity in California (Swain et al., 2014), it is essential to analyze the existing state of glacier masses in these regions.

1.3 Overview of glacier mass balance measurements techniques

Considering sensitivity of glaciers to the climatic variations; glacier extent and mass balance are measured as a part of hydrology and climate studies. The glacier mass balance could be analyzed by applying the glaciological (direct), geodetic (mapping), or hydrological methods. Following subsections provides the brief overview of different measurement methods, and about the process, used in this dissertation for the analysis.

1.3.1 Glaciological or direct measurement

The glaciological or in-situ method is conventional method successfully used worldwide for analysis of a glacier mass balance. This method needs interaction and extensive field work on the glacier site. It includes measurement of snow mass variations in the accumulation zone with snow pits or core drill or stack observations in the ablation zone. In which ice core drill measurements provide information about paleo-climatic conditions (Kaser et al., 2003). Generally, snow pits are preferred over core drills in the mass balance studies as it provides more sampling area and accurate snow density (Singh, 2001). At some sampling points, mass balance is calculated by differencing snow thickness through the reference and following summer dates. Conversely, stack measures

mass balance in the ablation zone, where stacks are drilled into the ice surface. The difference between a top of a stack and reference ice surface measured between the beginning and end of the balance period (Singh, 2001). Later this difference is converted into the water equivalent using known density value.

1.3.2 Hydrological method

Glacier mass balance controls melt runoff. Therefore, it is a valuable parameter for hydrological modeling. The hydrological method accounts water balance to estimate glacier mass. Therefore, a method involves estimation of parameters such as evaporation, precipitation, runoff, and variation in storage elements (S) of catchment area such as ground water (equation 1) (Kaser et al., 2003).

$$B = Precipitation - Runoff - Evaporation \pm \Delta S \quad (1)$$

The hydrological method is least used among other methods for determining mass balance changes because of the high uncertainty in the estimation of many parameters in the equation (Kaser et al., 2003; Singh, 2001).

1.3.3 Geodetic method

Direct or in-situ measurements gives better results as compared to the geodetic methods. But ease of taking an ample number of measurements and that too on rough terrains makes geodetic methods suitable for large-scale glacier studies (Fischer, 2011). Geodetic methods are also known as indirect methods of mass balance measurements. In this study, analysis of mass balance is based on the geodetic methods. The geodetic method provides an opportunity to report glacier mass balance in inaccessible areas on the mountain ranges such as the Andes and the Sierra Nevada. Also, it is efficient in

analyzing glacier mass balance on the larger scale. It includes analysis of topography using differential GPS, remotely sensed elevation models or other elevation datasets. Typically, in contrast to the glaciological method, the geodetic method provides measurements of entire glacier rather than at specific locations. However, recent advancements in remote sensing provide elevation datasets (laser altimeters) which provide accurate elevations at specific locations. This study used a geodetic method, where spatiotemporal analysis of glaciers mass balance was performed based on the digital elevation models. Where different year datasets were compared to understand changes in surface elevation. A product of snow thickness and near surface density was quantified for the different regions to get the water equivalent. Generally, ice density is considered as 900 kg m^{-3} and snow density as of 600 kg m^{-3} (Huss, 2013).

1.4 Glacier mass balance calculation

Glacier mass balance is a relationship between mass accumulation and loss (Kaser et al., 2003). In other words, glacier mass balance or budget is the alteration in the snow or ice mass on a glacier as a function of time (Ostrem M., 1991). Following equation (2) represents mass balance (*mb*) at a specific point.

$$mb_{glac} = \int_{t1}^{t} mb\ dt \tag{2}$$

Where *dt* is a time difference between two measurements at a specific point. Similarly, the geodetic method compares surface thickness (*dh*) at any point on a glacier to find mass change on a glacier. The result of equation (2) is expressed in [M T^{-1}] mass

change per period. Equation (3) (Kaser et al., 2003) is a representation of mass balance at a specific point using surface elevation variation.

$$dh = \frac{mb}{id_{ice}} - \hat{k} \tag{3}$$

In equation (3), *mb* and id_{ice} are mass balance change and ice density respectively. The horizontal gradient of ice flux (k) becomes zero in the computation of ice volume for the entire glacier area (Kaser et al., 2003). Then equation becomes

$$mb = dh * id_{ice} \tag{4}$$

Based on the availability of data, the mass budget can be computed at a specific point or for the entire glacier. The total mass balance of the entire glacier computed by integrating glacier extent in equation (2).

$$MB_{glac} = \iint mb(dt)(da) \tag{5}$$

In the above equation (5) (Kaser et al., 2003), *dt* and *da* represent temporal value and total glacier surface area respectively. The cumulative change in mass balance is expressed as unit's mass [M] or mass per area [M L^{-2}]. Generally mass is expressed in kilogram (kg) or Gigatonne (Gt). Mass balance can also be expressed in meter water equivalent (m.w.e.) by dividing mass per unit area by density (Kaser et al., 2003). We can rewrite equation (5) by using elevation difference values (dh) and ice density (id_{ice}). While performing preliminary glacier analysis in the Andes, study computed the glacier mass balance for the entire region of Chile and Argentina using specific ICESaT elevation footprints applying equation (4). More details about data and methodology are discussed in the second chapter. On the other hand, the analysis of snow mass in California is based on the equation (5), where a change in elevation was computed from

DEM generated from ASTER. Additional information about ASTER data and detailed methodology are discussed in Chapter III.

Throughout the year glacier experiences cyclic patterns of accumulation and ablation (Ostrem M., 1991). Accumulation is a process which adds the snow and ice mass on existing glacier body. Mass gained in the accumulation process is expressed as a positive number. There are different processes that add mass into the glacier system includes snowfall, freezing rain, drifting snow, refreezing of percolated waters, avalanches, etc. Likewise, mass lost in the ablation process is represented as a negative number. Some of the ablation processes that reduces the glacier mass include melting, avalanching, sublimation, calving, etc.

$$Mass\ balance = Accumulation - Ablation \quad (6)$$

As in some regions in the winter season glacier surface receives mass in the form of snow. For example, in glaciers of Sierra Nevada accumulation months are November, December, January, February, March, and April. On the other hand, other months represents ablation period.

Glacier is in equilibrium when mass lost during the ablation period recovers during the accumulation season. While disequilibrium status represents the imbalance in the state of mass between two seasons (equation 6). This disequilibrium in accumulation and ablation results in conditions either as positive mass balance or negative mass balance. Generally, in positive mass balance scenario glacier system gains mass in the form of snow. Subsequent positive mass balance periods lead glaciers to grow as well as to cover the low-altitude regions (Singh, 2001). On the other hand, negative mass balance

results in recession in snow and ice mass. Prolonged negative mass balance periods leads to the significant retreat of glaciers (Singh, 2001)

1.5 Study objectives

This dissertation analyzes a decadal state of mountain glaciers in south western territories of North and South American continent. The study covers two sites, Southern Andes and California. Following is brief overview of specific objectives and the methodology used to achieve those goals.

1.5.1 Spatial Patterns of glacier mass change in the southern Andes (Chapter-II)

Specific objectives of Chapter II are as follows:

- To estimate the rate of mass balance change of glaciers in Southern Andes using ICESat campaign and SRTM data.
- To compare contrasting patterns of glacier mass change in different sub-regions of the Southern Andes.

Glaciers in Chile and Argentina are distributed widely along latitude and longitude. Due to this widespread extent, topography and microclimatic conditions, region cover different types of glaciers, therefore this study analyzed footprints based on sub-regions. In addition the elevation footprints classified into snow and ice using multispectral Landsat images. The first section in Chapter II explains in detail different meteorological scenarios in the Southern Andes. To achieve the goals the study compared elevation models of ICESat laser footprints with SRTM data. The study precisely analyzed elevation footprints between 2000 and 2008 over the clean ice. The methodology section in Chapter II covers sequential order of the process.

As GLAS (ICEsat) instrument is aboard polar satellite specifically designed to study Polar Regions leads to scarcity of footprints in the outside regions. This issue of an uneven number of sample points in each year in each sub-region was addressed by performing the bootstrap analysis. ICESat laser altimeter data provides undoubtedly very precise measurements on the glaciers, but there are challenges in the data processing and unbiased elevation analysis. This study was the first attempt to use GLAS/ICESat data over clean ice to estimate mass wastage rates in the Southern Andes. Chapter II methodology elaborates in detail the processing challenges of the datasets. The study unearths patterns of glacier wastage in the South Andean sub-regions.

1.5.2 Spatiotemporal analysis of snow cover extent and mass anomalies in California (Chapter III)

Specific objectives of Chapter III are as follows:

- To quantify snow cover extent variations in the Sierra Nevada and Mt. Shasta, California.
- To estimate snow mass change in the Sierra Nevada and Mt. Shasta, California.
- To understand an impact of climatic variables on the snow mass change.

Glaciers in the California are mostly covered with the snowpacks. These snowpacks are less dense in comparison to the clean ice. Also, snowpacks in California are widespread and smaller in size. The study analyzes snowpacks in Sierra Nevada region based on the hydrological basins and the Mt. Shasta region separately. In this study, snow mass anomalies are quantified using digital elevation models generated from the Advanced Spaceborne Thermal Emission and Reflection Radiometer (ASTER) between the year

2000 and 2015. Further, Landsat scenes were used to measure snow cover extent variations during the same period.

The methodology section in Chapter III describes the chronological order of the process. It was challenging to acquire cloud-free and continuous timespan dataset. However, the study used best possible stereo ASTER elevation models and Landsat scenes to understand the spatial patterns of snow mass anomalies and snow extent. Uncertainty in the elevation models is computed by comparing elevation values of topographic benchmarks. The study results demonstrate the significant anomalies in mass balance and extent throughout the period between 2000 and 2015. Considering the current water crises in California, this study provides valuable insights into the possible role of climatic factors in snow mass anomalies in the region.

1.5.3 Effects of snow mass anomalies on the total water storage and agricultural yield in the California's Central Valley between 2003 and 2005 (Chapter IV)

Specific objectives of Chapter IV are as follows:

- To estimate changing Agricultural patterns in the Central Valley California
- To assess the effect of changing the climate on the Total Water Storage (TWS) and crop yield.

California is the major agricultural producer in the United States and also grows country's half of the fruits and vegetables worth billions of dollars. The chapter IV analyzes impacts of declining fresh water reserves and TWS in the four basins of the Central Valley agriculture. In this study, Landsat images were classified for the individual years 2003 and 2015 to understand patterns of agricultural change in the region. Hybrid classification technique was used by iteratively applying supervised and

unsupervised learning. While to understand total water storage in the central valley region study analyzed Gravity Recovery Research and Experiment (GRACE) data. These gravity anomaly coefficients provided information about the variations in the total water storage content (ground water, surface water, soil moisture, precipitation) in the Central Valley region. Lastly, study regressed and correlated Normalized Difference Vegetation Index (NDVI), TWS and temperature to understand the relation between these different parameters. An intention of this statistical analysis was to understand effects of snow melt on the TWS and the agricultural production in the California's Central Valley.

CHAPTER II

SPATIAL PATTERNS OF GLACIER MASS CHANGE IN THE SOUTHERN ANDES[1]

2.1 Abstract

The aim of this chapter was to analyze the spatial patterns of wastage trends of ice masses in the Southern Andes. The study compared digital elevation models from Shuttle Radar Topographic Mission (SRTM) (Year 2000) with the elevation footprints from the Geoscience Laser Altimeter System (GLAS) campaign for the years 2004 through 2008 in the Dry Central, North Wet, South Patagonia, and Cordillera Darwin regions. Overall, the mean elevation differences on clean ice were negative in all four regions. However, the higher mass balance trends were observed in the Cordillera Darwin (-0.126 ± 0.05 m w.e.a^{-1}) and the North Wet (–0.122 ± 0.12 m w.e.a^{-1}) regions. In contrast, no major change in mass balance trends was observed in Dry Central (-0.037 ± 0.13 m w.e.a^{-1}) and South Patagonian Icefield (-0.037 ± 0.05 m w.e.a^{-1}).

2.2 Introduction

The South American Cryosphere is composed of both tropical and temperate ice masses. The Patagonian Icefields in the Southern Andes is the major temperate ice mass in South America (Warren and Sudgen, 1993). Although the retreat of glaciers in the Southern Andes has been documented earlier (Lopez et al., 2010; Rignot et al., 2003; Willis et al., 2012), glacier of the Southern Andes has long been neglected for mass-balance measurements. Due to the remoteness, inaccessibility, and tough weather

[1] This chapter has been published as an applications paper in the journal Photogrammetric Engineering and Remote Sensing:
Inamdar, P., Ambinakudige, S., 2016. Spatial Patterns of Glacier Mass Change in the Southern Andes. Photogramm. Eng. Remote Sens. 82, 811–818.

conditions in the Andes, field-based mass-balance studies are sparse (Aniya et al., 1996). Because glaciers in this region have not been as closely studied, there is an uncertainty in the estimation of the contribution of these glacier-melts to the sea level rise (Rignot et al., 2003). Similar to other regions of the world, the recession of the glaciers and ice caps of the Andes is one of the most visible indications of the effects of climate change (Ambinakudige and Joshi, 2012; Ambinakudige, 2010; Lemke et al., 2007; Lliboutry, 1998; Warren and Sudgen, 1993). Because the annual temperatures of temperate ice masses are at the melting point, these glaciers respond very rapidly to climatic changes (Fountain, 2011). Climate change also affects the magnitude of the accumulation and ablation of the glaciers and the length of the mass balance seasons (Kaser et al., 2003; Pachauri et al., 2014). In addition, glaciers are the biggest wellsprings of fresh water in the Andes; therefore, the lack of records of water balances in the region is of great concern (Dixon and Ambinakudige, 2015). Hence, an estimation of mass balance trends in the Andean glaciers has broader impacts at the local, regional and global concerns on climate change and water resource management. This study will contribute to the existing knowledge of the glacial conditions in the Southern Andes. The study also contributes to the existing methodological approaches to use the sparingly available remote sensing data to model temporal changes in the glacial conditions in the region.

2.2.1 Status of glaciers in the Andes

The annual trends of glacial length and area of many glaciers in the Andes have fluctuated over time. Masiokas et al., (2009) reviewed glacial fluctuations over the last 1,000 years and found that in the Central Andes, glaciers retreated throughout the

twentieth century. They also found that after the little ice age (LIA), most glaciers in Southern Patagonia retreated and that has continued until today. Masiokas et al., (2009) also noticed isolated advances during the first half of the past millennium followed by a glacier reactivation between the seventeenth and nineteenth centuries and a widespread glacier shrinkage afterward.

According to Rivera et al. (2006), a significant frontal retreat trailed the glaciers located in the Central Andes. Similarly, Espizua and Pitte, (2009) using the historical data, aerial photographs and satellite images, observed area loss in Las Vacas, Güssfeldt, El Peñón, and El Azufre glaciers between 1894 and 2007. They also noted contrasting behavior of the glaciers in the Central Andes. Between 1894 and 1963, there was a pronounced glacier retreat followed by the glacial advance in 1963–1986, and nearly stationary conditions during 2004–2007 (Espizua and Pitte, 2009). In addition, an analysis of radiosonde data by Carrasco et al. (2005) over the central Chile from 1975 to 2001 revealed that tropospheric warming was the main cause of glacier retreat. Carrasco et al. (2005) also noticed a rise in the equilibrium line altitude (ELA) in the region during the study period. Furthermore, the comparison study of Shuttle Radar Topographic Mission (SRTM) digital elevation models with models generated from aerial photographs between 1955 and 2000 in the Cipreses glacier recorded a thinning rate of 1.06 ± 0.45 m a^{-1} (Rivera et al., 2006).

Most glaciers in the North Wet region of Andes are situated on active volcanoes. Rivera and Bown (2013) analyzed the contrasting morphology that glaciers adopt before and after volcanic eruptions. Using historical documents and remote sensing data, they studied the effects of volcanic events on glaciers and detected significant frontal retreats

and glacier areal change, with the maximum loss of -1.16 km^2 a^{-1} in Volcán Hudson. Rivera and Bown (2013) also concluded that the recovering capacity of glaciers was affected by the tropospheric warming and the decrease in precipitation. Another study of debris-covered ice at the Villarrica glacier showed an average shrinking of -0.4 km^2 a^{-1}, with an extent loss of 25 percent between 1961 and 2003 (Rivera et al., 2006). Figure 2.1 depicts an example of how glacier extents have changed in parts of the Southern Andes. Change in the area of Jorge Montt (in South Patagonian Icefield), Volcan Hudson (located in the North Wet region) and Marinelli (located in the Cordillera Darwin Icefield) glaciers shown in Figure 2.1 is an example for the glacial retreat in the region.

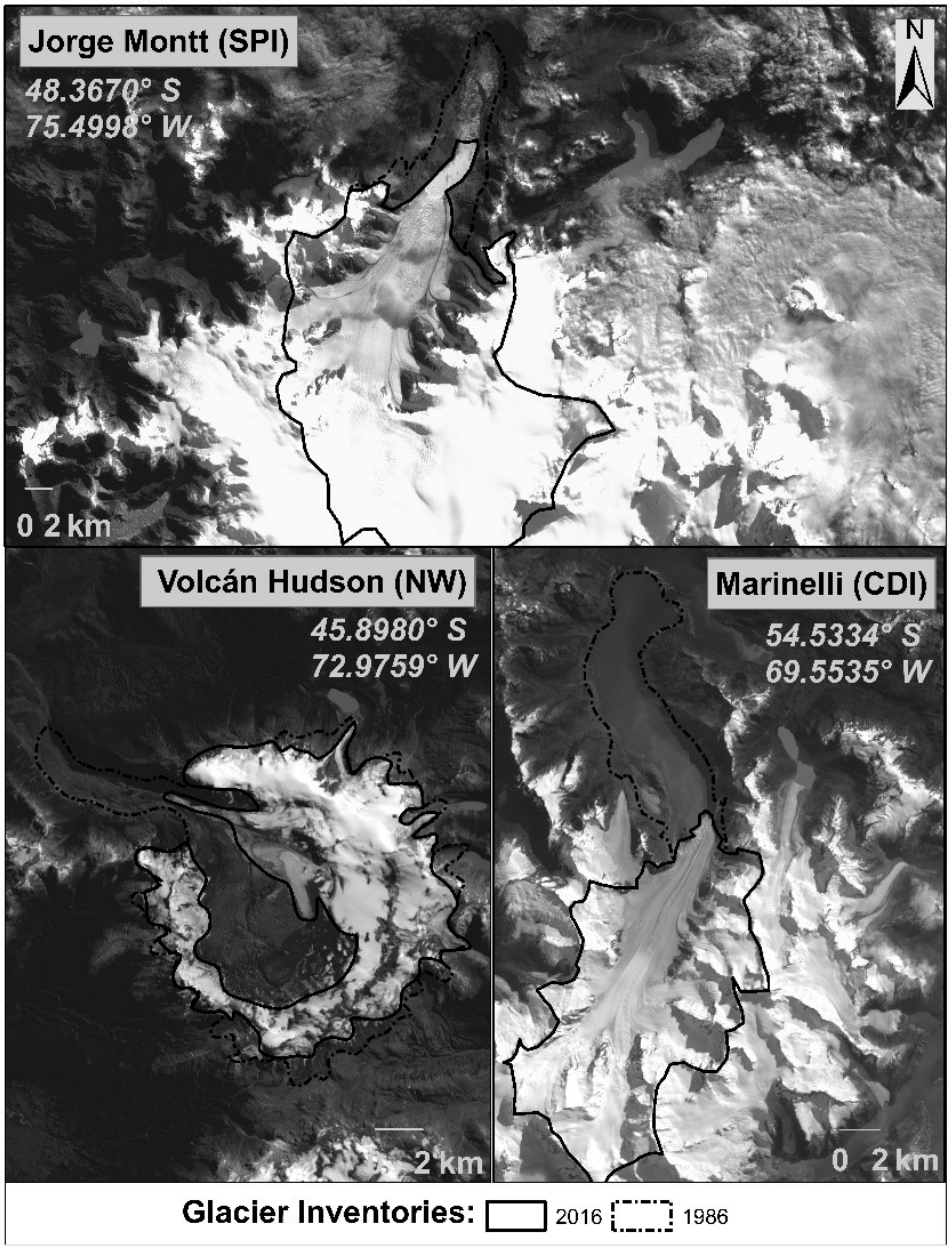

Figure 2.1 Current State of three glaciers in Southern Andes

Several studies have observed the retreat and mass loss of glaciers in the Andes over the last few decades (Dixon and Ambinakudige, 2015; Gardner et al., 2013; Lopez et al., 2010; Rabatel et al., 2013; Rignot et al., 2003). Mouginot and Rignot (2015) observed some of the fastest flowing glaciers using Interferometry Synthetic Aperture

Radar (InSAR), with velocities up to 10 km a^{-1} in the southern part of the South Patagonian Icefields (SPI). A recent spatiotemporal analysis of the San Rafael glacier using photogrammetric techniques showed a glacial velocity up to 16 meters per day (Maas et al., 2013).

Similarly, analysis based on satellite data between 1984 and 2011 in the SPI, showed that, there was, on an average 1.56 km retreat in 31 glaciers, with the maximum retreat more than 6 km in the Jorge Montt, HPS12, and Upsala glaciers (Sakakibara and Sugiyama, 2014). A gravimetric analysis using Gravity Recovery And Climate Experiment (GRACE) data from 2002 through 2006 in the Patagonian Icefields reported a mass loss rate of -24.3 ± 4.3 km^3a^{-1} (Chen et al., 2007). A time series analysis comparing ASTER and SRTM DEMs by Willis et al. (2012) also observed a mass loss rate of about −24.4 ± 1.4 Gt a^{-1} between 2000 and 2012 in Patagonian Ice fields, which is equivalent to +0.067 ± 0.004 mm a^{-1} of sea level rise. Likewise, another spatiotemporal analysis in the region by White and Copland (2013) found a net loss of the extent of the glaciers in 130 basins across the SPI from 1970 to late 2000. Dixon and Ambinakudige, (2015) also observed glacial retreat in the San Quintin, HPN1, Pared Norte, Strindberg, Acodado, Nef, San Quintin, Colonia, HPN4, and Benito glaciers in the North Patagonian Icefields by analyzing ASTER stereo and Landsat datasets. Lopez et al. (2010) recounted a maximum retreat of about 12 km in the Cordillera Darwin Icefield between 1945 and 2005 by comparing aerial photographs, Landsat and ASTER datasets. Melkonian et al., (2013) analyzed ASTER and SRTM data from 2000 to 2011and reported varied thinning behavior along the north-south axis of the Cordillera Darwin Icefield, with an average recession rate of −1.5 ± 0.6 m w.e.a^{-1}, which is equivalent to a sea level rise of 0.01 ±

0.004 mm a^{-1}. Given these observations of the glacial changes in the Andes, it is not surprising to note that during the twentieth century, melting glaciers of the Andes contributed about 10 percent of the water that caused the sea level rise (Bamber and Rivera, 2007; Rignot et al., 2003; Rivera et al., 2002).

Although many glaciers are retreating in the Andes, some glaciers have shown a positive mass budget. Schaefer et al. (2014) showed a progressive surface mass balance from 1975 to 2011 in the South Patagonian Icefield. Masiokas et al. (2009) also noted glacier growths in certain portions of SPI during the first half of the past millennium. Sakakibara and Sugiyama, (2014), in their analysis of 26 calving glaciers from 1984 to 2011, noticed small advancements in two termini of the Pío XI glacier. Espizua and Pitte, (2009) noticed some periods of minor advances in the Central Andes. They concluded that the positive mass balance during the period was the outcome of the warm El Niño–Southern Oscillation (ENSO) events.

Glaciers of Chile act as a valuable source of fresh water as their summer runoff contributes to several river basins. It is an important water resource to the populated and eco regions of the Chile (Rivera et al., 2006). But due to the inaccessible terrain and lack of data, the mass balance of the South American Cryosphere has not been documented extensively. As a result, the region has suffered from the absence of a systematic, long-term, and validated mass balance program (Bamber and Rivera, 2007; Dyurgerov and Meier, 1997; Rivera et al., 2007). In this paper, I use data that were generated using active and passive remote sensing techniques to analyze the state of glaciers in the Southern Andean Cryosphere from 2004 through 2008. I use GLAS and SRTM elevation

data to study trends in glacier wastage in the region. I examine regional elevation-difference trends in clean ice and analyze glacial thinning in the Southern Andes.

2.3 Study Area

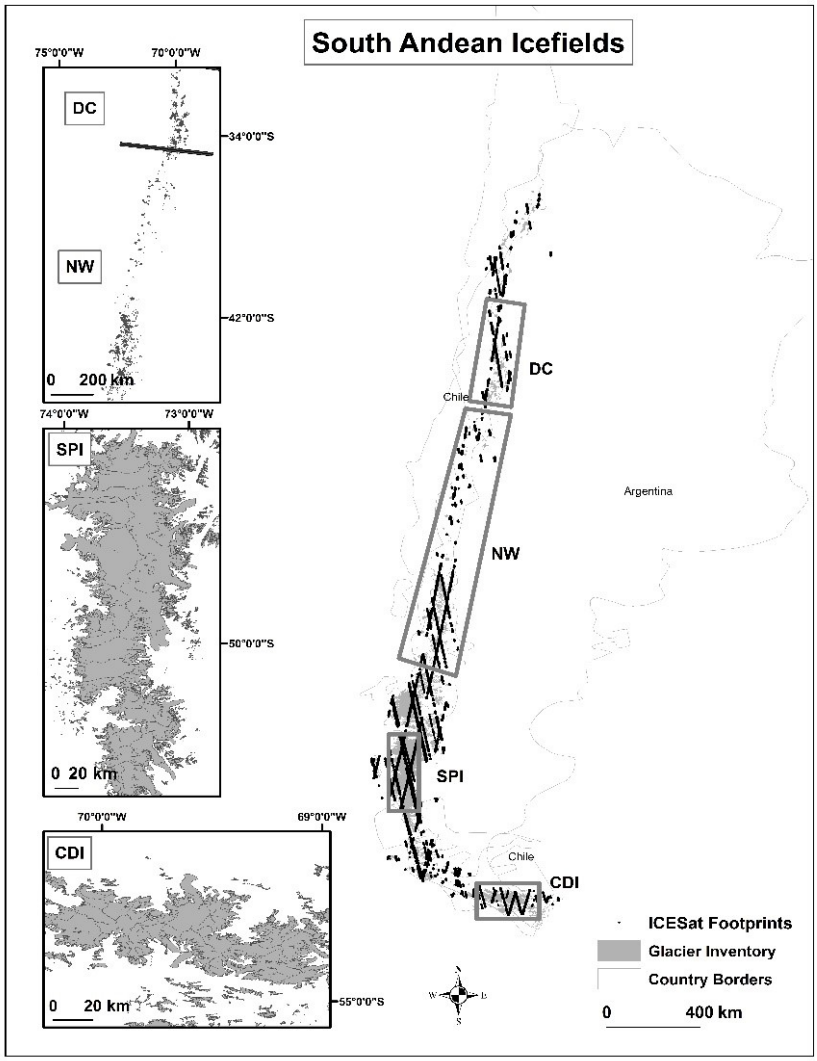

Figure 2.2 Illustration of the study area in South America

Most of the glaciers in the South America are located in Argentina and Chile. These glaciers are found typically in an area from 17° 30' S latitude to the southern tip of

South America at 55°S latitude (Figure 2.2). The Pacific Ocean in the West and the Andes Cordillera to the East influence the atmospheric conditions in the region. Varieties of glacier forms, such as mountain glaciers, valley glaciers, cirque glaciers, outlet glaciers, Piedmont glaciers, ice caps, and ice fields, spread across more than 4,000 km along the Andean mountains in Chile and Argentina (Lliboutry, 1998).

The climatic parameter differs along the longitude and latitude as the study region extends from northern Chile to Southern Argentina (Garreaud et al., 2009). Annual rainfall increases from 100 mm to 2,000 mm along the latitude within the central region (Montecinos and Aceituno, 2003). The studies on climate variability in the region reported a decrease in the precipitation and a diminutive increase in temperature (Favier et al., 2009; Rabatel et al., 2011). The complex landscapes of the Andes create numerous microclimatic zones in the study region (Rosenblüth et al., 1997). The varying climatic conditions and topography along the Andes influence the development of glacial masses. Therefore, I divided the study area into four regions based on climate and topography. These divisions help overcome statistical bias and avoid overlying dissimilar radar signal footprints (Kääb et al., 2012). These four climatic regions are Dry Central (31°S–35°S), North Wet (35.1°S–46°S), South Patagonian Icefields (48.15°S–51.4°S), and Cordillera Darwin Icefield (54.20°S–55°S) (Figure 2.2) (Lopez et al., 2010; Williams and Ferrigno, 1988).

In typical meteorological circumstances, stationary high pressure stretches out crosswise over South America at about 35°S and along these lines keeps any intrusion of moisture-laden air masses into the landmass (Lliboutry, 1998). In the regions, most precipitation occurs in the winter, between May and August. The summer months are

from December to February (Paruelo et al., 1998). In this study, I grouped ICESat footprints of December through February as dry season footprints. I restricted trend analysis to only the dry season ICESat footprints for an unbiased comparison with SRTM DEM, which is dated February 2000.

In the North Wet region, precipitation anomalies are prominent during the El Niño and La Niña periods in the Central Andes. The ENSO effect varies across geographic locations. In the El Niño years, above-average precipitation occurs between 30°S and 35°S latitudes from June to August, and between 35 and 38°S from October to November. In contrast, the opposite pattern is observed during La Niña years (Montecinos and Aceituno, 2003). On the western side of the Patagonian Icefields, near the Pacific Ocean, marine impact and westerly frontal frameworks affect the atmosphere. A heavy north-south atmospheric pressure gradient induces strong and moist westerly winds over Patagonia south of 45° 5' S (Lliboutry, 1998). The southern SPI receives the most extreme precipitation along the coast, at around 51° S (Lopez et al., 2010).

The CDI region (Figure 2.2) is by far the least inspected part of the Southern Andean cryosphere. The lessening of precipitation to the east is observed in the CDI. Throughout the winter, strong winds begin from the west and, at the same time, cold air comes from the polar region (Holmlund and Fuenzalida, 1995; Lopez et al., 2010).

These diverse climatic patterns influence glacial extent, mass and velocity in the Andes. Any deviation in normal climatic patterns will bring significant change in the Andean Cryosphere.

2.4 Data

I used all footprints of the elevation product of GLA14 release 533, Geoscience Laser Altimeter System (GLAS[2]) aboard the Ice, Cloud and land Elevation Satellite (ICESat) campaign from 2004 to 2008 that overlay glaciers in the Andean cryosphere. The GLAS transmits short pulses (40 pulses per second) of infrared light (1064 nm) and visible green light (532 nm). Laser footprints are about 70 m in diameter and spaced along-track direction at 170-meter intervals from a 600-km altitude orbit. Global Land Surface Altimetry (GLA 14) product provides surface elevations for land. It includes the laser footprint geolocation and reflectance (Kääb et al., 2012). The National Snow and Ice Data Center (NSIDC) distributes the ICESat GLAS data products. Also, I used a 90 m spatial resolution elevation model from the Shuttle Radar Topographic Mission (SRTM[3]) – version 4 for the year 2000. Moreover, I used Landsat ETM+ statellite data acquired close to the SRTM acquisition date. Table 2.1 provides acquisition dates of these scenes. I used these multispectral images to classify the spectral signatures into different land cover classes. I used glacier boundary shapefiles from the Global Land Ice Measurements from Space (GLIMS) and Randolph Glacier Inventory 5.0 (RGI) to identify glacial boundaries.

[2] Thomas, 2012. GLAS/ICESat L2 Antarctic and Greenland Ice Sheet Altimetry Data, Version 33, [GLA14]. Boulder, Colorado, NASA DAAC at the National Snow and Ice Data Center.

[3] Jarvis, A., H.I. Reuter, A. Nelson, E. Guevara, 2008, Hole-filled SRTM for the globe Version 4, available from the CGIAR-CSI SRTM 90m Database (http://srtm.csi.cgiar.org).

Table 2.1 List of Landsat (ETM+) scenes used in this study

Landsat path/row	Scene date	Cloud (%)	Landsat path/row	Scene date	Cloud (%)
231/095	10/14/01	2	232/084	1/20/00	0
232/090	12/8/01	0	232/085	2/7/01	0
232/091	12/8/01	0	232/086	2/7/01	0
232/092	3/11/01	0	232/087	2/7/01	0
232/093	3/11/01	8	232/088	12/8/01	0
232/089	12/8/01	0	233/085	1/29/01	1
233/083	12/26/99	0	233/086	1/27/00	0
226/099	12/14/01	18	233/087	11/29/01	0
227/098	2/7/02	12	232/086	2/7/01	0
229/096	2/21/02	6	233/082	2/28/00	1
229/098	3/19/00	32	232/094	5/14/01	10
230/096	10/2/99	7	232/083	12/5/00	0
230/097	8/4/01	9	233/080	11/26/00	0
231/094	10/27/00	10	233/081	3/21/02	0

2.5 Methods

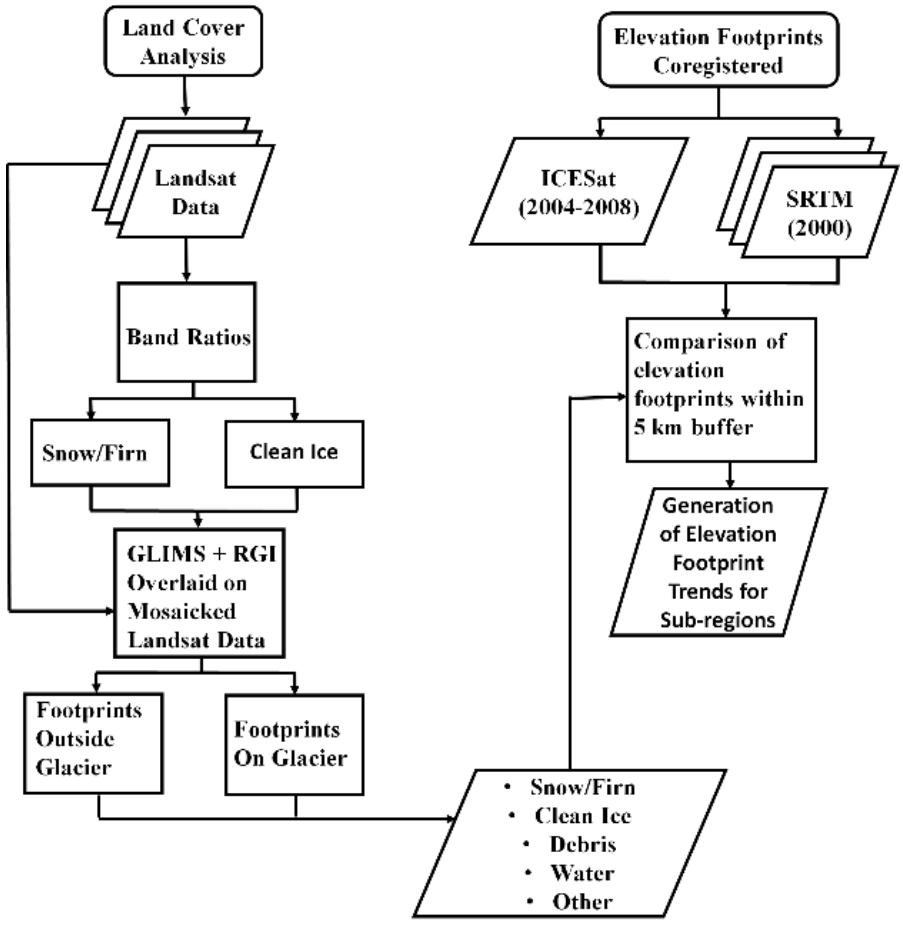

Figure 2.3 Flowchart summarizes the methodology

Figure 2.3 shows a flowchart of the methodology used to analyze the glacial change in the Andes. The ICESat elevation data was provided in Topex /Poseidon ellipsoid, and the SRTM data was in EGM 96 Geoid; therefore, I geo-referenced both ICESat and SRTM data to the WGS 84 ellipsoid before the analysis. I created a 5-km buffer around the glacier boundaries. Based on the location of the ICESat footprint, I

categorized ICESat footprints as ‘on-glacier’ and ‘off-glacier’ points (Figure 2.3). I used off-glacier footprints in the calculation of uncertainty in the estimation of glacier elevation differences and mass balance. I excluded the ICESat footprints that fall within the SRTM void mask to avoid possible bias in glacier mass estimation (Kääb et al., 2012).

I first georectified and mosaicked Landsat images. Then I classified the images into five land cover classes, Clean Ice, Snow, Debris, Water, and Others (Figure 2.3), using multiple band ratios and classification methods. The high albedo in the snow and clean ice helps to separate snow from the encompassing territory (Racoviteanu et al., 2008). I used the visual and near infrared (VIN) bands of Landsat to create a band ratio of Band 3/Band 5. I applied a threshold of 2.05 to this ratio to separate the clean ice and snow areas from the rest of the land cover. Although, individual Landsat image had different threshold, the value 2.05 was the highest value among all the images that separated ice and snow from other land cover class. Then I created a band ratio of (Band 4×Band 2)/ Band 5 (Kääb et al., 2012). This ratio helps to separate ice from snow because both ice and snow have unique spectral signatures in the VIN region (Ambinakudige and Joshi, 2012; Racoviteanu et al., 2008). I used a threshold value of 202 on the values of above band ratio (values ranged from 0 to 255) to separate ice and snow. Lastly, I classified water and debris manually and excluded those classes from the analysis. After the final image classification, in ArcGIS 10.2 software, I overlaid the ICESat footprints on the classified image and extracted classified pixel values. I used a total of 138,763 elevation footprints in the analysis. Of these footprints, 113,951 elevation were outside the glaciers, 12,009 were on clean ice, 11,279 were on glacier

firn/snow, and 1,524 were on debris-covered ice. There were 2119 footprints in DC, 5538 in NW, 5741 in SPI, and 1421 in CDI regions.

After the extraction of land cover classes from overlaying pixel to the ICESat footprints, I also extracted the elevation values from the SRTM DEM using the bilinear interpolation technique. Then I calculated elevation differences per year by subtracting ICESat (from the years 2004 to 2008) elevation and SRTM elevation (from 2000) in the clean ice zone during the dry season. I removed points with elevation differences greater than +150 and less than -150, because I assume that these are possible errors in the data due to clouds or other factors (Kääb et al., 2012; Phan et al., 2014). Finally, I used the remaining footprints to calculate the trends in the elevation differences over the study period.

I computed uncertainty in the trend estimation (u) as the root sum square of the standard error of elevation difference trends in glacier (SE_{gl}), elevation difference trends outside glaciers ($EDTnon_{gl}$) as shown in equation 1 (Gardner et al., 2013; Kääb et al., 2012; Neckel et al., 2014).

$$u = \sqrt{{SE_{gl}}^2 + {EDT_{nongl}}^2} \quad (1)$$

To prepare the parameters for equation 1, I conducted a bootstrap analysis to examine the possible error introduced in the analysis due to the uneven number of sample points in each year. From the elevation difference footprints on glaciers, I randomly selected points for bootstrap analysis with an increment of 10 percent points at each stage, until I covered 100 percent points. I used two hundred iterations at each stage (Kääb et al., 2012; Neckel et al., 2014). I fitted a second-order polynomial through all the

standard deviations of the elevation difference trend values obtained from the bootstrap analysis. I then used the fitted polynomial value at the 100 percent points in calculating standard error (SE_{gl}) and used in equation 1(Kääb et al., 2012; Neckel et al., 2014). I noticed representativeness of elevation footprints varies in the regions. In all regions except the NW, standard deviation values leveled off at around 55 percent of the points (Figure 2.4). In the NW region, standard deviation values leveled off at around 80 percent points (Figure 2.4). I therefore used the standard deviation value at 100 percent footprints in the uncertainty estimation.

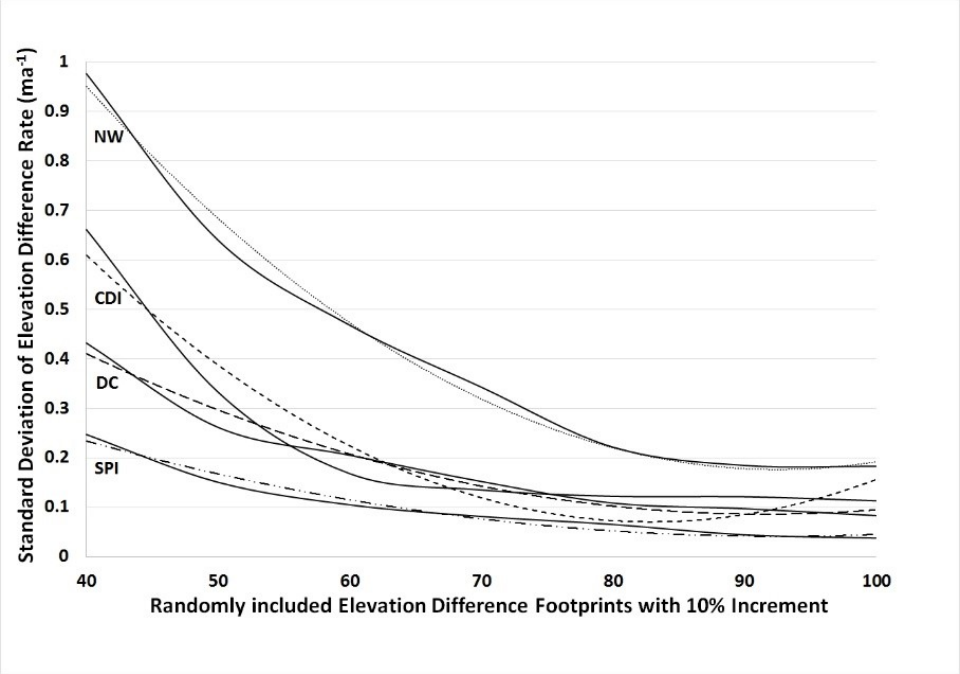

Figure 2.4 Trends of standard deviation of elevation difference from randomly selected points over clean ice

The accuracy of the ICESat's altimetry elevation measurement in the high slope areas is very low (Carabajal and Harding, 2005; Kääb et al., 2012; Neckel et al., 2014). Therefore, to get the precise error estimates in elevation differences in off-glacier areas, I

fitted a linear trend on elevation differences in off-glacier footprints in areas where slope values are less than 10 degrees. I used this trend value (EDT_{nongl}) in Equation 1. Although studies have noted that there could be inter-annual biases of about ± 0.03–0.06 m a^{-1} in the ICESat laser period (Gardner et al., 2013). I assume that the uncertainity estimation method is inclusive of any inter-annual biases. Finally, I computed glacier mass balance trend and associated uncertainty by multiplying a density value of 900 kg m^{-3} for clean ice (Huss, 2013).

2.6 Results and Discussions

The trends of elevation differences indicate varied glacial wastage rates throughout the study period. Figure 2.5 depicts the glacial thinning trends in DC, NW, SPI, and CDI regions on clean ice areas. I calculated these trends by fitting a linear model through all available elevation differences in ICESat footprints from 2004 to 2008 with respect to year 2000 SRTM elevation values. I fitted these trends through all footprints that fall within one and two standard deviations from the mean. I calculated the elevation difference trends and mass balance trends using all points. Figure 2.5 shows the trends of elevation differences fitted through all points.

Generally, in all four regions throughout the study period, elevation values were lower than the year 2000 SRTM values with some exceptions in the NW region. Over the study period in the Dry Central region, there was a negative elevation difference trend of -0.04 ± 0.14 m a^{-1}. This trend indicates a recession of glacial mass compared to the year 2000, but the uncertainty in this estimation is higher than the elevation difference trend. In the DC region, the maximum mean elevation difference (Table 2.2) (Figure 2.5) was -0.98 ± 0.29m in 2005, and minimum elevation difference was -0.13 ± 0.18m (Table 2.2)

in 2006. The overall mass balance in the DC region was -0.037 ± 0.13m w.e.a^{-1} on the clean ice region. Clearly, there were significant negative mass balance in DC in some years, but in other years, there were higher uncertainty in the estimated values.

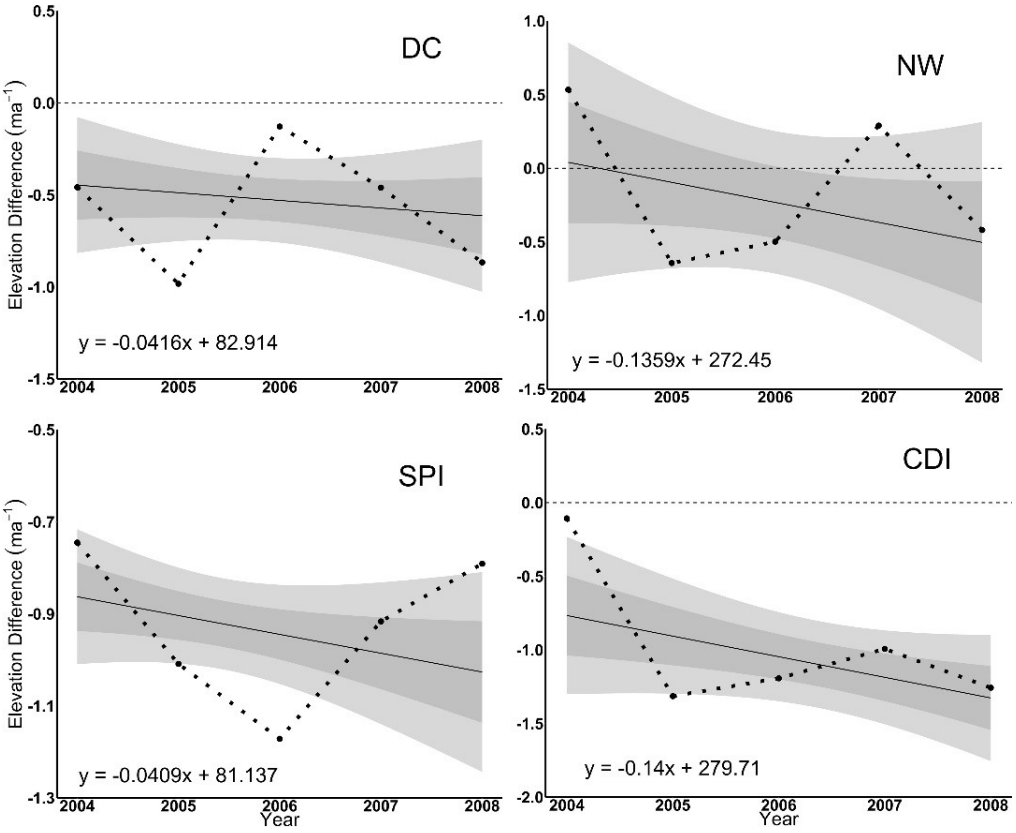

Figure 2.5 Average elevation differences per annum and linear trends between ICESat and SRTM data from 2004 through 2008 on clean ice in four regions

Table 2.2 Average elevation differences and trends between ICESat and SRTM data from 2004 through 2008

Regions	Average elevation difference per annum (ma^{-1})					Elevation Difference Trends (ma^{-1})	Mass Balance Trends (m $w.e.a^{-1}$)
	2004	2005	2006	2007	2008		
NW	0.53±0.9	**-0.64±0.5**	**-0.50±0.4**	0.29±0.4	**-0.42±0.3**	**-0.14±0.13**	**-0.122±0.12**
DC	**-0.46±0.3**	**-0.98±0.3**	-0.13±0.2	-0.46±0.2	-0.87±0.2	-0.04±0.14	-0.037±0.13
SPI	**-0.75±0.1**	**-1.01±0.1**	**-1.17±0.1**	**-0.92±0.1**	**-0.79±0.2**	-0.04±0.05	-0.037±0.05
CDI	-0.11±0.6	**-1.31±0.3**	**-1.19±0.3**	**-0.99±0.5**	**-1.26±0.2**	**-0.14±0.06**	**-0.126±0.05**

In the North Wet region, elevation differences on clean ice fluctuated significantly over the study period. However, the overall elevation difference trend was -0.14 ± 0.13m a^{-1}. The mean elevation values were lower than the year 2000 values in the years 2005, 2006, and 2008, while in 2007 and 2004, the mean elevation values were little higher than the 2000 value. The maximum mean elevation difference in this region was -0.64 ± 0.5m (Table 2.2) in 2005, and there was a positive elevation difference of 0.5 ± 0.9m (Table 2.2) in 2004. Over the study period, mass balance rate was -0.122 ± 0.12m $w.e.a^{-1}$ on the clean ice region.

In the SPI also there was a negative elevation difference trend of -0.04 ± 0.05m a^{-1} during the study period. In all the years, the mean elevation difference was lower than the values in 2000. The maximum mean elevation difference (Figure 2.5) I observed for this region was -1.17 ± 0.09m (Table 2.2) in 2006 and the minimum elevation difference I noticed was -0.75 ± 0.10m (Table 2.2) in 2004. Likewise, there was a negative trend in mass balance (-0.037 ± 0.05m $w.e.a^{-1}$).

In the Cordillera Darwin Icefields, there was a negative glacier elevation difference throughout the study period. The overall trend in the elevation difference was -0.14 ± 0.06 m a^{-1}. The maximum mean elevation difference (Figure 2.5) I observed in

this region was -1.31 ± 0.3m (Table 2.2) in 2005, and the minimum elevation difference I noticed -0.11 ± 0.6 m (Table 2.2) in 2004. The mass balance trend was -0.126 ± 0.05m w.e.a^{-1}. Among all the regions, CDI showed highest negative mass balance trend.

2.7 Conclusions

The objective of this study was to estimate the trends in glacial mass balance using GLAS-ICESat and SRTM elevation models in the Andes of Chile and Argentina. I classified the study area into DC, NW, SPI, and the CDI regions. One of the challenges of using ICESat data in non-polar regions is the scarcity of footprints outside the Polar Regions. This is because the ICESat campaign was originally developed to study polar ice dynamics, therefore, its coverage decreases as one moves toward the equator. The numbers of footprints across seasons and years varied significantly in the glaciated areas in this study region. Some areas covered with a very large number of footprints, but the others had only a few footprints. However, researchers have successfully used a limited number of ICESat footprints in non-polar regions such as Tibet and parts of the Himalayas to study glacial mass balance (Beaulieu and Clavet, 2009; Gardner et al., 2013; Kääb et al., 2012; Neckel et al., 2014). Highly accurate measurement of elevation in ICESat campaign makes it suitable for mass balance study at a regional or a sub-regional level. This study is the first attempt to use GLAS/ICESat data over clean ice in the Southern Andes. I used only the dry season footprints on clean ice areas of the glaciers in the analysis.

Generally, in all regions and all the years, the elevation values were lower than the elevation values from the year 2000, with some annual fluctuations especially in the NW region. But the elevation trends fitted through all data points have been always

negative (Figure 2.4 and Figure 2.5). Therefore, it is evident that there was a negative mass balance in the region. Several other studies in the region using various remote sensing satellite data also have indicated glacial retreat and mass balance decline (Chen et al., 2007; Dixon and Ambinakudige, 2015; Lopez et al., 2010; Masiokas et al., 2009; Mouginot and Rignot, 2015; Rignot et al., 2003; Rivera et al., 2006; Sakakibara and Sugiyama, 2014).

The mass balance of glaciers were significantly negative in the CDI and NW regions. The uncertainty in the estimation of mass balance is very low in the CDI ad NW. However, in SPI and DC regions, negative trends were not very significant as the uncertainties in the estimation of elevation differences are higher than the elevation differences. In the CDI region, glacial mass balance was -0.126 ± 0.05 m w.e.a^{-1}. Lopez et al. (2010) studied 25 glaciers in CDI and found 20 glaciers retreating and 5 glaciers remaining stationary between 945 and 2005. A recent study by Melkonian et al. (2013) used ASTER and STRM DEMs to record an average glacier thinning rate of -1.5 ± 0.6 m w.e.a^{-1} in the CDI region. Overall, it evident from this study and other studies that the Cordillera Darwin Icefield is losing mass more rapidly than other regions in the Southern Andes.

In the NW region, glacial mass balance was -0.122 ± 0.12 m w.e.a^{-1}. Rignot et al., (2003) and Rivera et al., (2006) studied the glacial retreat in this region and observed significant negative trends. This study reiterated these observations even though uncertainties in the estimations. Rignot et al., (2003) and Rivera et al., (2006) related these negative trends to trophospheric warming and reduced precipitation.

In Dry Central, I observed gradual but continuous mass loss at the rate of -0.037 ± 0.13 m w.e.a-1. Previously in this region, (Rivera et al., 2006) also found a negative mass balance of -1.06 ± 0.45 m a^{-1} in the Cipreses glacier between1955-2000. Similarly, these results in the SPI region reveal steady glacier mass balance rates of -0.037 ± 0.05 m $w.e.a^{-1}$. Considering the uncertainties, these results are comparable to the observations made by Willis et al. (2012) in this region where they found −24.4 ± 1.4 Gt a^{-1} loss in the mass between 2000 and 2012.

One possible reason for the negative mass balance in the region is the increased temperature in South America over the twentieth century, as reported by Carrasco et al., (2005), Favier et al., (2009), Rabatel et al., (2011), and Villalba et al., (2003). Similarly, there might be other climatic factors responsible for glacial melting and variation in the snow accumulation, like a fluctuation in the precipitation, as suggested by Favier et al., (2009), Prieto et al., (2001) and Rignot et al., (2003). More research is required to understand the role of micro-climatic conditions on glacial variations in the region. It is also important to understand the effects of ENSO events on Central Andean glaciers (Carrasco et al., 2005; Prieto et al., 2001; Rivera and Bown, 2013; Rivera et al., 2006). However, the lack of good quality climatic data in glacier regions (Masiokas et al., 2009) prevented such analysis. This study attempts to use limited data to study the status of glacial change in a large area, but further studies are still required.

CHAPTER III

SPATIOTEMPORAL ANALYSIS OF SNOW COVER EXTENT AND MASS ANOMALIES IN CALIFORNIA[4]

3.1 Abstract

The aim of this chapter was to analyze the melting patterns of snow cover in the Sierra Nevada and Mt. Shasta regions in California. I use digital elevation models generated from the Advanced Spaceborne Thermal Emission and Reflection Radiometer (ASTER) between the year 2000 and 2015 to study snow mass anomalies. Further, I use Landsat scenes to quantify snow cover extent in the hydrological region between 2000 and 2015. The study results demonstrate that the snow cover has been significantly receded throughout the period. This decline in snow cover is mainly attributed to a decrease in snowfall. Further, air temperature and glacier size also played a significant role. A remarkable reduction in snow cover extent of about 80% between 2000 and 2015 was observed in the studied watersheds. Similarly, during the period snow mass anomalies in Mt. Shasta and Crowley lake watershed (Sierra Nevada mountain ranges) were –96.85± 67.35 megaton and –162.12 ±130.49 megaton respectively. However, some glaciers had a surge in snow mass. Considering the current water crises in California, this study provides valuable insights into the possible role of climatic factors in snow mass anomalies in the region.

[4] This chapter is an extension of the work presented in ASPRS (IGTF) 2016 annual conference

3.2 Introduction

Water is essential not only to human sustenance, but it is also vital for all lifeforms on earth. Water covers more than 75% of the Earth's surface, yet just 3% of it is freshwater. Of this, ice caps and glaciers are the primary contributors. In the state of California, snow mass plays a significant role as natural water reservoirs. Because of the Mediterranean climatic conditions, the region gets most of its precipitation in winter. It makes snow mass as a primary source of freshwater for the rest of the year. Typically, it provides one-third of the water utilized in California's urban areas and ranches every year (Chou, 2014). Thus bearing in mind the water scarcity in California (Swain et al., 2014), it is essential to analyze the existing state of perennial and seasonal snow masses in the region.

Alpine glaciers are sensitive to slight changes in climate and similar to the other glaciers in the world, they act as pointers towards climate change (Ambinakudige and Joshi, 2015; Basagic and Fountain, 2011; Inamdar and Ambinakudige, 2016; Marcus et al., 1995). The changing climate affects the length of the mass balance season (Kaser et al., 2003) and also impacts the seasonal distribution of streamflow in the high altitude regions (Pachauri et al., 2014).

Over the past century, California has experienced severe and prolonged dry events, including those during 1976-1977, late 1980s, and the recent drought during 2012-2014 (Griffin and Anchukaitis, 2014; Swain et al., 2014). Analysis of nine different observational datasets by (Bonfils et al., 2007) to estimate California's average temperature trends between 1950-99 found increased temperature of about 2°C, with higher rates in the winter. They also noticed more warming at night than in day and

attributed this phenomenon to the anthropogenic activities. Additionally, climate prediction models forecasted a 20% decrease in precipitation by AD 2100 in the southern California (MacDonald, 2007). Howat and Tulaczyk (2005) in their study of climate sensitivity of spring snowpack in the Sierra Nevada analyzed historical climate data using a multivariate model and found that impact of the warming is considerably reliant on coexisting precipitation variation and watershed topography. Because of the high elevation of the most of the watersheds in California, snow amassing was found to be mainly controlled by precipitation than temperature (Costa-Cabral et al., 2012). Another climate model report in the region predicted significant fluctuations in cold season precipitations and temperature resulting in increased runoff in the winter as compared to the spring/summer (Ashfaq et al., 2013). Similarly, a hydro-meteorological study of California rivers (Maurer et al., 2007) reported the increased warming in the recent decade caused earlier streamflow timings. They attributed variation in stream flows to anthropogenic activities.

A study by Maurer (2007) in the Sierra Nevada region compared a hydrological model under two emissions scenarios (high and low) to determine the probable hydrologic changes by 2071–2100. Maurer (2007) study also predicted increased temperature, reduced and early stream flows, and reduced snowpack in winter due to the role of emissions. Stine (1994) provided the evidence of anomalous climate conditions with severe droughts in about AD~1112 and AD ~1350 due to the reorientation of the storm tracks in the Sierra Nevada. It shows that the region has suffered droughts in the past too. Therefore, Stine (1994) concluded that anthropogenic warming soon might result in another reorientation of storm tracks that might cause extreme droughts. Swain et

al.(2014) ascribed global warming to boost the probability of North Pacific ridging events, which might restate extreme 2013-14 droughts in California. Though probabilistic analysis based on Monte Carlo simulation (Margulis et al., 2016) expected the recovery period of four years since the recent snowpack drought. Changing climate with long-term fluctuations in the precipitation and high evaporation makes the condition vulnerable to the states like California, as it affects the discharge in the basins (MacDonald, 2007). After examining remotely sensed and climate data McCabe and Fountain, (2013) observed considerable spatiotemporal variability of glaciers occurred between 1900 to 2000 largely due to warming and fluctuations in rainfall in high elevation areas. However, despite fluctuation in temperature and precipitation, Howat et al. (2007) noticed surge in glaciers in Mt. Shasta due to events of high snow accumulation and positive ENSO phases.

Other than climatic parameters, impurities also decrease the snow albedo and thus results in higher melting rate. Several studies showed that trace amounts of aerosol impurities in snow affects the surface energy budget as it can remarkably degrade the amount of sunlight reflected by snow and ice fields (Hadley et al., 2010; Kirchstetter et al., 2008; Sterle et al., 2013). Hadley et al. (2010) studied the concentration of black carbon in the snow before and after the precipitation. They noticed deduction of aerosols from the atmosphere by snowflake and its subsequent deposition to the snowpacks of Sierra Nevada. A study by Hadley et al. (2010) reveals black carbon concentration in precipitation of about 1.7 ng/g to 12.9 ng/g. K. Sterle et al., (2013) reported black carbons and dust in the Sierra Nevada region for the year 2009 distressing about a quarter of the solar component in the energy balance.

Additional factor directly impacting the extent and the melting rate of snow mass is the topography of basin. Kessler et al. (2006) modeled irregular terrain in the Sierra Nevada during the last glacial maximum. They reported uneven terrain accounts for larger glacier extent towards the west as compared to the rain shadowed east draining glaciers. Also, glaciers on the west flank are on the low slope and receives high southwest precipitation (Kessler et al., 2006). Similarly, a recent analysis of variability in the snowmelt based on the topographic elevation by (Rice et al., 2011) observed higher melting of about 40-60% in the mid-elevation of Tuolumne and Merced River basins.

Furthermore, seasonal snow masses in semiarid regions, such as the Sierra Nevada, provides suitable habitat for microbial life (Painter et al., 2001). The presence of cold tolerant microbes on thawing snow covered regions has been reported in the Serra Nevada region and many other parts of the world (Dozier et al., 2009; Painter et al., 2001; Segawa et al., 2005; Takeuchi et al., 2006). Painter et al. (2001) developed a linear model to retrieve snow algal concentrations and reported red algae biomass concentration of 0.033 g. m^{-2} in the Sierra Nevada region.

In California and other western states, many small perennial snow and ice covered regions exist over a vast area. Because of this scattered distribution pattern, the region lacks in the comprehensive historical records of glacier extent before the development of modern topographic maps (Krimmel, 2002).

In this paper, I use data that was generated using remote sensing techniques to analyze the state of snow extent and mass anomalies in the California between 2000 and 2015. I compared classified raster land cover models to quantify snow cover extent in the region. Additionally, anomalies in snow mass were analyzed based on digital elevation models

generated from the Advanced Spaceborne Thermal Emission and Reflection Radiometer (ASTER). Here I present results of snow extent and mass analysis based on the watersheds and named glaciers in the region.

3.3 Study Area

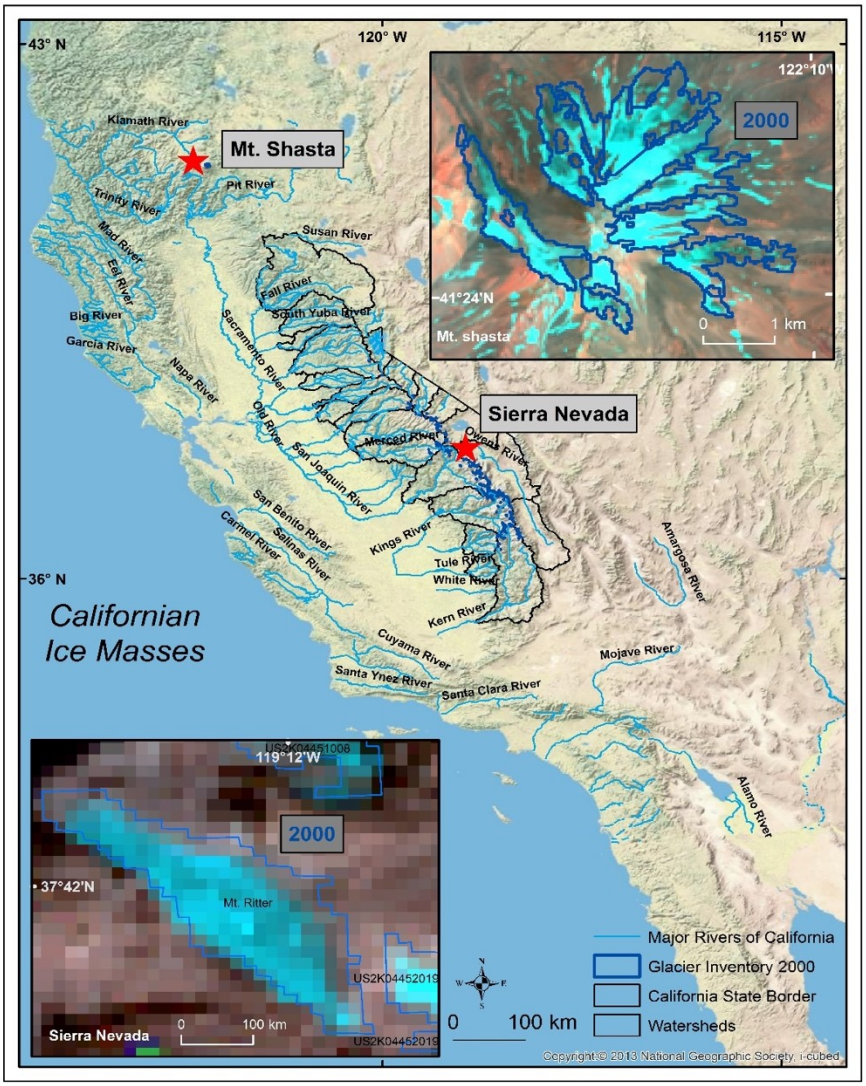

Figure 3.1 Illustration of the study area in California

Perennial snow and ice covered regions in California are mainly located in the Sierra Nevada and Mt. Shasta. The Sierra Nevada mountain range extends from around

35°N to 39°N about 650 km (Figure 3.1), situated on the eastern border of California. In the northern California, Mt. Shasta is located at 44.4°N-112.20°W (Figure 3.1). This potentially active volcano marks the end of Cascade Range. Also, Mt. Shasta is the largest stratovolcano with a second highest peak (about 4320m) in the Cascade Range. During the Pleistocene period, the entire region was significantly glaciated (Clark and Gillespie, 1997). At present, the region contains small but scattered perennial snow and ice covered regions (Basagic and Fountain, 2011; Krimmel, 2002). California has Mediterranean and semi-arid climates with dry summers. It gets precipitation in the form of snow during the cool winters between November and May (Serreze et al., 1999). Low-pressure systems over the Pacific Ocean control the moisture deposition in the region. Also, the amount of precipitation varies along the crest based on the rain shadow area in the east (Danskin, 1999; Gillespie and Clark, 2011). In this study, snow cover and mass change on about 30 named glaciers as small as 0.01 km^2 were enumerated. Also, I provide quantitative results of the anomalies in the extent and mass loss in the major watersheds. This analysis considers American, Crowley Lake, East Walker, Kaweah, Kern, Kings, Merced, Mokelumne, Mono, Owens, San Joaquin, Stanislaus, Tahoe, Tuolumne, Upper Carson, and West Walker watersheds. In this study, I also measured snow cover and mass on named glaciers of the Mt. Shasta such as Bolam, Hotlum, Whitney, Wintum, Watkins, and Konwakiton.

3.4 Data

Landsat TM, and L8 scenes were acquired with the minimal cloud cover and with acquisition dates in the month of August. Finest images were available for the years 2000, 2002, 2008, 2010, and 2014 covering Sierra Nevada. While scenes of the years

2000, 2003, 2008, 2011, and 2015 were available for the Mt. Shasta. These multispectral images were used to develop raster land cover models of snow cover in the region. List of Landsat data is given in Table 3.1.

Table 3.1 List of Landsat scenes used in this study.

Date	Path/Row	Cloud cover	Landsat	Region
8/27/2000	043/033	0	5	Sierra
8/20/2000	042/034	0	5	Sierra
8/27/2000	043/033	0	5	Sierra
8/1/2002	043/033	0	5	Sierra
8/3/2002	041/035	0	5	Sierra
8/10/2002	042/034	0	5	Sierra
8/1/2008	043/033	1	5	Sierra
8/3/2008	041/035	0	5	Sierra
8/26/2008	042/034	0	5	Sierra
8/16/2010	042/034	0	5	Sierra
8/23/2010	043/033	0	5	Sierra
8/16/2010	042/034	0	5	Sierra
8/18/2014	043/033	0.11	8	Sierra
8/27/2014	042/034	0.18	8	Sierra
8/27/2014	042/035	0.15	8	Sierra
8/25/2000	045/031	0	5	Shasta
8/18/2003	045/031	0	5	Shasta
8/15/2008	045/031	0	5	Shasta
9/9/2011	045/031	0	5	Shasta
8/19/2015	045/031	35	8	Shasta

Other remote sensing data used was the Advanced Spaceborne Thermal Emission and Reflection Radiometer (ASTER) elevation data product (4A01) processed by Japanese Space systems utilized for the analysis. The ASTER is a high spatial resolution multispectral imaging radiometer onboard NASA's Terra spacecraft. Obtained three-dimensional data product is generated using the nadir-looking VNIT (3N) and backward looking 3B. I used available ASTER scenes with minimal cloud cover between the year

2000 and 2015 that overlay on perennial and seasonal snow covered regions in Mt. Shasta and the Sierra Nevada. Specifically, for the Sierra Nevada available ASTER scenes were acquired for the years 2000, 2002, 2008, 2010, 2012 and 2014. Similarly, for the Mt. Shasta available ASTER scenes were acquired for the years 2000, 2003, 2008, 2011, and 2015. Obtained ASTER scenes were between the month of June and October to understand the state of snow mass cover in the regions. These months were selected to coincide the study period with the end of the hydrological year. The ASTER elevation data was provided in WGS84 ellipsoid with the transverse Mercator projection. Moreover, 7.5-minute series quadrangle topographic maps (1:24000) in mid-nineties were obtained from the National Geologic Database project (NGMDB); managed by USGS National Geospatial Program (NGP). List of topographic maps used in the analysis given in Table 3.2. Whereas watershed boundary shapefiles was acquired from the California Department of Forestry and Fire Protection's Fire and Resource Assessment Program (FRAP). Additionally, Global Land Ice Measurements from Space (GLIMS), Randolph Glacier Inventory 5.0 (RGI), World Glacier Inventory (World glacier monitoring service (WGMS)) and United States Geological Survey report on inventories of Sierra Nevada (Raub et al., 2006) were used to identify glacial boundaries and locations. Lastly, monthly summaries of mean temperature degree Celsius (1996-2015) and total monthly snowfall millimeter (1991-2015) data were obtained from the United States National Climate Data Center (NCDC).

Table 3.2 List of 7.5-minute series (1:24000) quadrangle maps used in this study.

Topographic Map	Year	Topographic Map	Year
Mt. Shasta	1998	Mt. Henry	1994
Tioga Pass	1994	Mt. Hilgard	1994
Mt. Dana	1994	Mt. Thompson	1994
Koip Peak	1994	Mt. Goddard	1994
Mt. Ritter	1992	North Palisade	1994
Mt. Lyell	1992	Split Mtn.	1994
Mt. Abbot	1994	Mt. Whitney	1994
Mt. Tom	1994	Triple Divide peak	1993
Mt. Darwin	1994	Mt. Clarence King	1994

3.5 Methods

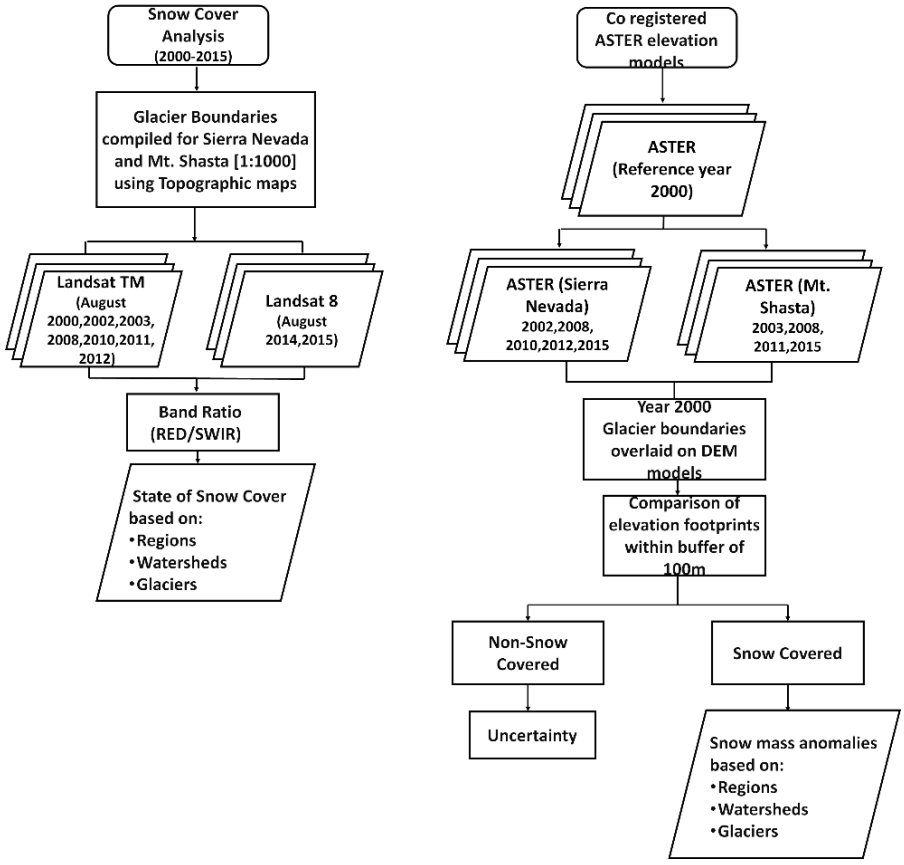

Figure 3.2 Flowchart summarizes the methodology

Figure 3.2 shows a flowchart of the methodology used to analyze snow cover and mass anomalies in California. Section 3.5.1 comprises extent analysis of snow cover in the region. Snow covered region was analyzed at the end of the hydrological year in named glaciers. While the change in the snow extent was quantified based on the major watersheds. Section 3.5.2 describes methods used to calculate snow mass anomalies in the major watersheds. Uncertainty calculations of mass differences are provided in section 3.5.3. Lastly climate data analysis is described in section 3.5.4.

3.5.1 Snow cover change

Landsat TM and Landsat-8 scenes were first georectified and mosaicked covering Mt. Shasta and Sierra Nevada (Figure 3.2). Several glaciers in this region were missing in the GLIMS and Randolph Glacier Inventory (RGI) database mainly because of their smaller extent (about 0.01 km^2) (H. Basagic and Fountain, 2011; Krimmel, 2002). Therefore, I digitized glaciers manually using 7.5-minute series quadrangle maps on a scale of 1:1000. Later, I used these as reference glacier boundaries. Topographic maps used in the study are listed in Table S2. Additionally, glacier boundaries from GLIMS, RGI, World Glacier Monitoring Service (WGMS) and USGS report on inventories of Sierra Nevada (Raub et al., 2006) were used as references to determine locations of the perennial snow masses in the region.

Land cover in the study area was classified into two classes: snow covered and non-snow covered regions using a band ratio (Red/SWIR) (Figure 3.2). This ratio helps to separate high reflectance snow/ice pixels from other land cover classes. A threshold value should be selected that separates snow/ice from other land cover class. In this study, the highest Red/SWIR band ratio value of 2.05 was selected as the threshold value. I also visually

checked each classified area with the actual image to see any area that is visually identifiable that has been misclassified. I manually corrected miss-classified water and debris pixels. Later I used the zonal statistic tool in the ARCGIS 10.2 to quantify snow covered pixels within the glacier and watershed boundaries. The snow covered extent at the end of particular hydrological years was measured in the named glaciers. While I analyzed the change in the amount of snow cover extent between the year 2000 and subsequent years within watershed boundaries. Finally, results of percent snow cover extent with linear trends were presented for the two study regions (Mt. Shasta and the Sierra Nevada), named glaciers and watersheds.

3.5.2 Snow mass difference

To study anomalies in snow mass, for the Sierra Nevada, I used ASTER DEMs for years 2002, 2008, 2010, 2012 and 2015. Similarly, for Mt. Shasta available ASTER DEMs for years 2003, 2008, 2011, 2015 were used. Available images capturing the end of the water year were acquired in the months of June-October. Elevation differences were calculated by subtracting subsequent ASTER DEMs from the reference ASTER elevation (the year 2000) (Figure 3.2). Further, pixels in the elevation difference raster data were converted into points. Supplementary glacier boundaries overlapping period (2000) compiled for the precise classification of elevation difference points. I manually digitized glacier boundaries in the region for the specific year 2000 using the Landsat data for the August month. Later the year 2000 inventory area was used to calculate mass change. I created a 100m buffer around the glacial boundaries. Subsequently based on the location of the elevation points, they were categorized as ‘snow covered’ or ‘non-snow covered’ points (Figure 3.2).

A total of 366,640 elevation points were used in the analysis. Out of which, 262,018 elevation points were off snowfield, and 104,622 were on the snowfield. In the Mt. Shasta and the Sierra Nevada, I analyzed 28,504 and 76,118 elevation points respectively. The non-snow covered elevation points were used to calculate the standard error as well as uncertainty in the estimation of snow elevation differences. Additionally, elevation points with very extreme elevation differences were removed, as these are a possible error in the data (Kääb et al., 2012; Phan et al., 2014). As I was specifically comparing snow mass at the end of hydrological year, I decided to use density value of 750 kg m^{-3} which is an average of snow (600 kg m^{-3}) and clean ice (900 kg m^{-3}) density scenarios (Huss, 2013). Finally, results of snow mass changes in megaton were presented based on named glaciers, regions (Mt. Shasta), and watersheds (Sierra Nevada).

It is important to note that these results of snow cover extent and geodetic snow mass analysis of named glaciers cannot be compared merely to each other. Primarily because in snow cover analysis I quantified the snow cover extent at the end of the hydrological year. While the mass analysis was based on the surface elevation difference between the reference (the year 2000) and successive years. Besides, it covers diverse seasonal snow cover extent. However, both outcomes can be compared to the broader scenario.

3.5.3 Uncertainty assessment

Initially, the uncertainty in the estimation of elevation differences calculated as the root sum square of the standard error of the mean (SE_{nongl}) and mean elevation difference (ED_{mean}) of the non-glaciated region (Bolch et al., 2011).

$$EDu = \sqrt{ED_{mean}{}^2 + SE_{nongl}{}^2 + DEM_{bias}} \quad (1)$$

Where the mean elevation difference (ED_{mean}) was calculated by averaging the all the non-snow covered pixels in the 100m buffer zone. The parameter standard error of the mean (SE_{nongl}) in the equation 1, is estimated by the amount of dispersion in the non-snow covered points divided by the square root of its sample size. DEM_{bias} (systematic error) in the equation 1, measures the degree to which predicted successive elevation models (ASTER) are on average differs the true elevation at topographic map benchmark locations (Wechsler and Kroll, 2006). I used forty benchmarks.

$$DEM_{bias} = \frac{\sum_{j=1}^{n}(\hat{Y}_j - Y_j)}{n} \quad (2)$$

Where, n is the number of benchmark locations, $\hat{Y}_j$ and Y_j refers to the ASTER and topographic elevations. Lastly uncertainty in mass differences was quantified by using reference inventory area, elevation difference uncertainty (Edu) and using density scenario of 750 kg m^{-3}

3.5.4 Climate data analysis

Monthly climate summaries were acquired from NOAA's National Centers for Environmental Information (NCEI). Fluctuations in temperature (°C) and snowfall (mm) parameters analyzed for the years between 1991 and 2015. To get an accurate representation of climate during the study period; weather stations were selected based on their proximity to the named glaciers. Stations located within the radius of about 10 miles from the Sierra Nevada and Mt. Shasta glaciers were used. List of the stations with details are provided in Table S3. The rate of fluctuation analyzed based on the average of dry season months (June, July, August, September, and October) and average of wet months (November, January, February, March, April, and May). Finally, results of trend

analysis were presented based on seasons (Dry and Wet) and regions (Mt. Shasta and the Sierra Nevada).

3.6 Result and discussion

The objective of this study was to analyze anomalies in snow extent as well as mass. Initially, glacier and watershed boundaries were compiled, and raster land cover models were developed to study the state of snow cover in glaciers and watersheds. Snow mass change was also quantified in glaciers and watersheds. Finally, outcomes of climatic variables are discussed. The results presented in the following three sections.

3.6.1 Extent of snow cover change in California

The snow cover analysis in California shows a substantial decrease in the extent of snow cover in both Sierra Nevada and Mt. Shasta regions between the years 2000 and 2015. I investigated changes in the extent of snow cover in the Mt. Shasta region in six glaciers, namely, Konwakinton, Watkins, Whitney, Wintum, Bolam, and Hotlum (Figure 3.3). In 2015, glaciers in the region had an average snow cover area of 44% of the total glacier extent. In Whitney glacier, only 26% of the glacier area had snow cover in 2015 (Figure 3.3). However, in Wintum glacier, the entire glacier was covered with snow during the years 2000, 2003, and 2011. But, in 2008 and 2015, only 62% and 56% area of the glacier was covered with snow (Figure 3.3). It is important to notice that all other glaciers in the Shasta region never recovered but rather showed the continuous loss in snow cover during the period.

If we look at the trends in snow covered region during the study period, without any exceptions, all glaciers showed a negative trend. Bolam glacier showed a highest negative

trend of -3.1% followed by Watkins (-2.8 %), Wintum (-2.4%), Whitney (-2.2 %), Konwakinton (-1.4%) and Hotlum (-1.3%) (Figure 3.3). Higher negative growth rate shows the uninterrupted retreat in snow cover extent of the glaciers.

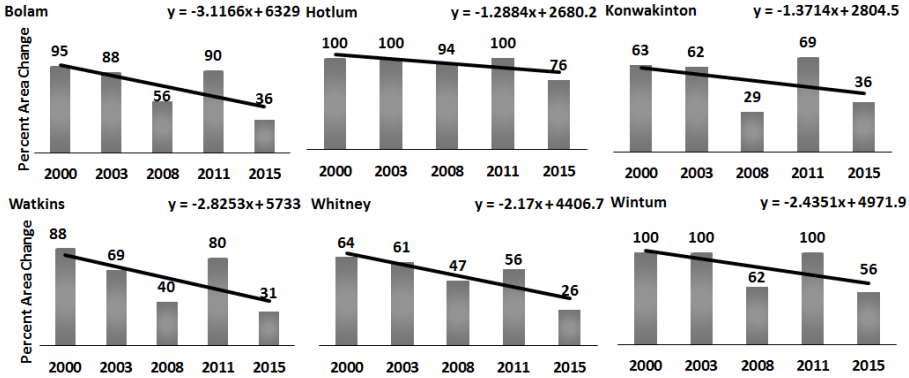

Figure 3.3 Percent snow cover extent in major glaciers in Mt. Shasta

The figure 3.3 represent linear trend fitted through percent extent of snow cover at the end of hydrological year in the region.

I analyzed the state of snow cover extent of 33 glaciers in the Sierra Nevada region. Similar to the glaciers of Mt. Shasta region, glaciers of Sierra Nevada also showed a large decrease in snow covered area at the end of the hydrological years during the study period. On an average snow cover extent in 2014 was found to be 11%. In the year 2014, Winchell, Keyhole, Scylla, Mt. Lamarck, Mt. Dade, Mt. Warlo, Matthes, Four Gables, Charybdis and most other glaciers were almost completely snow free (Figure 3.4). Following in the year 2008, only 34% of the glacier area was under snow cover. While I observed in the years 2000 and 2010, there was highest snow cover in many glaciers. Mt. Ritter glaciers, for example, had full snow cover in the year 2000 (Figure 3.4). On

average 87% and 78% of the total glacier area was under snow cover for the water year 2000 and 2010 respectively.

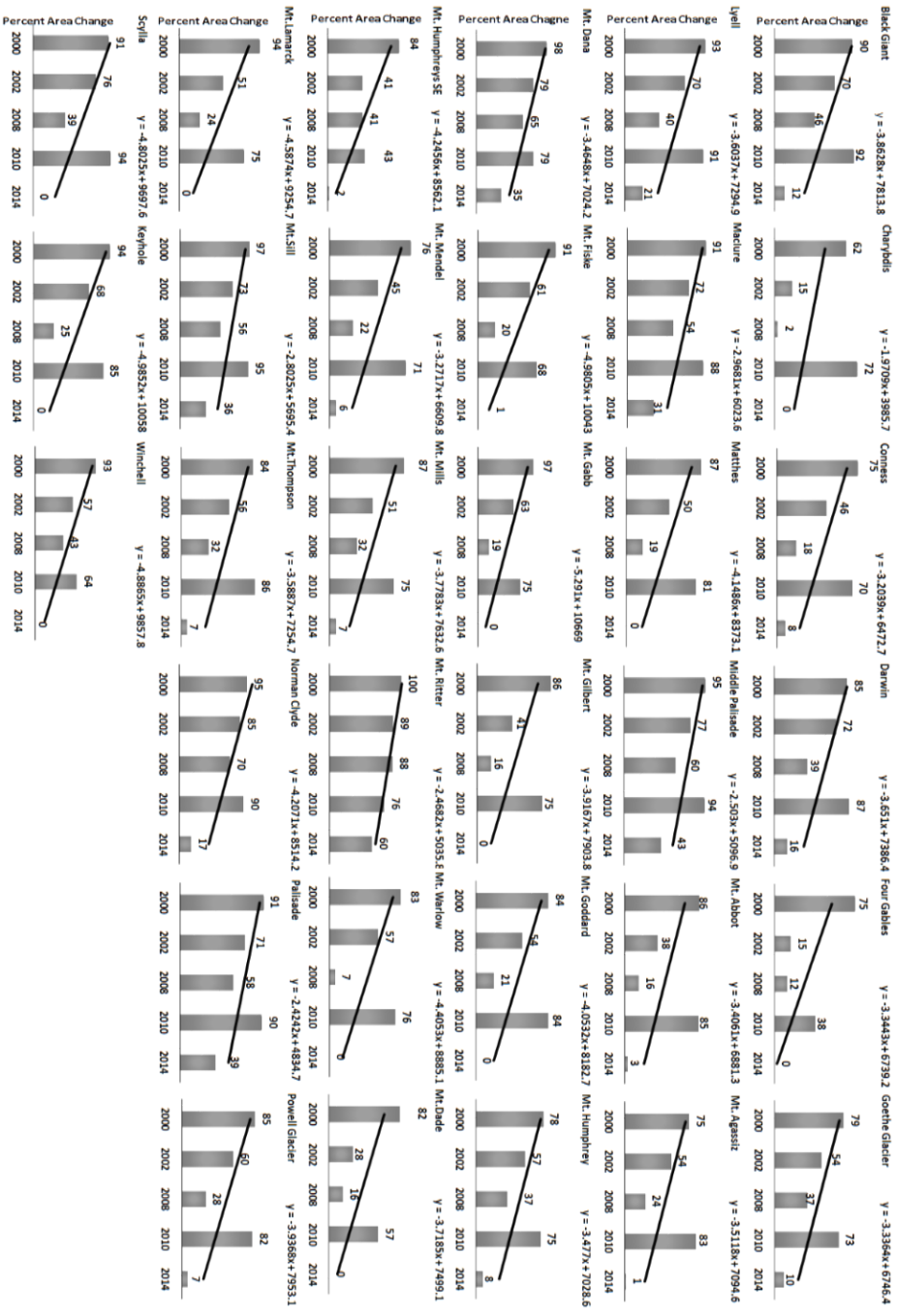

Figure 3.4 Percent snow cover extent in major glaciers in the Sierra Nevada

The figure 3.4 represent linear trend fitted through percent extent of snow cover at the end of hydrological year in the region.

Linear trends fitted over percent snow covered extent in each glacier found to be negative at the end of the hydrological year throughout the study period in all glaciers. Mt. Gabb had the highest negative growth rate (-5.3%) (Figure 3.4). The Charybdis glacier had the lowest negative growth rate of snow cover extent (-2.0 %) (Figure 3.4). Palisade Glacier, one of the largest glaciers (Krimmel, 2002) in the Sierra Nevada region, covered snow in about 39% of the glacier the area in 2014 (Figure 3.4). In essence, negative trends in the region demonstrate a steady decrease in the extent of snow cover with minor fluctuation throughout the period. Generally, the Sierra Nevada region showed the high snow cover extent loss as compared to the Mt. Shasta.

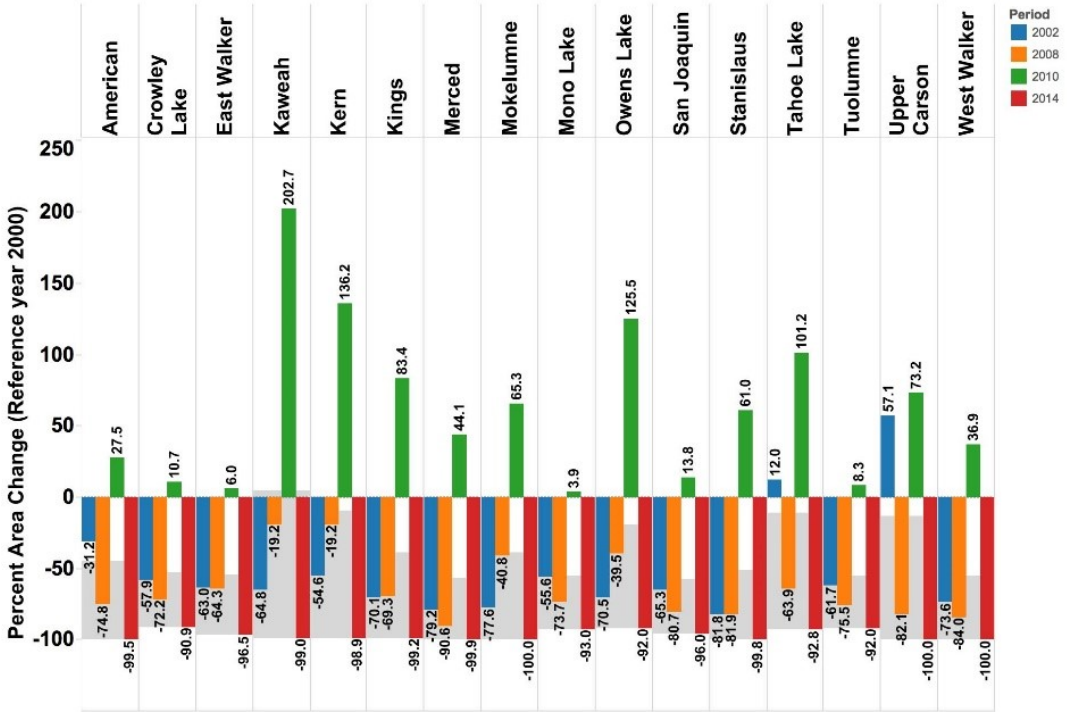

Figure 3.5 Percent snow cover extent change in major watersheds in Sierra Nevada California

Shaded region demonstrates maximum to average (percent) change in the area

I also compared snow cover change at the end of the hydrological year 2000 with the successive years within sixteen watersheds in the Sierra Nevada. Like the glacier level in overall watersheds, loss in the snow cover area was substantial in all years except for the year 2010. In 2010, all sixteen watersheds showed higher snow cover. For example, in 2010, Kaweah watershed snow cover area increased by 200% (Figure 3.5) as compared to the year 2000. However, Mono Lake watershed showed only about 4% increase in 2010 when the average recovery in the region was about 20% in that year (Figure 3.5). In the year 2014, there was almost no snow cover in any of the watersheds in August. Obviously, the downstream areas of these watersheds faced drought (Griffin and Anchukaitis, 2014; Swain et al., 2014).

3.6.2 Snow mass change 2000-2015

Snow mass anomalies indicate varied snow mass loss throughout the study period. Figure 3.6 depicts the overall glacial thinning in the regions of Mt. Shasta and the Sierra Nevada. Here I studied eight river watersheds in the Sierra Nevada based on the availability of ASTER data. Generally, in both regions, elevation values on snow covered areas were lower than the year 2000 ASTER values throughout the study period.

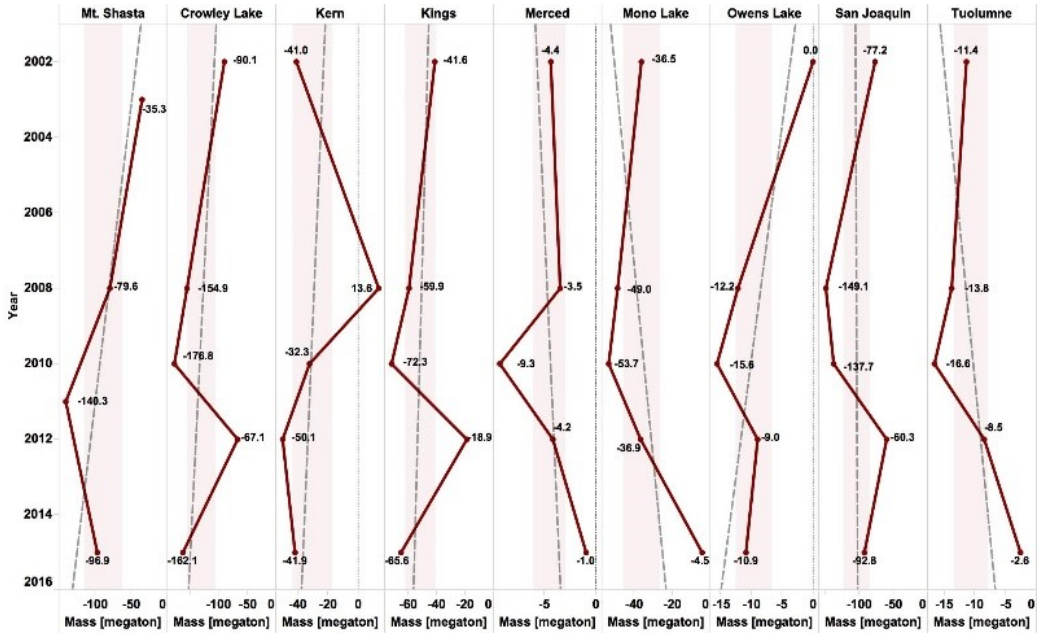

Figure 3.6 Average snow mass anomalies (megaton) and linier trends between reference ASTER 2000 and ASTER data through 2002-2015

The figure 3.6 represents linear trend fitted through average snow mass anomalies in the Mt. Shasta and major watersheds of Sierra Nevada. Shaded region of the confidence interval (68.27%) represents the spread of data in accordance to mean.

In the Sierra Nevada, over the study period, there was a remarkable mass loss in snow covered areas (Figure 3.6) (Table 3.3) (Table 3.4). Between 2000 and 2015, the high snow mass loss of –162.12± 130.49 megaton was noticed in Crowley Lake watershed (Table 3.3) (Figure 3.6) and the lowest negative snow mass observed at Merced watershed (-1.01± 1.66 megaton) (Table 3.3) (Figure 3.6). Similarly, Mt. Shasta region showed a significant snow mass loss of -96.85 ± 67.35 megaton (Table 3.5).

Table 3.3 Snow mass anomalies in watersheds of Sierra Nevada. Base year: 2000

	Snow mass anomalies (megaton)				
	2002	2008	2010	2012	2015
Crowley Lake	-90.10 ± 35.49	-154.87 ± 100.12	-176.76 ± 173.43	-67.12 ± 70.05	-162.12 ± 130.49
Kern	-41.00 ± 17.40	13.63 ± 28.18	-32.27 ± 25.05	-50.08 ± 30.96	-41.88 ± 25.89
Kings	-41.58 ± 23.20	-59.88 ± 48.11	-72.34 ± 63.11	-18.88 ± 18.73	-65.63 ± 53.71
Merced	-4.35 ± 1.01	-3.48 ± 2.22	-9.26 ± 9.19	-4.20 ± 1.81	-1.01 ± 1.66
Mono Lake	-36.49 ± 19.63	-48.97 ± 30.81	-53.68 ± 44.34	-36.93 ± 18.48	-4.51 ± 10.34
Owens Lake	0.05 ± 1.41	-12.16 ± 5.11	-15.63 ± 14.60	-8.99 ± 5.19	-10.90 ± 5.78
San Joaquin	-77.17 ± 30.38	-149.12 ± 102.23	-137.69 ± 119.55	-60.28 ± 37.51	-92.82 ± 68.02
Tuolumne	-11.38 ± 6.35	-13.80 ± 8.47	-16.56 ± 11.05	-8.54 ± 4.84	-2.61 ± 1.94

Mass anomalies quantified by using reference inventory area, elevation difference and using density scenario of 750 kg m^{-3}

Table 3.4 shows the list of named glaciers with corresponding snow mass anomalies in the Sierra Nevada region. A maximum snow mass loss of -19.68±12.06 megaton observed on snow masses of Lyell glacier in the Sierra Nevada for the year 2010 as compared to 2000. Additionally, Goethe and McClure glaciers also showed significant recession of -10.16±7.19 megaton and -7.38±4.60 megaton (Table 3.4) respectively for the year 2010 as compared to 2000.

Table 3.4 Snow mass anomalies in named glaciers of Sierra Nevada. Base year: 2000

Mass anomalies quantified by using reference inventory area, elevation difference and using density scenario of 750 kg m^{-3}

	Snow mass anomalies (megaton)				
	2002	2008	2010	2012	2015
Black Giant	-2.94 ± 2.71	-3.42 ± 3.14	-4.51 ± 3.83	-1.21 ± 0.80	-4.17 ± 4.16
Black Giant E	-1.82 ± 1.55	-2.94 ± 2.79	-3.15 ± 2.74	-0.92 ± 0.89	-2.18 ± 2.19
Charybdis	-0.30 ± 0.36	-0.19 ± 0.17	-0.21 ± 0.25	0.06 ± 0.09	-0.39 ± 0.52
Conness	-6.90 ± 1.85	-7.01 ± 2.12	-5.10 ± 3.10	-9.24 ± 1.21	1.09 ± 0.96
Darwin	-4.92 ± 4.17	-4.58 ± 2.62	-4.96 ± 3.21	-1.21 ± 1.63	-6.07 ± 5.31
Goethe	-6.27 ± 1.85	-7.46 ± 4.43	-10.16 ± 7.19	-1.71 ± 1.61	-5.49 ± 1.20
Kuna	-2.87 ± 1.78	-3.93 ± 3.06	-5.64 ± 4.53	-3.40 ± 2.81	-1.74 ± 0.66
Lamarck	-3.29 ± 1.43	-4.23 ± 2.88	-4.89 ± 4.76	-1.34 ± 1.63	-4.45 ± 2.54
Lyell	-13.49 ± 3.97	-16.48 ± 9.75	-19.68 ± 12.06	-10.07 ± 5.76	-3.03 ± 3.12
Matthes	-2.23 ± 0.60	-6.22 ± 4.20	-6.34 ± 5.96	-0.32 ± 1.30	-5.53 ± 3.60
McClure	-5.01 ± 1.69	-5.18 ± 2.06	-7.38 ± 4.60	-4.40 ± 1.20	-1.88 ± 0.88
Mt. Abbot	-1.41 ± 0.24	-1.76 ± 0.94	-2.02 ± 2.12	-2.01 ± 1.41	-1.71 ± 1.47
Mt. Dade	-1.92 ± 0.23	-3.11 ± 2.10	-2.66 ± 1.98	-2.83 ± 1.70	-3.43 ± 2.99
Mt. Dana	-2.07 ± 1.65	-1.76 ± 1.39	-2.25 ± 2.24	-1.73 ± 1.36	-0.11 ± 0.72
Mt. Gabb	-0.36 ± 1.39	-2.12 ± 0.57	-2.21 ± 3.73	-2.65 ± 0.75	-0.27 ± 4.29
Mt. Gilbert	-2.67 ± 0.45	-5.60 ± 2.96	-6.15 ± 5.58	-0.82 ± 2.56	-5.58 ± 6.25
Mt. Goddard	-0.63 ± 0.14	-0.88 ± 0.14	-0.90 ± 0.63	-0.26 ± 0.11	-0.48 ± 0.14
Mt. Mendel	-1.67 ± 1.06	-2.24 ± 1.62	-2.05 ± 1.13	-0.06 ± 0.44	-3.65 ± 2.28
Mt. Mills	-1.58 ± 2.59	-1.54 ± 0.80	-1.80 ± 0.40	-2.87 ± 1.43	-2.43 ± 0.84
Mt. Powell	-1.95 ± 0.63	-2.43 ± 1.29	-2.94 ± 2.88	0.19 ± 0.47	-2.94 ± 1.69
Mt. Ritter	-3.21 ± 1.37	-5.33 ± 3.92	-3.43 ± 3.84	-3.77 ± 4.35	-1.07 ± 0.65
Mt. Warlow	-1.43 ± 0.78	-1.96 ± 0.66	-2.16 ± 1.56	-0.49 ± 0.36	-2.11 ± 1.49
Parker Creek	-1.18 ± 0.21	-1.42 ± 0.66	-2.41 ± 1.42	-1.14 ± 0.35	-0.67 ± 0.33
Scylla	-1.71 ± 0.81	-2.57 ± 1.83	-2.87 ± 2.42	-0.81 ± 0.40	-2.85 ± 2.29
Keyhole	-0.77 ± 0.65	-1.40 ± 0.34	-1.66 ± 1.40	0.02 ± 0.29	-1.24 ± 0.47

Almost all glaciers showed perennial snow mass decline except Conness glacier (between 2000 and 2012), Mt. Gilbert (2010), Mt. Ritter (2008), Goethe (2008) glaciers (Table 3.4). Conversely, the lowest snow mass loss was observed between the year 2000 and 2015 in Mt. Dana and Mt. Gabb with the snow mass loss of -0.11±0.72 megaton and -0.27±4.29 megaton respectively. Whereas snow masses in the Conness (between 2000 and 2012), Charybdis (2012), Keyhole (2012), and Mt. Powell glaciers (2012) demonstrated recovery (Table 3.4).

Table 3.5 Snow mass anomalies in named glaciers of Mt. Shasta. Base year: 2000

	Snow mass anomalies (megaton)			
	2003	2008	2011	2015
Mt. Shasta	-35.29 ± 38.15	-79.61 ± 68.19	-140.33 ± 111.18	-96.85 ± 67.35
Bolam	-12.23 ± 10.95	2.16 ± 7.56	-9.01 ± 5.34	-7.64 ± 2.86
Hotlum	-15.82 ± 10.45	-25.77 ± 20.50	-46.58 ± 34.28	-32.92 ± 21.68
Konwakiton	2.16 ± 2.66	-2.89 ± 1.03	-9.73 ± 7.60	-4.23 ± 2.09
Watkins	0.38 ± 0.53	-2.12 ± 1.32	-2.69 ± 2.22	-1.78 ± 1.31
Whitney	-8.61 ± 7.63	-1.99 ± 6.24	-10.70 ± 9.04	-5.31 ± 9.38
Wintum	-0.31 ± 4.56	-35.75 ± 22.48	-44.30 ± 37.54	-33.67 ± 21.74

Mass anomalies quantified by using reference inventory area, elevation difference and using density scenario of 750 kg m^{-3}

Table 3.5 provides a list of glaciers with snow mass anomalies in the Mt. Shasta. Over the study period, in the Hotlum Glacier in Mt. Shasta, the maximum negative snow mass of -46.58±34.28 megaton (between 2000 and 2011) (Table 3.5) was noticed. While the minimum mass loss of -1.78±1.31 megaton was noticed in Watkins Glacier (between 2000 and 2015). It is important to observe that all glaciers in Mt. Shasta displayed snow mass decline, but Hotlum and Wintum glaciers lost snow mass severely. Conversely, snow mass loss was lowest in Konwakiton and Watkins glaciers, throughout the period (Table 3.5).

3.6.3 Climate data analysis

The climate data analysis for the Mt. Shasta and the Sierra Nevada region (Figure 3.7 and Figure 3.8) shows fluctuations in temperature and snowfall throughout the period. But it is important to notice the positive trend in temperature anomalies. It demonstrates that

there is an overall increase in temperature for dry as well as wet months in the region. Also, a noticeable steady increase in temperature can be seen in the wet season after 2011 till 2015 throughout the year (Figure 3.7).

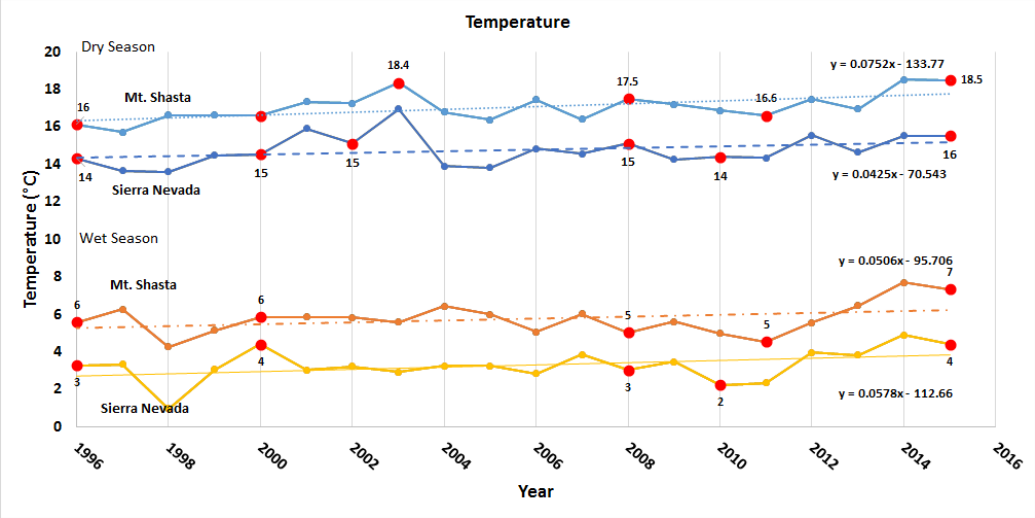

Figure 3.7 Average monthly mean temperature from 1996 through 2015 during dry and wet seasons.

The figure represents linear trend fitted through average temperature (°C) for the Mt. Shasta and Sierra Nevada region. Highlighted symbol represents study data period.

Here I present results of average monthly summaries of climate data based on the regions and seasons. I considered NOAA weather stations within 10-mile radius of the glaciers. I analyzed region-wise anomalies in temperature for the dry and wet seasons between 1996 and 2015. Both the regions show a similar pattern but in the dry season, Mt. Shasta region warmed at a rate of 0.08 °C and the Sierra Nevada region warmed by 0.04°C (Figure 3.7). Similar to the Dry season, Wet season showed the similar trends. While Mt. Shasta region warmed at the rate of 0.05 °C, Sierra Nevada exhibited a rate of 0.06 °C (Figure 3.7). It is important to notice that warming rate is slightly higher in the

Mt. Shasta region (around 0.01 °C) for the dry and wet seasons. In the dry season for the years 2003, 2014, and 2015, both the regions had above average temperature (about 16-18 °C). While, below average temperature noticed in the years 2004, 2005, 2010 and 2011 in the dry season, during the wet seasons, highest warming was observed for the year 2014 (about 5-7 °C) whereas, the lowest temperature was noted in the years 1998, 2010 and 2011.

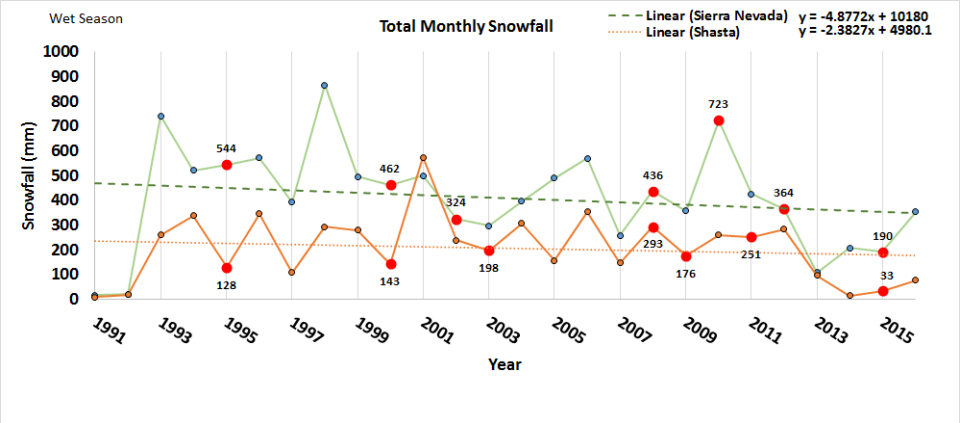

Figure 3.8 Average monthly mean snowfall from 1991 through 2015 during the wet season.

The figure represents linear trend fitted through average snowfall (mm) for the Mt. Shasta and Sierra Nevada region. Highlighted symbol represents study data period.

On the other hand, snowfall fluctuated significantly but the snowfall trend was negative between 1991 and 2016 (Figure 3.8). Because snow deposits in the winter, I considered only wet season for the analysis. A negative rate of -2.4 mm and -4.9 mm observed in the Mt. Shasta and the Sierra Nevada region (Figure 3.8). It is important to notice that decline in snowfall is slightly higher in the Sierra Nevada region (around -4.9 mm). In the Mt. Shasta region more than average snowfall observed for the years 1994, 1996, 2001, 2004, and 2006 (about 300 mm). While in the Sierra Nevada region, more than average

snowfall observed for 1993, 1998, and 2010 (about 700 mm) (Figure 3.8). Conversely, lowest snowfall is recorded for the year 2013, 2014 and 2015 in both the regions (Figure 3.8).

3.7 Conclusions

The objective of this study was to estimate the extent and mass anomalies in the snow-covered regions using ASTER elevation models and Landsat multispectral scenes in the Mt. Shasta and Sierra Nevada region. The anomalies in snow cover extent and mass were quantified for individual glaciers and watersheds in the region. For this study, I identified best available ASTER DEMs that overlaid on the snow-covered areas of the California. I compared elevation of snow covered regions from reference ASTER DEMs (the year 2000) with ASTER DEMs (from 2002-2015). In all regions, the elevation values were lower than the 2000 year's ASTER elevation values. Snow mass anomalies were always negative as compared to the reference year. After comparing glacier boundaries and mass, it is evident that there is a substantial loss in snow cover area as well snow mass. The research outcomes clearly indicate that snow mass never recovered after heavy snowfall event of 1998. I noticed that recession in the region is mainly a result of reduced snowfall than increased temperature similar to the findings of Costa-Cabral et al. (2012). I also encountered contrasting patterns of years with snow mass loss and events of snow surge at the individual glacier level. Additionally, I noticed that the snow mass depletion in the Sierra Nevada region is higher as compared to the Mt. Shasta region. The study results of the snow cover analysis are similar to the finding of Howat et al. (2007) where they noticed advances to no change on the glaciers of Mt. Shasta. These results also can be compared to the observations of McCabe and Fountain (2013)where they noticed

spatiotemporal variation between 1900-2000 on some of the glaciers of Sierra Nevada. The other possible reason for higher recession rate in the Sierra Nevada might be the result of increased temperature in the wet season as compared to dry months. It is evident that slight fluctuation in the snowfall and temperature impacts the state of snow masses in the region. For instance for the year 2010, most of the snow cover in the Sierra Nevada hydrologic regions recovered the extent that might be the result of below average temperatures in both dry (about 15 °C) and wet (about 3.5 °C) seasons. Also in the same year, the region received above average snowfall (about 700 mm).

The study results found aligned with the observations by most of the climate studies in the region (Ashfaq et al., 2013; MacDonald, 2007; Maurer et al., 2007; Stine, 1994; Swain et al., 2014) and showed that negative mass balance in the region might be the direct result of fluctuations in snowfall and temperature. The increase in temperature and decrease in snowfall in 2013-2014 (Figure 3.7) (Figure 3.8) were the main cause of 2014 drought like conditions (Griffin and Anchukaitis, 2014; Swain et al., 2014) in California that resulted in a massive snow cover loss of about 87%.

It is important to study microclimatic conditions for the individual glaciers as well as regions. I noticed varied snow mass anomalies in two adjacent glaciers of Black Giant and Black Giant E. in Sierra Nevada. The difference in microclimatic conditions of these glaciers have resulted in these differences. Not all the glaciers lost mass, for example, Kern River watershed had positive snow mass of 13.63±28.18 megaton in the year 2008 (Table 3.3) (Figure 3.6). It may attributed to high snowfall in the alternate years between 2006 and 2008 (Figure 3.8), and steady temperature in the dry season, and low temperature in the wet season for the years 2007 and 2008(Figure 3.7). But during the

same period, snow mass in the other river watersheds continued to regress. So, it is important to find the particular effect of climatic and topographic parameters on the snow masses in the region. Additionally, there might be other factors such as the traces of aerosol (black carbon), dust, red algae, topography etc. in snow that may be impacting the magnitude of ablation (Hadley et al., 2010; Kessler et al., 2006; Kirchstetter et al., 2008; Painter et al., 2001; Rice et al., 2011; Sterle et al., 2013). More work is required to understand the role of different climatic factors as well ENSO (Howat et al., 2007) effects because of the importance of these freshwater reservoirs.

CHAPTER IV

EFFECTS OF SNOW MASS ANOMALIES ON THE TOTAL WATER STORAGE AND AGRICULTURAL YIELD IN THE CALIFORNIA'S CENTRAL VALLEY BETWEEN 2003 AND 2015

4.1 Abstract

The aim of this chapter was to observe impacts of climate forcing on the total water storage and agriculture land cover in the California's Central Valley. I classified Landsat images for the individual year 2003 and 2015 using hybrid classification technique. Besides, I quantified total water storage (TWS) in the region using Gravity Recovery Research and Experiment (GRACE) data signals. Lastly, regressed and correlated Normalized Difference Vegetation Index (NDVI), TWS and temperature to unearth an interdependence between the variables.

The study observed the change in the land cover area of about 20% (6993 sq.km) due to the alteration of Agriculture land covers to impervious or non-moist (barren) lands. I noticed that out of this change most of the alteration in the agriculture land cover of about 4403 sq.km occurred in the San Joaquin and Tulare Basins of southern Central Valley region. I also observed that the Sacramento and Delta basins in the Central Valley region shared the same rate of water depletion of -0.26±0.25 (equivalent water height cm) between 2003 and 2015. While in the southern half of the Central Valley, San Joaquin experienced slightly higher water depletion rate of -0.49±0.27 (equivalent water height cm) than Tulare (-0.48±0.26 equivalent water height cm). It is important to notice that total water storage depletion rate was found to be almost double in the southern half (San Joaquin, Tulare) than the northern half of the Central Valley. Moreover, study reports

decrease in crop yield with an increase in anomalies in TWS in the Central Valley region. Whereas I suspect that increased temperature was the reason behind increasing crop water demand in the area. In essence, the research concludes that the depleting water resource and changing agriculture land cover was the result of increased temperature in the past decade.

The high depletion rates of total water storages than its recharge suggests possible severe future impacts on the Californian Agricultural production. Considering current water crises in California this study provides valuable insights into the potential role of total water storage anomalies on the billion-dollar agricultural and dairy industries in the central valley.

4.2 Introduction

California is the major agricultural producer in the United States. California's Central Valley not only adds $40 billion to the US economy but also grows country's half of the fruits and vegetables. Additionally, it supports $3 billion dairy industry and employs more than million people (Schlenker et al., 2007). With high crop diversity, central valley produces over 250 different commodities, which makes California fifth largest supplier of food and in other agricultural products (L. Jackson et al., 2011a). Central Valley has been one of the most productive regions in the world due to its fertile soil and ample availability of water for irrigation (Reilly et al., 2008). The rich agricultural production in the region has been made possible through ample water supply through engineered irrigation infrastructures as the federal Central Valley Project (CVP), All-American Canal, and the State Water Project (SWP) (Cooley et al., 2009).

Ground water has strategic importance as the world's largest scattered store of fresh water for agriculture use and sustaining ecosystems (Gleeson et al., 2012; Taylor et al., 2013). But increasing population, changing land use, urban sprawl and economic development are key drivers of an increasing demand for water worldwide. Thus, mounting water stress in several parts of the world. Due to Mediterranean climatic conditions, California gets most of its precipitation in the form of snow. Snow amasses in the mountains and serves as freshwater reserves for the California state in the summer. But findings of Chapter III showed the anomalies with an incremental loss in snow mass in the California in the last decade. Therefore, it is viable to study dependence between NDVI and TWS which represents surface and ground water.

4.2.1 Water depletion in the Central Valley

Groundwater stored in aquifers beneath the soil and porous rock accounts for 33% of total water withdrawals globally. Groundwater is being extracted at far greater rates than it replenished and will very likely accelerate mid-latitude drying (Famiglietti, 2014). Many areas in the world are facing groundwater depletion because of overexploitation of ground water resources than its recharge (Wada et al., 2010). Konikow (2011) calculated water depletion using calibrated groundwater models, analytical approaches or volumetric budget for multiple aquifer systems. The study (Konikow, 2011) estimated global groundwater depletion during 1900, and 2008 of around 4500 km^3, equivalent to sea level rise of 12.6 mm with maximum loss rates occurred between 2000 and 2008. Groundwater depletion in the irrigated high planes and central valley accounts for half of groundwater depletion in the United States since 1900 and continues totaling 80 km^3 even after engineered irrigation infrastructures Scanlon et al. (2012b). Excessive utilization of

groundwater could significantly affect agriculture production because more than 50% of irrigation relies on aquifers. Scanlon et al. (2012a) also observed a high rate of water loss in the South (Tulare Basin) and primarily during droughts. The overexploitation of groundwater plays a direct role in land subsidence by causing gentle down warping and the sudden sinking of discrete segments of the ground surface (Galloway and Burbey, 2011). The USGS groundwater availability study report for the period 1962-2003 pointed the over extraction of ground water in the central valley region leading to land subsidence in the San Joaquin (Reilly et al., 2008).

Analysis of groundwater depletion in the Central Valley region by Scanlon et al. (2012b) using Gravity Recovery and Climate Experiment (GRACE) satellite showed reduction totaled about 31.0 ± 3.0 km^3 from October 2006 through March 2010. Similar analysis using GRACE data by Famiglietti et al. (2011) shows that Central Valley had lost 20.4 ± 3.9 mm yr^{-1} of ground water during the 78-month period between October 2003 and March 2010. They claimed that groundwater loss at this might would damage the economy and food security of the United States. Actual agricultural water use remains largely unknown, but ground water exploitation during drought will slowly exhaust groundwater storages at a higher cost (Howitt et al., 2014).

4.2.2 Effects of climate change on the Central Valley agriculture

Many reports foresaw possible impacts of climate change on the agriculture in the California's Central Valley. If global warming continues unchecked, anomalies in precipitation and continuously increasing temperatures will severely affect the agricultural industry. A recent study by Cayan et al. (2009) projected increase in temperature by 1°C -2°C through 2050. While Christy et al. (2006) carried out time series

analysis of temperatures in irrigated San Joaquin Valley and nearby non-irrigated Sierra Nevada region between 1910 and 2003. Their findings suggest minimum valley temperatures are warming at a highly significant rate, on the other hand, minimum temperatures in Sierra Nevada Mountains cooling with the less significant rate. Another study by Ladochy et al. (2007) on the air temperature patterns in California from 1950 to 2000, noted that urbanization showed the largest positive trends while rural, non-agricultural regions showed the least warming. However, the study also observed a pattern of warming with highest rates of warming in the Southern California and minimum warming in northeastern basins. Ladochy et al. (2007) recounted positive correlation between Pacific sea surface temperatures, Pacific Decadal Oscillation (PDO) values, also account for temperature variability throughout the state.

Most of the agriculture based literature claims that plant growth is directly dependent on temperature only within a certain range (Schlenker et al., 2007). Climate warming suspected to disturb this balance between crop water demand and its supply. In California's Central Valley, continuously increasing temperatures likely to intensify crop water demand, while supply will become less consistent due to depleting and early melting snowpack in the mountains. Lo and Famiglietti (2013) demonstrated the effects of the resulting increase in evapotranspiration and water vapor distribution, not only will significantly impact the atmospheric circulation in the southwestern United States but also strengthens regional hydrological cycle. A similar study also identified that irrigation in the central valley begins anthropogenic loop in the regional hydrological cycle (L. Jackson et al., 2011b).

Climate forcing and the effects of greenhouse gas emissions are complex and likely to be severe in the dry season than winter, with depletion of precipitation (L. Jackson et al., 2011b) investigated climate change effects on the irrigation water supply in the Central Valley and found that irrigation demand will increase by 26% and 32% under B1 and A2 baseline climate scenarios. Jackson et al., (2011b) extensively reviewed the possible positive and negative effects of climate forcing on the agricultural products. The findings show that continuously increasing temperatures will adversely affect the yields of tomato, rice, and fruits like grapes but might result in better production of citrus fruits and drought tolerant olives in the region (Jackson et al., 2011b). Similarly, the statistical analysis of 22 climate models and IPSS global emission scenarios (A1, A2, and B1), Lobell et al. (2006) reported that slight increase of 1˚C would moderate yields such as almonds, walnut and table grapes by 2050. In California, Lee et al. (2011) analyzed effects of climate forcing on agricultural production in the 21st century. Using emission scenarios (A2 and B1), climatic models and by eleven year moving averages for the period, 1956 to 2094, (Lee et al., 2011) and predicted 2 % to 9 % decrease in wheat, Cotton, Sunflower by 2050 compared to 2009. Lee et al. (2011) also concluded that climate forcing would decrease crop production in the Central Valley in the long term except for alfalfa crop breed. Agricultural crop production is fully expected to be impacted by water depletion in the region (Lee et al., 2011). Further analysis of the climate change impacts and potential adaptations strategies were assessed by Joyce et al. (2011) using an application Water Evaluation and Planning (WEAP) system in the Central Valley region. Results of the study by Joyce et al. (2011) suggested an increasing agricultural demand in the Sacramento and San Joaquin may amplify stress on the

management of water resources, and warm climate might impose additional $400 million/year as an operating cost.

California's Central Valley is one of the highly productive agronomic regions in the world. In this chapter, I analyzed effects of snow mass anomalies on the agriculture in the Central Valley using remote sensing and GIS technique. Where, I analyzed gravity models generated using GRACE data set to determine variation in not only ground water but total water storage in the region. Also, using supervised and unsupervised learning, I classified Landsat multispectral dataset and quantified changes in agriculture land cover by comparing hybrid classified images between 2003 and 2015. Lastly, I correlated and regressed total water storage (TWS), and Normalized Difference Vegetation Index (NDVI), temperature. This study provides valuable insights on the effects of Snowmass anomalies on the ground water recharge and indirectly on the agricultural yield.

4.3 Study Area

California's Central Valley marks the geographical center of the California state (Fig 4.1). The Central Valley is a large, low altitude valley with Mediterranean climatic conditions. The Central Valley extends about 720 km along a north-south axis with the breadth of 60-90 km and covers approximately 46,620 sq.km area (Reilly et al., 2008).

The Central Valley is subdivided into northern one-third Sacramento Valley and southern two third as San Joaquin Valley (Reilly et al., 2008). The climate of the Central Valley allows long growing season with hot summers and moderate winters. Sacramento Valley gets about ten inches more average annual precipitation than San Joaquin basin (Reilly et al., 2008). The Central Valley basin can be further subdivided into four sub-regions: Sacramento, Delta, San Joaquin, and Tulare. The southern part of the San

Joaquin Valley, the semiarid region is known as the Tulare Basin. Whereas Delta is the region where the Sacramento and San Joaquin Rivers meet, and discharge in the Pacific Ocean (Fig 4.1) (Reilly et al., 2008).

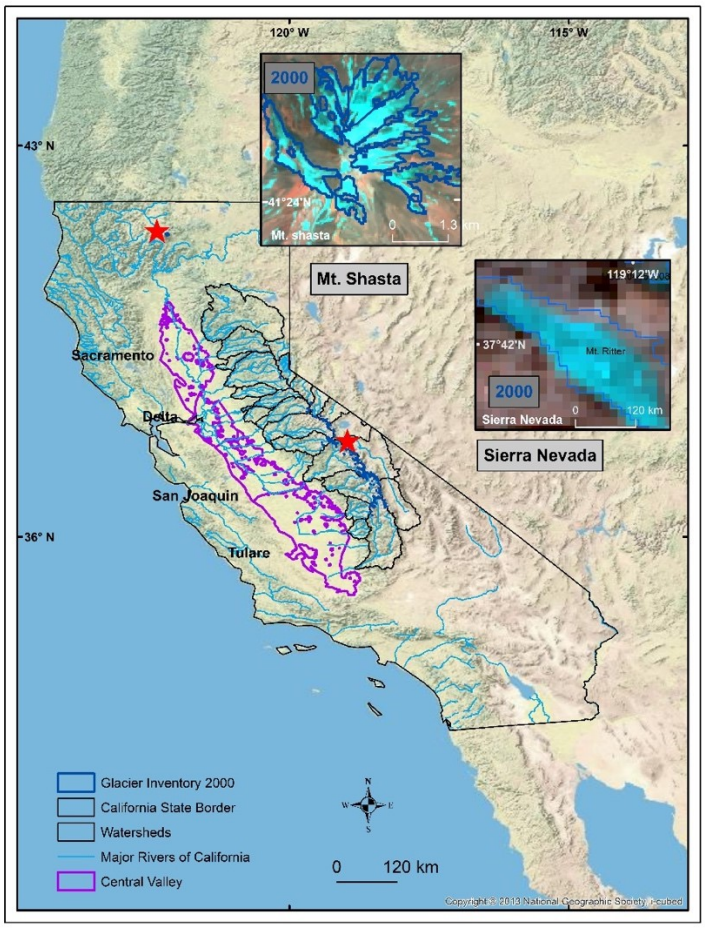

Figure 4.1 Illustration of the study area in California

4.4 Data used

Landsat TM and L8 scenes for years 2003 and 2015 were acquired with the minimal cloud cover and with acquisition dates in the month of July covering California's Central Valley. These multispectral Landsat images were used to classify land covers and to perform change detection analysis.

All overlapping signals of Gravity Recovery & Climate Experiment (GRACE[5]) monthly land mass grid dataset used to analyze total water storage (TWS). Where all available gravity anomalies data footprints based on the RL-05 spherical harmonics were acquired from GFZ for the years between 2003 and 2015. This preprocessed data was obtained in the raster format with 300 km Gaussian filter and spatially sampled for grids approximately ~100 km.

In addition, to understand and quantify crop pattern and yield I acquired preprocessed Normalized Difference Vegetation Index (NDVI) data generated using Moderate Resolution Spectroradiometer (MODIS) from Earth Explored (USGS). Monthly 7-10-day composite 250 m NDVI data over the agricultural land cover for the period between 2003 and 2015 was used.

Lastly, monthly summaries of mean temperature degree Celsius (2003-2015) data for one hundred and thirty-six stations in California's Central Valley was obtained from the United States National Climate Data Center (NCDC). Temperature data was used for statistical analysis and analyzed based on sub-regions.

4.5 Methods

The methodology used for the analysis includes GIS and remote sensing techniques. Firstly, multispectral scenes were classified into different land covers using iterative combinations of supervised and unsupervised learnings. Further based on the two major subregions: Sacramento and San Joaquin change detection analysis was carried out between two-year 2003 and 2015. As per the objective of the study, priority was given to

[5] S.C. Swenson. 2012. GRACE monthly land water mass grids NETCDF RELEASE 5.0. Ver. 5.0. PO.DAAC, CA, USA. Dataset accessed [2016-05-01] at http://dx.doi.org/10.5067/TELND-NC005.

the Agriculture land cover and its associated land (AL, AS). Later additional variables like Total water storage and NDVI were used to understand effects of changes in water levels on the crop yield in the region. Following sections describes in detailed methods of hybrid classification, change detection and statistical analysis.

4.5.1 Hybrid classification

Hybrid classification is an iterative combination of supervised and unsupervised classification learnings (Singh et al., 2013). Landsat scenes with a minimal cloud cover of July month for the year 2003 and 2015 were selected. This specific month was selected because it marks the pick of the growing season and end of the hydrological year. Hybrid classification takes the advantages of both supervised and unsupervised learnings. This classification technique provides an object oriented control over the dataset (Singh et al., 2013). In the classification priority was given to agriculture, and related land covers such as moist soil. Therefore, before classifying images, urban and mountainous barren terrain were digitized and masked out from the multispectral images.

In the first step of hybrid image classification, unadulterated pixels were mapped out. Then image scenes were classified using the unsupervised classification technique, which identified and clustered pixels with similar spectral signatures. During the first attempt of unsupervised classification, unique spectral signatures were placed into 150 ISODATA clusters. These unique spectral clusters were assigned labels as “Agriculture (A)”, “Agriculture Soil (AS),” “Agriculture low (AL),” “Water (W),” “Barren Land (BL),” “Urban (U).” It is important to note that Agriculture Soil and Agriculture low are two additional classes included especially to improve the accuracy of agricultural land cover

classification. These two classes were identified based on the uniqueness of spectral signatures, their association, and shape of the field. Agricultural soil represents fertile land with human-made shape and moisture content. While Agricultural low defines low crop cover on fertile soil marking intermediate phase in the crop growing cycle. Later these different land covers were quantified to understand changes in the crop pattern.

In the second step of classification, the cluster belonging to respective classes with the highest accuracy were selected and removed from the main image. This process was iterated, where classified images were recoded to a binary image ('0' was assigned to the accurately classified clusters and '1' assigned to 'non-classified' cluster) (Singh et al., 2013). In the third step, a masked image obtained in the second step was again classified using the unsupervised technique. This time unclassified clusters were placed into 50 ISODATA clusters.

After the thrid step, unclassified pixels or the pixels with the mixed signatures were classified using supervised learning (maximum likelihood classifier), where training set was selected based on the visual interpretation, an association of pixels and shape of the agriculture land cover. The three images obtained through two unsupervised, and one supervised classification were then overlaid, and the final classified images for 2003 and 2015 were generated.

An independent sample sixty pixels (10 per each class) were randomly selected on the google earth and compared to check the image classification accuracy. Kappa statistic was generated (Congalton and Green, 2008) and found the accuracy of over 90% for the agricultural land cover.

Following the classification of imagery from the individual years 2003 and 2015. Recoded classified images were subtracted from each other to detect changes in the region. The post-subtraction approach provides "from–to" change information, and new values tell the landscape transformation patterns that have occurred. These changes in Agriculture Land cover were later quantified and visualized. Lastly, a change detection map based on the two major sub-regions were generated.

4.5.2 GRACE data analysis

Total water storage was derived from the Gravity Recovery & Climate Experiment (GRACE) monthly land mass grid dataset. First attenuations in GRACE signals due to sampling was corrected by grid scaling as recommended by the data providers. The provided scaling coefficients were used for each overlying grid cell, and the product was calculated. For the analysis, missing month's values in the data sets were filled with averaging bounded months. In total twelve grid cells, completely and partially overlying central valley region was considered for the analysis. Further, these selected Grid cells were classified based on the four sub-regions in the Central Valley. Uncertainties and errors associated with each GRACE footprint were calculated using leakage error and measurement error values supplemented by the data providers. Uncertainty associated with the scaled and processed GRACE signal footprint was computed as the root of the sum of squares of leakage (residual error) and measurement error. Lastly these monthly total water storage values in meter water equivalent used for the regression analysis. Statistical analysis was conducted to find a relationship between the variables such as total water storage, Normalized Difference Vegetation Index, and Temperature. The intention of the statistical analysis was to unearth effects of anomalies in total water

storage, and temperature on the agricultural yield in the four hydrological basins of California's Central Valley. Dry season months May, June, July, August, September, October, November between 2003 and 2015 were considered for the analysis. Monthly mean values were selected for the regression analysis. Where NDVI was used as the dependent variable and Temperature, TWS were used as the independent variables. The results of linear regression were generated for the four sub-regions: Sacramento, San Joaquin, Delta, and Tulare hydrological basins.

4.6 Results and Discussion

The results of statistical and change detection analysis demonstrate adverse effects of anomalies in snow mass and climate on the agricultural land cover and total water storage in the region. The results are organized and discussed here for change detection analysis, total water storage (TWS) and statistical analysis of different factors such as TWS, Temperature, and NDVI.

4.6.1 Change detection analysis

Figure 4.2 represents hybrid classified images for the individual years 2003 and 2015. It is important to note that results presented here are based on the area after exclusion of major urban centers, mountainous terrain and some of the wetland. I analyzed six land classes approximately covering 35483 sq.km of California's Central Valley.

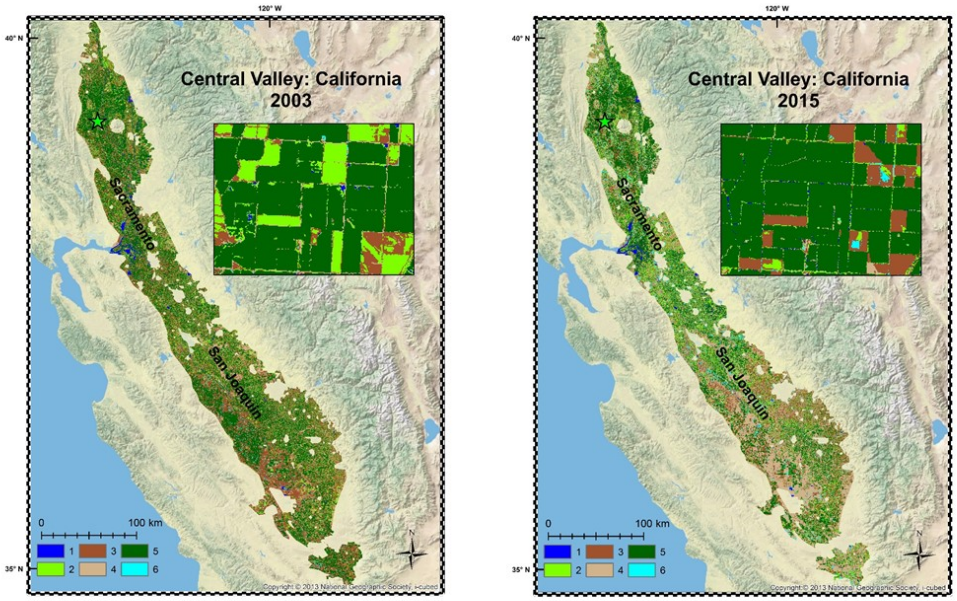

Figure 4.2 Hybrid classified images for the year 2003 and 2015

Image is classified into six land cover classes: 1-Water, 2-Agriculture Low, 3-Agriculture Soil, 4Barren Land, 5-Agriculture, 6-Urban

In 2003 agricultural (A) and associated land covers i.e. agricultural Low (AL) and Agricultural Soil (AS) together covered 82.7% of the land cover area in the Central Valley 4.3. While in 2015, combined A, AL and AS land cover area found reduced to 62.5%. I observed that the change in the land cover area of around 20% occurred due to the shift of Agriculture and associated land covers to impervious or non-moist barren lands. This 20% alteration accounts for approximately 6993 sq.km. Out of these most of the alteration in the agriculture land cover of about 4400 sq.km occurred in the San Joaquin and Tulare Basins of southern Central Valley region.

The study also observed around 3% increase in the urban area. I suspect this increase of around 1036 sq.km in the urban area was due to the increased infrastructures on or near

the agricultural field other than urban centers. While the area of non-moisture or barren land cover increased in the Central Valley by about 17% that accounts for around 5957 sq.km land cover. Out of this 5957 sq.km barren land about 84% of the barren land, around 4662 sq.km, endowed by the southern San Joaquin region. Moreover, about 35% of the Agriculture and associated land covers (AL, AS) interchanged between each other. For example, A to Al, Al to A, A to AS, AS to A and so on. I suspect this was because imageries used for classification represent an instance in the crop growth cycle. Therefore, this transition between A, Al and AS was not given too much significance as it's a natural phenomenon. Other than that, analysis observed about 30% of the land cover area remain unchanged which accounts approximately 10619 sq.km of land.

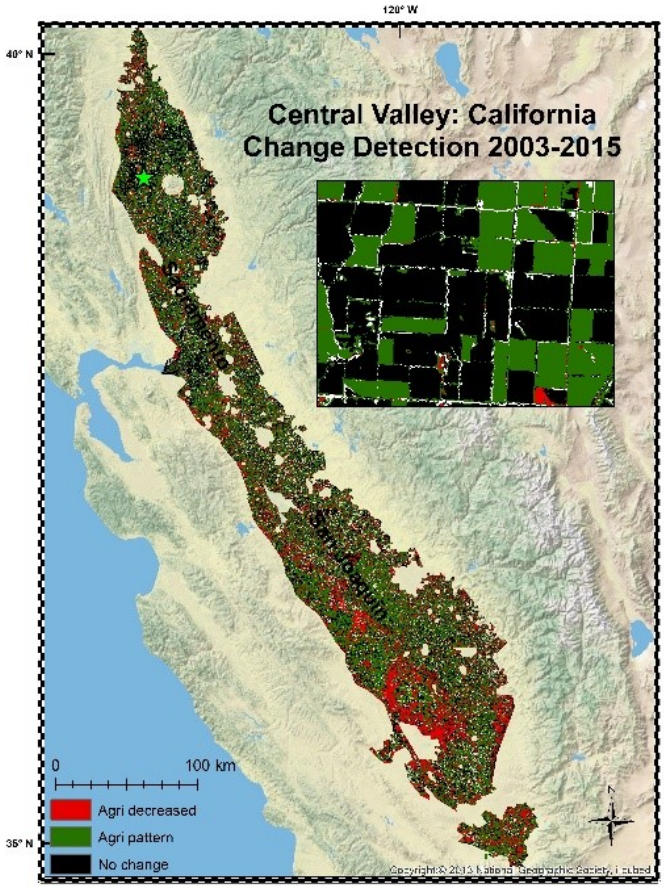

Figure 4.3 Illustration of change detection analysis:2003-2015

Figure 4.3 demonstrates the regions in California's Central Valley with decreased agriculture, agriculture pattern (A, AL, AS), No change

4.6.2 Total Water Storage (TWS)

This study made use of Gravity Recovery and Climate Experiment (GRACE) to examine total water storage change in the Central Valley, California. The results demonstrate an uninterrupted decrease of total water equivalent in the region. Total water storage which is an amalgamation of snowmelt, groundwater, surface water, precipitation, evaporation

does follow a cyclic pattern of recharge (Wet season) and discharge (Dry season) in most of the years except years following 2011 (Figure 4.4). The GRACE results of diminishing water equivalent height can be coupled with findings of snow mass anomalies in the Sierra Nevada (Chapter III). I noticed the relation between receding perineal snow mass in the Sierra Nevada region and the declining water content of the central valley aquifers with the maximum change in drought period year 2014. Effects of receding source of fresh water reserve, snow packs in the Sierra Nevada, shows clear impacts on the total water storage in the region. This incremental depletion in the snow mass and anomalies in total water storages suggest possible severe future impacts on the Californian Agricultural industry.

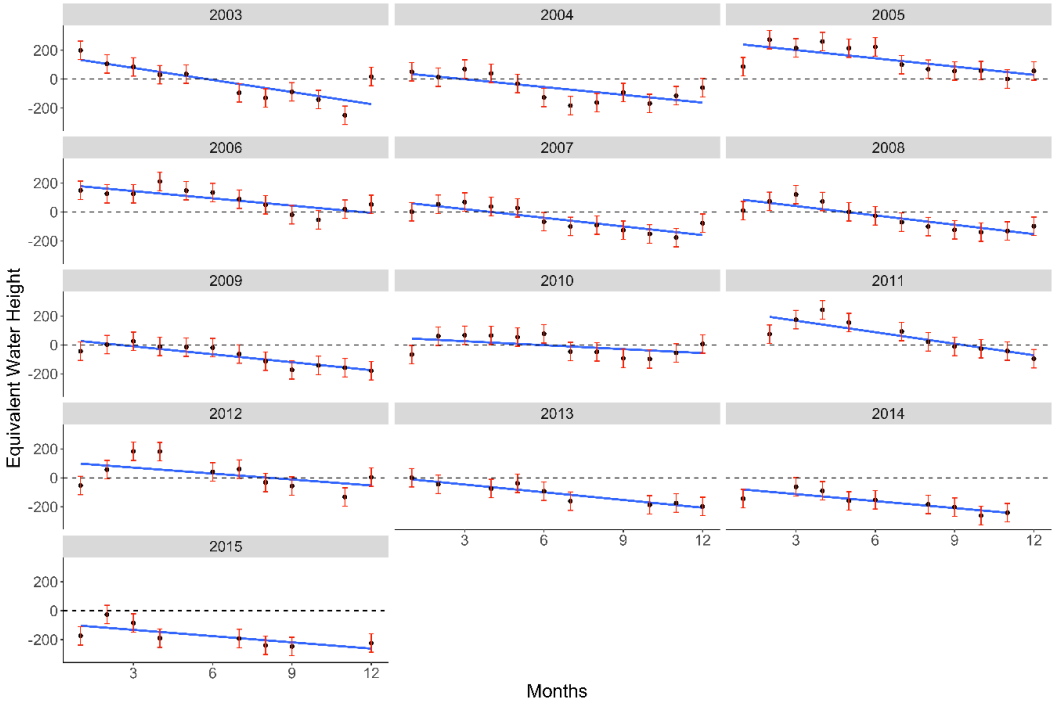

Figure 4.4 GRACE data anomalies (equivalent water height) monthly and annually

Figure 4.4 represents available GRACE data (equivalent water height (cm)) for the California's Central Valley. First part represents month wise data available between 2003 and 2015.

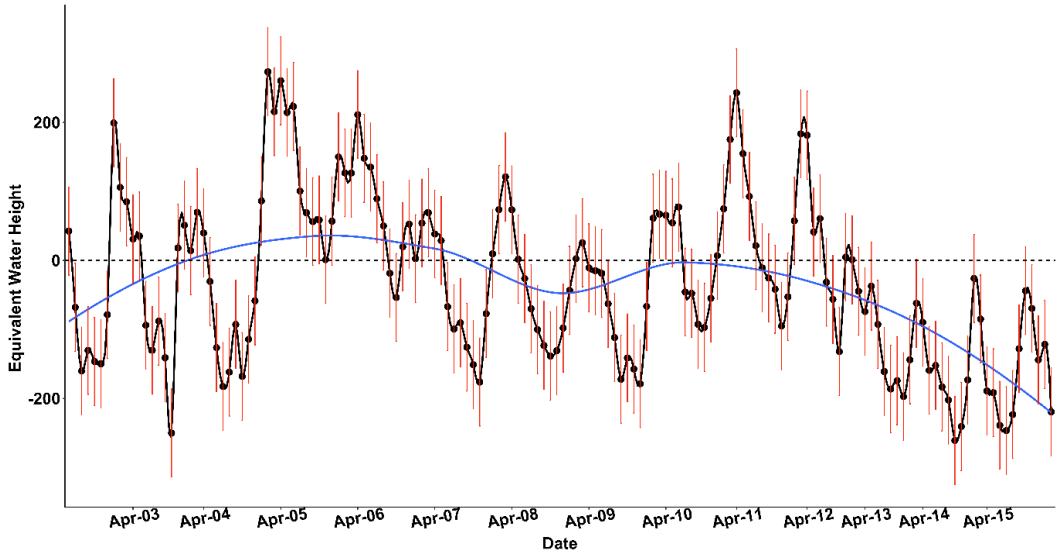

Figure 4.4 (continued)

Figure 4.4 Second part represents polynomial trend fitted over all available data between 2003 and 2015.

Here I contrasted total water storage anomalies in the central valley with the snow thickness change in the Sierra Nevada reported by (Chapter III). Figure 4.5 shows mean dry season total water storage anomalies in equivalent water height (cm) between 2003 and 2015 (blue line). While histogram displays snow thickness in meters at the end of the hydrological year reported for the years (2003, 2008, 2010, 2012, 2015) (Chapter III). Figure 4.5 shows direct effects of changing water reserves on the total water storage in the Central Valley region. Especially it is important to notice that, negative mass balance years 2003, 2012, and 2015 severely affected surface and ground water levels. Whereas

the good snowfall years 2008, 2010 helped recovering the water levels but not for a long time. As consecutive drought years around years, 2013 and 2014 worsened the conditions and the ground water levels reached to its lowest with almost 90% snowmelt in the region (figure 4.5) (Chapter III).

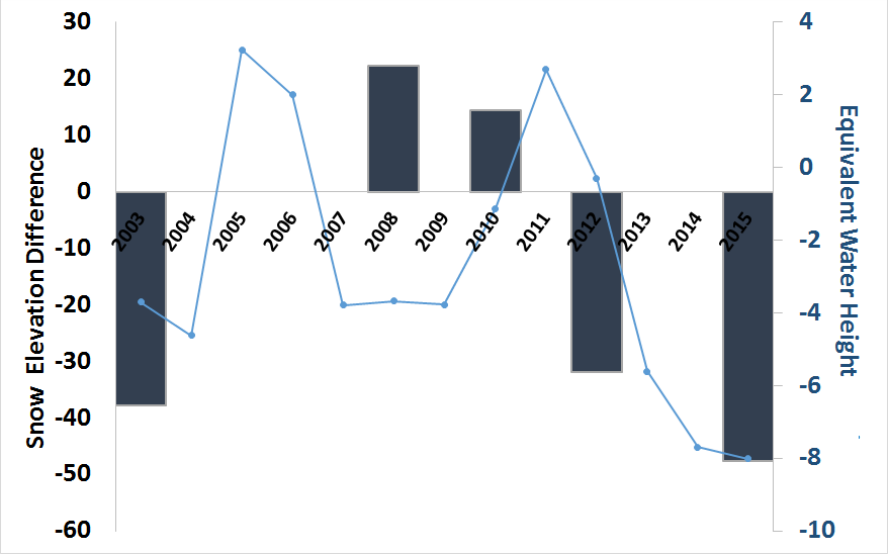

Figure 4.5 Association between snow mass anomalies in the snow elevation difference in the Sierra Nevada and total water storage in the Central Valley.

Figure 4.5 represents snow elevation difference in meters with base year 2000. Blue line represents Total Water Storage anomalies in equivalent water height (cm).

Furthermore, monthly graphical representation of total water storage change between 2003 and 2015 (Figure 4.6) demonstrates a bimodal pattern. The TWS change in the region demonstrates positive values for the years 2005 and 2011, because of high snowfall during the period. These positive water equivalent heights can be contrasted with the Chapter III findings of positive snow mass surge reported in the Sierra Nevada and Mt. Shasta for those years.

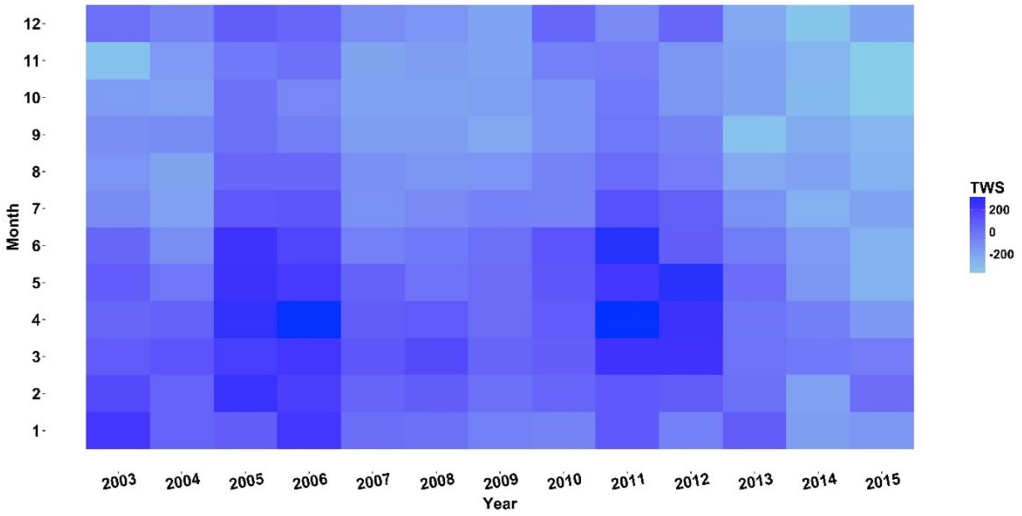

Figure 4.6 Monthly graphical representation of TWS between 2003 and 2015 in the California's Central Valley

4.6.3 Statistical Analysis

TWS, temperature and NDVI parameters were studied based on sub-region aquifers namely Sacramento, Delta, San Joaquin and Tulare to understand north-south geographical pattern between them. Specifically, dry months are taken into consideration to understand impacts of changes in TWS on the agricultural land cover.

The Linear trend is fitted through the mean dry season (May-Nov) TWS (water equivalent heights), Temperature (°C), NDVI though 2003 to 2015 for individual sub-region (Figure 4.7) (Table 4.1). All four sub-regions demonstrate changing agricultural pattern with depleting water levels.

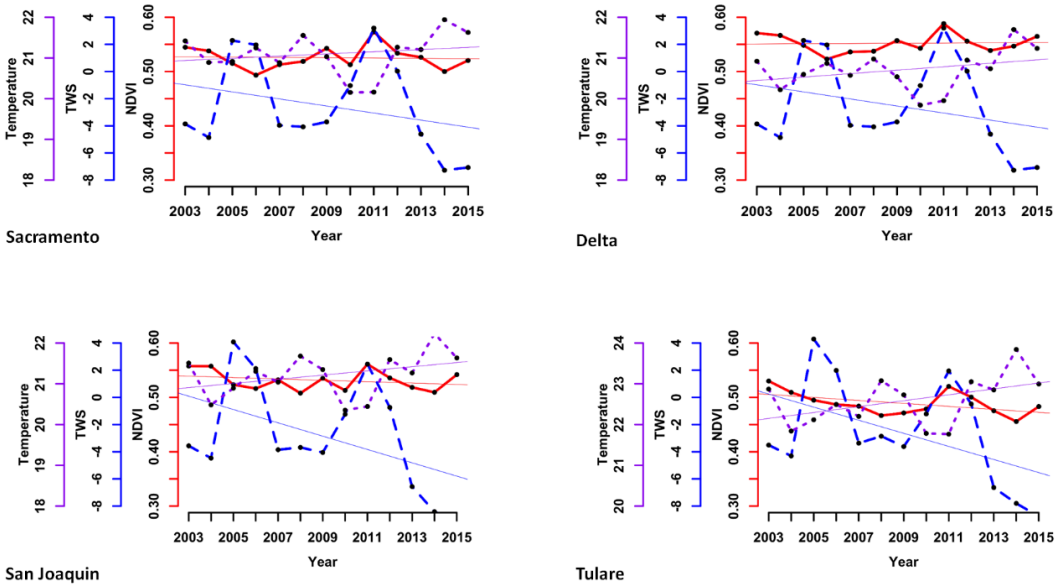

Figure 4.7 Linear trend fitted through Temperature, TWS, and NDVI through 2003 to 2015 for the four sub regions.

Note: Temperature is in (°C) and TWS (equivalent water height in cm)

Table 4.1 Rate of change for TWS and Temperature between 2003 and 2015

Regions	TWS (cm)	Temperature (°C)
Sacramento	-0.26±0.25	0.03±0.04
Delta	-0.26±0.25	0.04±0.03
San Joaquin	-0.49±0.27	0.05±0.04
Tulare	-0.48±0.26	0.07±0.04

Monthly graphical representation of temperature between 2003 and 2015 suggest a slight increase in the temperature with the early summer in the recent years (figure 4.8). Linear trend fitted through temperature showed a slight positive trend in all four sub-regions. However, I noticed geographical dissimilarity in the warming rate, as the Sacramento basin observed 0.03±0.04 (°C) while southern tip of the Central Valley observed warming rate of 0.07±0.04 (°C).

Figure 4.8 Monthly graphical representation of Temperature (°C) between 2003 and 2015 in the California's Central Valley

Four regions show depletion in the ground as well as surface water, with a major reduction in levels in the total water storages in the southern part of the Central Valley. Regression analysis demonstrates a negative trend in all sub-region aquifers.

I observed that Sacramento and Delta basins in the Central Valley region share the same rate of water depletion of -0.26±0.25 (equivalent water height cm) between 2003 and 2015. While in the southern half of the Central Valley, San Joaquin experienced slightly higher depletion rate of -0.49±0.27 (equivalent water height cm) than Tulare (-0.48±0.26 equivalent water height cm). It is important to notice that ground and surface water rate was found to be almost double in the southern half (San Joaquin, Tulare) than the northern half of the Central Valley (Figure 4.9).

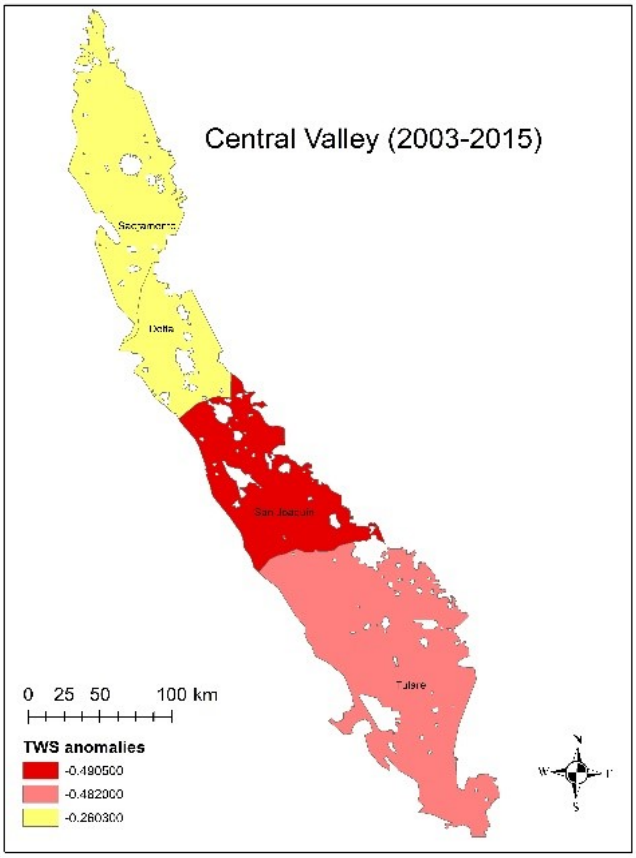

Figure 4.9 Sub-region wise Total water storage anomaly

The difference of crop yields between northern half (Sacramento) and a Southern half (San Joaquin) of the central valley was analyzed by visualizing the monthly distribution of vegetation index values for years between 2003 and 2015 (Figure 4.10). Figure 4.3 demonstrates change detection findings, which showed more agriculture area less barren land in the Sacramento as compared to the San Joaquin. Linear trend fitted through normalized vegetation index suggest a slight increase in the crop yield in the Sacramento region. While San Joaquin and Tulare region showed a constant decrease in crop yield.

To confirm assumptions of the impact of TWS change on the agricultural land cover, findings are regressed and correlated with the NDVI. Outcomes of least square regression support the assumptions and demonstrate significant positive relation (Table 4.2, 4.3) between decreasing NDVI and decreasing TWS in all four sub-regions. The positive coefficient suggests the decrease in crop yield with an increase in anomalies in TWS in the Central Valley region. While positive coefficient between NDVI and temperature suggest continuously increasing crop water demand. Furthermore, these results can be compared with the change detection analysis finding. Change detection analysis (Figure 4.3) findings demonstrate the decreased agricultural land cover in the San Joaquin. It is important to note that coefficients for NDVI (agriculture cover) and TWS (Table 4.3) are not significant primarily because of the size of the GRACE data unique footprint.

Table 4.2 Statistical analysis based on the sub regions in the Central Valley using NDVI, TWS and Temperature for the dry season months between 2003 and 2015

Model Summary

Region	R	R Square	Std. Error est.
Delta	0.68	0.47	0.04
Sacramento	0.83	0.69	0.06
San Joaquin	0.72	0.52	0.04
Tulare	0.81	0.66	0.07

Note: dependent Variable: NDVI

Table 4.3 Statistical analysis: Regression between TWS, NDVI and Temperature

Region	Variables	Coefficients	Sig.
	TWS	0.08	0.25
Delta	Temperature	**0.67**	0.00
	TWS	0.06	0.25
Sacramento	Temperature	**0.82**	0.00
	TWS	0.03	0.71
San Joaquin	Temperature	**0.72**	0.00
	TWS	0.20	0.00
Tulare	Temperature	**0.76**	0.00

Note: dependent Variable: NDVI

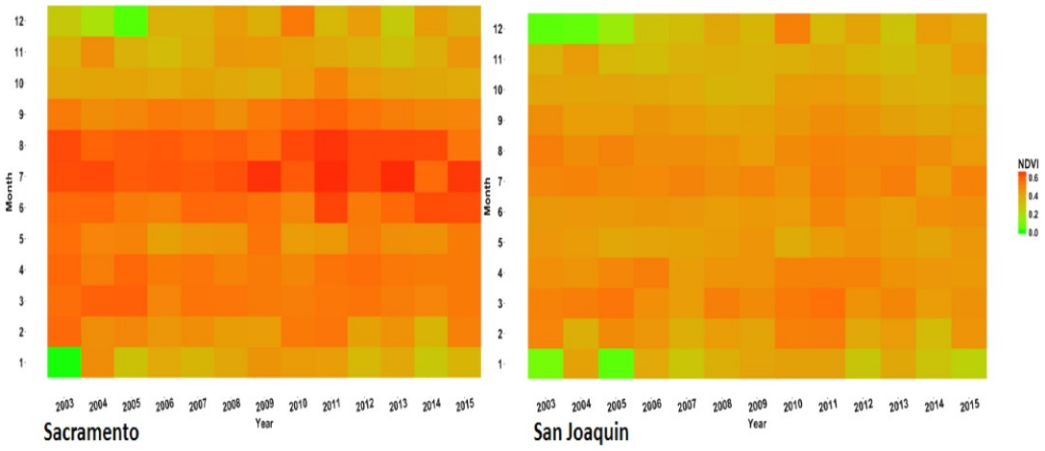

Figure 4.10 Monthly graphical representation of crop yield (NDVI) between 2003 and 2015 in the California's Central Valley

4.7 Conclusion

The objective of this analysis was to observe impacts of climate forcing on the total water storage and agriculture cover in the California's Central Valley. To achieve this goal first I classified multispectral Landsat image for the individual years 2003 and 2015. Then I compared and analyzed these hybrids classified images to quantify changes in agriculture and associated land cover. As the amount of agricultural yield is directly dependent on water accessibility in the region, I used Gravity Recovery Research and Experiment (GRACE) data signals and studied changes in equivalent water height (cm) for the California's Central Valley. Lastly, I statistically identified the relation between crop yield, TWS, and temperature.

I conclude that groundwater and surface water in the region was found to be declining continuously at an incremental rate. The water levels in the aquifers were noticed to be sensitive to changes in the freshwater reserves in the Sierra Nevada. Statistical analysis between NDVI and TWS showed the decrease in crop yield with an increase in TWS anomalies in the Central Valley region.

During the study period region also experienced minor changes in the agriculture land cover and increased warming. I suspect the increased temperature might have resulted in high crop water demand. To maintain the crop water demand and yield; farmers depend on the ground waters. This assumption can be substantiated by the findings of the other studies, reported depletion of groundwater levels in the region (Famiglietti et al., 2011; Mehta et al., 2013; Scanlon et al., 2012b).

The study results indicate that the conditions are severe in the southern regions (San Joaquin and Tulare Basins) of California's Central Valley. The ground and water levels

in the San Joaquin and Tulare Basins are depleting with the rate almost double to the basins in the North (Sacramento and Delta). Besides, the region lost more agricultural land in the south compared to the North parts of the central valley. These findings are aligned with the observations of Reilly et al., (2008) and Scanlon et al. (2012b) where they observed a high rate of water loss and followed land subsidence in Southern Basins (San Joaquin and Tulare Basins). Also, results of total water storage are comparable to the findings of Famiglietti et al. (2011) where they found negative ground water levels between 2003 and 2010 in the central valley.

Also, increasing population and urban areas are building stress on water resources. Proper water management techniques like drip irrigation, controlled water extraction, and use, alternate use of drought-tolerant species like olives, citrus, water holding structures and water literacy will help sustainable management. This study provides insights into the state of ground and surface water levels and the agricultural pattern using the limited available data. More research is required to understand impacts of Pacific sea surface temperatures in the region. Also, more work is required to understand detailed impacts of changing water levels on the region wise specific crop and soil types.

CHAPTER V

CONCLUSIONS

5.1 Discussions on the overall outcomes and scope for the future research

The overall objective of this dissertation was to understand spatial patterns and state of cryospheric components in southwestern regions of North and South America. Specifically, this study performed temporal analysis of large glaciers in Southern Andes and snowpacks of California. Also, study quantified, geovisualized and statistically reported potential effects of increased glacier and snow melting on the fresh water reserves and agricultural cover.

In the Southern Andes and California, the elevation values over glaciers and snow covers were found lower in the past decade than the elevation values for the year 2000. It shows that cryospheric components are retreating irrespective of geolocations and their proximity to the polar region. Specifically, in the Southern Andes, the mass balance of glaciers was significantly negative in the Cordillera Darwin Icefields (CDI) and the North Wet (NW) region. Of which CDI represents the southern tip of Chile and is close to Antarctica, while NW region is situated in the north-central region of Chile. In CDI, Lopez et al. (2010) noticed major retreat in twenty major glaciers between 1945 and 2005, which is indirectly comparable to the negative mass balance of -0.126 ± 0.05 m w.e.a^{-1} reported in this study in Chapter II. Besides, recent findings by Melkonian et al. (2013) also found similar recession in in CDI (-1.5 ± 0.6 m w.e.a^{-1}.)

The study reports second highest negative mass balance rate of -0.122 ± 0.12 m w.e.a^{-1} in the NW region. Rignot et al., (2003) and Rivera et al., (2006) linked these negative trends in NW region to tropospheric warming and reduced precipitation. In essence, it is evident

from this study and other studies that the CDI region, which is a southern end near the south pole is losing ice mass more rapidly. While, SPI and DC regions showed insignificant but continuous melting. To understand the factors responsible for this phenomenon, it is necessary to study microclimatic conditions of the individual glaciers as well as of the sub-regions. The results of several other studies in the region on glaciers and climate data found aligned with the findings of state of glaciers in Southern Andes reported in Chapter II (Chen et al., 2007; Dixon and Ambinakudige, 2015; Lopez et al., 2010; Masiokas et al., 2009; Mouginot and Rignot, 2015; Rivera et al., 2006).

It is essential to note that in California, the snow mass depleted more rapidly in the Sierra Nevada than in Mt. Shasta. Like in the Andes, the elevation values over the perennial snow cover were lower than the year 2000 elevation values. The research outcomes indicate that snow mass never recovered after heavy snowfall event of 1998 in the California region. These findings of the snow extent and mass anomalies in California (Chapter IV) are comparable to other similar cryosphere and climate studies in the region (Ashfaq et al., 2013; MacDonald, 2007; Maurer et al., 2007; Stine, 1994).

Conversely, this study also observed positive mass balances and contrasting patterns in some of the basins and glaciers for the individual years. For example, there was a positive snow mass in the Kern River basin in the year 2008, and fluctuating snow mass anomalies in two adjacent glaciers of Black Giant and Black Giant E. in the Sierra Nevada.

This contrasting behavior of the some of the glaciers for the individual years could be attributed to the varied topography. Also, high snowfall in the alternate years between 2006 and 2008 and the steady temperatures in the dry season, while the low temperatures

in the wet season for the years 2007 and 2008 might have played an important role in amassing snow. But to substantiate this theory, more information on climatic parameters and underlying factors is required, as, during the same period, snow mass in the other river basins and many other glaciers of California continued to regress.

The study concludes that the increased melting in both the regions is a result of rapidly changing climate after the industrial revolution. The primary reason for the negative mass balance in the Southern Andes and California might be increased temperature over the twentieth century, as reported by recent reports (Carrasco et al., 2005; Favier et al., 2009; Griffin and Anchukaitis, 2014; Rabatel et al., 2011; Villalba et al., 2003). Besides, as suggested by many studies, there might be other climatic parameters accountable for glacier and snow mass anomalies, like a fluctuation in the precipitation (Favier et al., 2009; Prieto et al., 2001; Rignot et al., 2003). The increase in temperature and decrease in snowfall in California between 2013 and 2014 was the main cause of 2014 drought like conditions (Griffin and Anchukaitis, 2014; Swain et al., 2014) in the California state that resulted in a massive snow cover loss of about 87%.

The depleting fresh water reserves in the California region are directly affecting total water storage and agricultural production in the Central Valley region. Analysis of GRACE data (Chapter IV) shows that groundwater and surface water in the region are declining continuously at an incremental rate. This variation in surface and ground water in the region found related to the increased melting patterns in the Sierra Nevada watersheds. The study observed the relation between receding perineal snow mass in the Sierra Nevada region and the declining water content of the central valley aquifers with the maximum change in the drought year 2014. Effects of receding source of fresh water

reserve, snow packs in the Sierra Nevada, shows clear impacts on the total water storage in the region. This incremental depletion in the snow mass and anomalies in total water storages suggest possible severe future impacts on the Californian Agricultural industry. Especially it is important to understand that, negative mass balance years 2003, 2012, and 2015 severely affected surface and ground water levels. Whereas the good snowfall years 2008, 2010 helped recovering the water levels but not for a long time. As consecutive drought years around years, 2013 and 2014 worsened the conditions and the ground water levels reached to its lowest with almost 90% snowmelt in the region. This indicates the cyclic pattern of snow mass deposition and ablation with dominant negative mass balance trend in the region.

During the study period (Between 2003 and 2015) the change in the land cover area of around 20% occurred due to the shift of Agriculture land cover to impervious or non-moist barren lands. This 20% alteration accounts for approximately 6993 sq.km. Out of these most of the alteration in the agriculture land cover of about 4400 sq.km occurred in the San Joaquin and Tulare Basins of southern Central Valley region. The study also observed around 3% increase in the urban area. This increase of around 1036 sq.km in the urban area might be a result of the increased infrastructures on or near the agricultural field other than urban centers. While the area of non-moisture or barren land cover increased in the Central Valley by about 17% that accounts for around 5957 sq.km land cover. Out of this 5957 sq.km barren land about 84% of the barren land, around 4662 sq.km, endowed by the southern San Joaquin region.

The statistical analysis between NDVI and TWS showed the decrease in crop cover with an increase in TWS anomalies in the Central Valley region. It shows that continuously

increasing temperature leads to increased snow melt and crop water demand. This has resulted in more utilization of surface and ground water leading to drought-like conditions in the region (Famiglietti et al., 2011; Mehta et al., 2013; Scanlon et al., 2012a). The ground and surface water levels in the southern regions (San Joaquin and Tulare Basins) are depleting with the rate almost double to the basins in the North (Sacramento and Delta). In this research, geographical dissimilarity in the warming rate was detected, as the Sacramento basin observed 0.03±0.04 (°C) while southern tip of the Central Valley observed warming rate of 0.07±0.04 (°C). Similarly, GRACE data analysis showed variation in depletion rate along north-south axis in California's Central Valley. Where Sacramento and Delta basins in the Central Valley region observed sharing the same rate of water depletion of -0.26±0.25 (equivalent water height cm) between 2003 and 2015. However, in the southern half of the Central Valley, San Joaquin experienced slightly higher depletion rate of -0.49±0.27 (equivalent water height cm) than Tulare (-0.48±0.26 equivalent water height cm). It is important to comprehend that ground and surface water rate was found to be almost double in the southern half (San Joaquin, Tulare) than the northern half of the Central Valley.

The study results indicate that the conditions are severe in the southern regions (San Joaquin and Tulare Basins) of California's Central Valley. Besides, the region lost more agricultural land in the south and compared to the North parts of the central valley. These findings are aligned with the observations of Reilly et al., (2008) and Scanlon et al. (2012b). Where the USGS report for the period 1962-2003 found the over extraction of ground water in the central valley region leading to land subsidence in the San Joaquin

(Southern region) (Reilly et al., 2008). Besides, results of total water storage are comparable to the findings of Famiglietti et al. (2011).

More research is required to understand the role of regional and micro-climatic conditions on glacial and snow mass variations in the Southern Andes and California. It is also important to understand the effects of ENSO events on Central Andean glaciers and the Sierra Nevada glaciers (Carrasco et al., 2005; Howat et al., 2007; Prieto et al., 2001; Rivera and Bown, 2013; Rivera et al., 2006). Future work should also focus on the potential factors such as the traces of aerosol (black carbon), dust, red algae, topography, etc. in snow that are capable of impacting the magnitude of ablation as reported by many studies (O. Hadley et al., 2010; Kessler et al., 2006; Kirchstetter et al., 2008; Painter et al., 2001; Rice et al., 2011; K. Sterle et al., 2013). More detailed research work is required in future to evaluate crop specific water requirement and irrigation potential using high spatio-temporal resolution datasets. An, increasing population and urban areas are constantly building stress on water resources. But proper water management techniques like drip irrigation, controlled water extraction, and use, alternate use of drought-tolerant species like olives, citrus, water holding structures and water literacy will help sustainable management. This dissertation provides valuable insights into the state of cryospheric components in the Southern Andes and California. Also, highlights the effects of snow mass anomalies on the ground and surface water levels and the agricultural pattern in the last decade. This research study has used possible limited available data to understand phenomenon on the larger scale. More focused and detailed work is required to recognize other underlying factors.

CHAPTER VI

REFERENCES

Ambinakudige, S., 2010. A study of the Gangotri glacier retreat in the Himalayas using Landsat satellite images. Int. J. Geoinformatics 6, 7–12.

Ambinakudige, S., Joshi, K., 2015. Multi-Decadal Changes in Glacial Parameters of the Fedchenko Glacier in Tajikistan. Int. J. Adv. Remote Sens. GIS 4, 911–919.

Ambinakudige, S., Joshi, K., 2012. Remote Sensing of Cryosphere, in: Escalante-Ramirez, B. (Ed.), Remote Sensing Applications. InTech, pp. 369–380.

Aniya, M., Sato, H., Naruse, R., Skvarca, P., Casassa, G., 1996. The Use of Satellite and Airborne Imagery to Inventory Outlet Glaciers of the Southern Patagonia Icefield, South America. Photogramm. Eng. Remote Sens. 62, 1361–1369.

Ashfaq, M., Ghosh, S., Kao, S.C., Bowling, L.C., Mote, P., Touma, D., Rauscher, S.A., Diffenbaugh, N.S., 2013. Near-term acceleration of hydroclimatic change in the western U.S. J. Geophys. Res. Atmos. 118, 10676–10693. doi:10.1002/jgrd.50816

Bamber, J.L., Rivera, A., 2007. A review of remote sensing methods for glacier mass balance determination. Glob. Planet. Change 59, 138–148. doi:10.1016/j.gloplacha.2006.11.031

Basagic, H., Fountain, A.G., 2011. Quantifying twentieth century glacier change in the Sierra Nevada, California. Arctic, Antarct. Alp. Res. 43, 317–330.

Basagic, H.J., Fountain, A.G., 2011. Quantifying 20th Century Glacier Change in the Sierra Nevada , California. Arctic, Antart. Alp. Res. 43, 317–330. doi:10.1657/1938-4246-43.3.317

Beaulieu, A., Clavet, D., 2009. Accuracy Assessment of Canadian Digital Elevation Data using ICESat. Photogramm. Eng. Remote Sens. 75, 81–86.

Bolch, T., Kulkarni, a, Kääb, a, Huggel, C., Paul, F., Cogley, J.G., Frey, H., Kargel, J.S., Fujita, K., Scheel, M., Bajracharya, S., Stoffel, M., 2012. The state and fate of Himalayan glaciers. Science 336, 310–4. doi:10.1126/science.1215828

Bolch, T., Pieczonka, T., Benn, D.I., 2011. Multi-decadal mass loss of glaciers in the Everest area (Nepal Himalaya) derived from stereo imagery. Cryosphere 5, 349–358. doi:10.5194/tc-5-349-2011

Bonfils, C., Duffy, P.B., Santer, B.D., Wigley, T.M.L., Lobell, D.B., Phillips, T.J., Doutriaux, C., 2007. Identification of external influences on temperatures in California. Clim. Change 87. doi:10.1007/s10584-007-9374-9

Carabajal, C.C., Harding, D.J., 2005. ICESat validation of SRTM C-band digital elevation models. Geophys. Res. Lett. 32, 1–5. doi:10.1029/2005GL023957

Carrasco, J.F., Casassa, G., Quintana, J., 2005. Changes of the 0°C isotherm and the equilibrium line altitude in central Chile during the last quarter of the 20th century / Changements de l'isotherme 0°C et de la ligne d'équilibre des neiges dans le Chili central durant le dernier quart du 20ème siècle. Hydrol. Sci. J. 50, 37–41. doi:10.1623/hysj.2005.50.6.933

Carturan, L., Baroni, C., Brunetti, M., Carton, A., Dalla Fontana, G., Salvatore, M.C., Zanoner, T., Zuecco, G., 2015. Analysis of the mass balance time series of glaciers in the Italian Alps. Cryosph. Discuss. 9, 5849–5883. doi:10.5194/tcd-9-5849-2015

Cayan, D., Tyree, M., Dettinger, M., Hidalgo, H., Das, T., Maurer, E., Bromirski, P., Raham, N., Flick, R., 2009. Climate change scenarios and sea level rise estimates for the California 2008 Climate Change Scenarios Assessment, California Climate Change Center CEC-500-2009-014-D.

Chen, J.L., Wilson, C.R., Tapley, B.D., Blankenship, D.D., Ivins, E.R., 2007. Patagonia Icefield melting observed by Gravity Recovery and Climate Experiment (GRACE). Geophys. Res. Lett. 34, 1–6. doi:10.1029/2007GL031871

Chou, B., 2014. NRDC fact sheet California Snowpack and the Drought [WWW Document]. Nat. Resour. Def. Counc. URL https://www.nrdc.org/sites/default/files/ca-snowpack-and-drought-FS.pdf

Christy, J.R., Norris, W.B., Redmond, K., Gallo, K.P., 2006. Methodology and Results of Calculating Central California Surface Temperature Trends : Evidence of Human-Induced Climate Change ? J. Clim. 19, 548–564.

Clark, D.H., Gillespie, A.R., 1997. Timing and significance of late-glacial and Holocene cirque glaciation in the Sierra Nevada, California. Quat. Int. 21–38.

Congalton, R.G., Green, K., 2008. Assessing the accuracy of remotely sensed data: principles and practices. CRC Press.

Cooley, H., Christian-smith, J., Gleick, P.H., 2009. Sustaining California Agriculture in an Uncertain Future. Pacific Institute.

Costa-Cabral, M., Roy, S.B., Maurer, E.P., Mills, W.B., Chen, L., 2012. Snowpack and runoff response to climate change in Owens Valley and Mono Lake watersheds. Clim. Change 116, 97–109. doi:10.1007/s10584-012-0529-y

Danskin, W.R., 1999. Evaluation of the hydrologic system and selected water-

management alternatives in the Owens Valley, California. US Department of the Interior, US Geological Survey.

Dixon, L., Ambinakudige, S., 2015. Remote Sensing Study of Glacial Change in the Northern Patagonian Icefield. Adv. Remote Sens. 4, 270–279.

Dozier, J., Green, R.O., Nolin, A.W., Painter, T.H., 2009. Interpretation of snow properties from imaging spectrometry. Remote Sens. Environ. 113. doi:10.1016/j.rse.2007.07.029

Dyurgerov, M.B., Meier, M.F., 1997. Mass Balance of Mountain and Subpolar Glaciers: A New Global Assessment for 1961-1990. Arct. Alp. Res. 29, 379–391.

Espizua, L.E., Pitte, P., 2009. The little ice age glacier advance in the Central Andes (35 S), Argentina. Palaeogeogr. Palaeoclimatol. Palaeoecol. 281, 345–350. doi:10.1016/j.palaeo.2008.10.032

Famiglietti, J.S., 2014. The global groundwater crisis. Nat. Clim. Chang. 4, 945–948.

Famiglietti, J.S., Lo, M., Ho, S.L., Bethune, J., Anderson, K.J., Syed, T.H., Swenson, S.C., Linage, C.R. De, Rodell, M., 2011. Satellites measure recent rates of groundwater depletion in California ' s Central Valley. Geophys. Res. Lett. 38. doi:10.1029/2010GL046442

Favier, V., Falvey, M., Rabatel, A., Praderio, E., López, D., 2009. Interpreting discrepancies between discharge and precipitation in high-altitude area of chile's norte chico region (26-32°S). Water Resour. Res. 45, 1–20. doi:10.1029/2008WR006802

Fischer, A., 2011. Comparison of direct and geodetic mass balances on a multi-annual time scale. Cryosphere 5, 107–124. doi:10.5194/tc-5-107-2011

Fountain, A., 2011. Temperate Glaciers, in: Singh, V., Singh, P., U, H. (Eds.), Encyclopedia of Snow, Ice and Glaciers. Springer, The Netherlands, p. 1145.

Galloway, D.L., Burbey, T.J., 2011. Review : Regional land subsidence accompanying groundwater extraction. Hydrogeol. J. 19, 1459–1486. doi:10.1007/s10040-011-0775-5

Gardner, A.S., Moholdt, G., Cogley, J.G., Wouters, B., Arendt, A. a, Wahr, J., Berthier, E., Hock, R., Pfeffer, W.T., Kaser, G., Ligtenberg, S.R.M., Bolch, T., Sharp, M.J., Hagen, J.O., van den Broeke, M.R., Paul, F., 2013. A reconciled estimate of glacier contributions to sea level rise: 2003 to 2009. Science 340, 852–7. doi:10.1126/science.1234532

Garreaud, R.D., Vuille, M., Compagnucci, R., Marengo, J., 2009. Present-day South American climate. Palaeogeogr. Palaeoclimatol. Palaeoecol. 281, 180–195. doi:10.1016/j.palaeo.2007.10.032

Gillespie, A.R., Clark, D.H., 2011. Glaciations of the Sierra Nevada, California, USA. Dev. Quat. Sci. 15, 447–462.

Gleeson, T., Wada, Y., Bierkens, M.F.P., Beek, L.P.H. Van, 2012. Water balance of global aquifers revealed by groundwater footprint. Nature 488, 197–200. doi:10.1038/nature11295

Griffin, D., Anchukaitis, K.J., 2014. How unusual is the 2012 – 2014 California drought ? Geophys. Res. Lett. 41, 9017–9023. doi:10.1002/2014GL062433.1.

Hadley, O., Corrigan, C.E., Kirchstetter, T.W., Cliff, S.S., Ramanathan, V., 2010. Measured black carbon deposition on the Sierra Nevada snow pack and implication for snow pack retreat. Atmos. Chem. Phys. 7505–7513. doi:10.5194/acp-10-7505-2010

Hadley, O.L., Corrigan, C.E., Kirchstetter, T.W., Cliff, S.S., Ramanathan, V., 2010. Measured black carbon deposition on the Sierra Nevada snow pack and implication for snow pack retreat. Atmos. Chem. Phys. 10, 7505–7513. doi:10.5194/acp-10-7505-2010

Hansen, J., Sato, M., Ruedy, R., Lo, K., Lea, D.W., Medina-elizade, M., 2006. Global temperature change, in: Proceedings of the National Academy of Sciences. pp. 14288–14293.

Holmlund, P., Fuenzalida, H., 1995. Anomalous glacier responses to 20th century climatic changes in Darwin Cordillera, southern Chile. J. Glaciol. 41, 465–473.

Howat, I.M., Tulaczyk, S., 2005. Climate sensitivity of spring snowpack in the Sierra Nevada. J. Geophys. Res. Earth Surf. 110, 1–9. doi:10.1029/2005JF000356

Howat, I.M., Tulaczyk, S., Rhodes, P., Israel, K., Snyder, M., 2007. A precipitation-dominated, mid-latitude glacier system: Mount Shasta, California. Clim. Dyn. 28, 85–98. doi:10.1007/s00382-006-0178-9

Howitt, R., Lund, J., Sumner, D., 2014. Economic Analysis of the 2015 Drought For California Agriculture, Center for Watershed Sciences, University of California, Davis.

Huss, M., 2013. Density assumptions for converting geodetic glacier volume change to mass change. Cryosph. 7, 877–887. doi:10.5194/tc-7-877-2013

Inamdar, P., Ambinakudige, S., 2016. Spatial Patterns of Glacier Mass Change in the Southern Andes. Photogramm. Eng. Remote Sens. 82, 811–818.

Jackson, L., Wheeler, S., Hollander, A.D., O'Geen, A., Orlove, B., Six, J., Sumner, D.A., Santos-Martin, Fernando Kramer, J., Horwath, W.R., 2011a. Case study on potential agricultural responses to climate change in a California landscape. Clim. Change 109, 407–427.

Jackson, L., Wheeler, S.M., Hollander, A.D., Orlove, B.S., Six, J., Sumner, D.A., Kramer, J.B., Horwath, W.R., Howitt, R.E., Tomich, T.P., 2011b. Case study on potential agricultural responses to climate change in a California landscape. Clim. Chang. 109, 407–427. doi:10.1007/s10584-011-0306-3

Johnson, A.J., Larsen, C.F., Murphy, N., Arendt, A.A., Lee Zirnheld, S., 2013. Mass balance in the Glacier Bay area of Alaska, USA, and British Columbia, Canada, 1995-2011, using airborne laser altimetry. J. Glaciol. 59, 632–648. doi:10.3189/2013JoG12J101

Joyce, B.A., Mehta, V.K., Purkey, D.R., Dale, L.L., Hanemann, M., 2011. Modifying agricultural water management to adapt to climate change in California ' s central valley. Clim. Chang. 109, 299–316. doi:10.1007/s10584-011-0335-y

Kääb, A., Berthier, E., Nuth, C., Gardelle, J., Arnaud, Y., 2012. Contrasting patterns of early twenty-first-century glacier mass change in the Himalayas. Nature 488, 495–498. doi:10.1038/nature11324

Kaser, G., Fountain, A., Jansson, P., 2003. A manual for monitoring the mass balance of mountain glaciers. Unesco Paris.

Kessler, M.A., Anderson, R.S., Stock, G.M., 2006. Modeling topographic and climatic control of east-west asymmetry in Sierra Nevada glacier length during the Last Glacial Maximum. J. Geophys. Res. Earth Surf. 111, 1–15. doi:10.1029/2005JF000365

Kirchstetter, T.W., Aguiar, J., Tonse, S., Fairley, D., Novakov, T., 2008. Black carbon concentrations and diesel vehicle emission factors derived from coefficient of haze measurements in California: 1967-2003. Atmos. Environ. 42, 480–491. doi:10.1016/j.atmosenv.2007.09.063

Konikow, L.F., 2011. Contribution of global groundwater depletion since 1900 to sea - level rise. Geophys. Res. Lett. 38, 1–5. doi:10.1029/2011GL048604

Krimmel, R.M., 2002. Glaciers of the conterminous United States, Satellite image atlas of glaciers of the world: North America: US Geological Survey Professional Paper.

Ladochy, S., Medina, R., Patzert, W., 2007. Recent California climate variability : spatial

and temporal patterns in temperature trends. Clim. Res. 33, 159–169.

Lee, J., Gryze, S. De, Six, J., 2011. Effect of climate change on field crop production in California ' s Central Valley. Clim. Chang. 109, 335–353. doi:10.1007/s10584-011-0305-4

Lemke, P., Ren, J., Alley, R., Allison, I., Carrasco, J., Flato, G., Fujii, Y., Kaser, G., Mote, P., Thomas, R., Zhang, T., 2007. Observations: Changes in Snow, Ice and Frozen Ground. In: Climate Change 2007: The Physical Science Basis. Contribution of Working Group I to the Fourth Assessment Report of the Intergovernmental Panel on Climate Change. Cambridge University Press, Cambridge, United Kingdom and New York, NY, USA.

Lliboutry, L., 1998. Glaciers of Chile and Argentina. Geol. Surv. Prof. Pap. 1386, 1103.

Lo, M., Famiglietti, J.S., 2013. Irrigation in California ' s Central Valley strengthens the southwestern U . S . water cycle. Geophys. Res. Lett. 40, 301–306. doi:10.1002/grl.50108

Lobell, D., Field, C., Cahill, K., Bonfils, C., 2006. Impacts of Future Climate Change on California Perennial Crop Yields : Model Projections with Climate and Crop Uncertainties. Agric. For. Meteorol. 141, 208–218.

Lopez, P., Chevallier, P., Favier, V., Pouyaud, B., Ordenes, F., Oerlemans, J., 2010. A regional view of fluctuations in glacier length in southern South America. Glob. Planet. Change 71, 85–108. doi:10.1016/j.gloplacha.2009.12.009

Maas, H.-G., Casassa, G., Schneider, D., Schwalbe, E., Wendt, A., 2013. Photogrammetric techniques for the determination of spatio-temporal velocity fields at Glaciar San Rafael, Chile. Photogramm. Eng. Remote Sens. 79, 299–306.

MacDonald, G.M., 2007. Severe and sustained drought in southern California and the West : Present conditions and insights from the past on causes and impacts. Quarternary Int. 174, 87–100. doi:10.1016/j.quaint.2007.03.012

Marcus, M.G., Chambers, F.B., Miller, M.M., Lang, M., Marcus, M.G., Chambers, F., Miller, M.M., Lang, M., 1995. Recent trends in the Lemon Creek Glacier, Alaska. Phys. Geogr. 16, 150–161.

Margulis, S.A., Cortés, G., Girotto, M., Huning, L.S., Li, D., Durand, M., 2016. Characterizing the extreme 2015 snowpack deficit in the Sierra Nevada (USA) and the implications for drought recovery. Geophys. Res. Lett. 1–9. doi:10.1002/2016GL068520

Masiokas, M.H., Rivera, A., Espizua, L.E., Villalba, R., Delgado, S., Aravena, J.C., 2009.

Glacier fluctuations in extratropical South America during the past 1000years. Palaeogeogr. Palaeoclimatol. Palaeoecol. 281, 242–268. doi:10.1016/j.palaeo.2009.08.006

Maurer, E.P., 2007. Uncertainty in hydrologic impacts of climate change in the Sierra Nevada, California, under two emissions scenarios. Clim. Change 82, 309–325. doi:10.1007/s10584-006-9180-9

Maurer, E.P., Stewart, I.T., Bonfils, C., Duffy, P.B., Cayan, D., 2007. Detection, attribution, and sensitivity of trends toward earlier streamflow in the Sierra Nevada. J. Geophys. Res. Atmos. 112, 1–12. doi:10.1029/2006JD008088

McCabe, G.J., Fountain, A.G., 2013. Glacier Variability in the Conterminous United States during the Twentieth Century. Clim. Chang. 116, 565–577.

Mehta, V.K., Haden, V.R., Joyce, B.A., Purkey, D.R., Jackson, L.E., 2013. Irrigation demand and supply , given projections of climate and land-use change , in Yolo County , California. Agric. Water Manag. 117, 70–82. doi:10.1016/j.agwat.2012.10.021

Melkonian, A.K., Willis, M.J., Pritchard, M.E., Rivera, A., Bown, F., Bernstein, S.A., 2013. Satellite-derived volume loss rates and glacier speeds for the Cordillera Darwin Icefield, Chile. Cryosph. 7, 823–839. doi:10.5194/tc-7-823-2013

Montecinos, A., Aceituno, P., 2003. Seasonality of the ENSO-related rainfall variability in central Chile and associated circulation anomalies. J. Clim. 16, 281–296. doi:10.1175/1520-0442(2003)016<0281:SOTERR>2.0.CO;2

Mouginot, J., Rignot, E., 2015. Geophysical Research Letters Ice motion of the Patagonian Icefields of South America: 1984–2014. J. Issue Geophys. Res. Lett. Geophys. Res. Lett 42, 1984–2014. doi:10.1002/2014GL062661

Neckel, N., Kropáček, J., Bolch, T., Hochschild, V., 2014. Glacier mass changes on the Tibetan Plateau 2003–2009 derived from ICESat laser altimetry measurements. Environ. Res. Lett. 9, 014009. doi:10.1088/1748-9326/9/1/014009

Ostrem M., G. and B., 1991. Glacier mass-balance measurements: A manual for field and office work, NHRI Science Report No. 4.

Pachauri, R.K., Allen, M.R., Barros, V.R., Broome, J., Cramer, W., Christ, R., Church, J.A., Clarke, L., Dahe, Q., Dasgupta, P., 2014. Climate Change 2014: Synthesis Report. Contribution of Working Groups I, II and III to the Fifth Assessment Report of the Intergovernmental Panel on Climate Change. IPCC.

Painter, T.H., Duval, B., Thomas, W.H., Heintzelman, S., Dozier, J., Mendez, M., 2001.

Detection and Quantification of Snow Algae with an Airborne Imaging Spectrometer Detection and Quantification of Snow Algae with an Airborne Imaging Spectrometer. Appl. Environ. Microbiol. 67, 5267–5272. doi:10.1128/AEM.67.11.5267

Paruelo, J.M., Beltran, A., Jobbagy, E., Sala, O.E., Golluscio, R.A., 1998. The climate of Patagonia: general patterns and controls on biotic. Ecol. Austral 8, 85–101.

Phan, V.H., Lindenbergh, R.C., Menenti, M., 2014. Orientation dependent glacial changes at the Tibetan Plateau derived from 2003–2009 ICESat laser altimetry. Cryosph. Discuss. 8, 2425–2463. doi:10.5194/tcd-8-2425-2014

Prieto, R., Herrera, R., Doussel, P., Gimeno, L., Ribera, P., Garcia, R., Hernandez, E., 2001. Interannual oscillations and trend of snow occurrence in the Andes region since 1885. Aust. Meteorol. Mag. 50, 164–168.

Rabatel, A., Castebrunet, H., Favier, V., Nicholson, L., Kinnard, C., 2011. Glacier changes in the Pascua-Lama region, Chilean Andes (29° S): recent mass balance and 50 yr surface area variations. Cryosphere 5, 1029–1041. doi:10.5194/tc-5-1029-2011

Rabatel, A., Francou, B., Soruco, A., Gomez, J., Cáceres, B., Ceballos, J.L., Basantes, R., Vuille, M., Sicart, J.-E., Huggel, C., Scheel, M., Lejeune, Y., Arnaud, Y., Collet, M., Condom, T., Consoli, G., Favier, V., Jomelli, V., Galarraga, R., Ginot, P., Maisincho, L., Mendoza, J., Ménégoz, M., Ramirez, E., Ribstein, P., Suarez, W., Villacis, M., Wagnon, P., 2013. Current state of glaciers in the tropical Andes: a multi-century perspective on glacier evolution and climate change. Cryosph. 7, 81–102. doi:10.5194/tc-7-81-2013

Racoviteanu, A.E., Williams, M.W., Barry, R.G., 2008. Optical Remote Sensing of Glacier Characteristics: A Review with Focus on the Himalaya. Sensors 8, 3355–3383. doi:10.3390/s8053355

Rahmstorf, S., Foster, G., Cahill, N., 2017. Global temperature evolution: recent trends and some pitfalls. Environ. Res. Lett. 12, 054001.

Raub, W., Brown, C.S., Post, A., 2006. Inventory of glaciers in the Sierra Nevada, California. U.S. Geological Survey.

Reilly, T.E., Dennehy, K.F., Alley, W.M., Cunninggham, W.L., 2008. Ground-Water Availability in the United States-1323. U.S.Geological Survey.

Rice, R., Bales, R.C., Painter, T.H., Dozier, J., 2011. Snow water equivalent along elevation gradients in the Merced and Tuolumne River basins of the Sierra Nevada. Water Resour. Res. 47, 1–11. doi:10.1029/2010WR009278

Rignot, E., Rivera, A., Casassa, G., 2003. Contribution of the Patagonia icefields of South America to global sea level rise. Science (80-.). 302, 434–437.

Rivera, A., Acuña, C., Casassa, G., 2006. Glacier Variations in Central Chile (32° S-41° S). Glacier Sci. Environ. Chang. 246–247.

Rivera, A., Acuña, C., Casassa, G., Bown, F., 2002. Use of remotely sensed and field data to estimate the contribution of Chilean glaciers to eustatic sea-level rise. Ann. Glaciol. 34, 367–372. doi:10.3189/172756402781817734

Rivera, A., Benham, T., Casassa, G., Bamber, J., Dowdeswell, J.A., 2007. Ice elevation and areal changes of glaciers from the Northern Patagonia Icefield, Chile. Glob. Planet. Change 59, 126–137. doi:10.1016/j.gloplacha.2006.11.037

Rivera, A., Bown, F., 2013. Recent glacier variations on active ice capped volcanoes in the Southern Volcanic Zone (37°–46° S), Chilean Andes. J. South Am. Earth Sci. 45, 345–356. doi:10.1016/j.jsames.2013.02.004

Rosenblüth, B., Fuenzalida, H. a, Aceituno, P., 1997. Recent temperature variations in Southern South America. Int. J. Clim. 17, 67–85.

Sakakibara, D., Sugiyama, S., 2014. Ice-front variations and speed changes of calving glaciers in the Southern Patagonia Icefield from 1984 to 2011. J. Geophys. Res. Earth Surf. 119, 2541–2554. doi:10.1002/2014JF003148.Received

Scanlon, B.R., Faunt, C.C., Longuevergne, L., Reedy, R.C., Alley, W.M., Mcguire, V.L., Mcmahon, P.B., 2012a. Groundwater depletion and sustainability of irrigation in the US High Plains and Central Valley, in: Proceedings of the National Academy of Sciences. pp. 9320–9325. doi:10.1073/pnas.1200311109/-/DCSupplemental.www.pnas.org/cgi/doi/10.1073/pnas.1200311109

Scanlon, B.R., Longuevergne, L., Long, D., 2012b. Ground referencing GRACE satellite estimates of groundwater storage changes in the California Central Valley , USA. Water Resour. Res. 48, 1–9. doi:10.1029/2011WR011312

Schaefer, M., Machguth, H., Falvey, M., Casassa, G., Rignot, E., 2014. Quantifying mass balance processes on the Southern Patagonia Icefield. Cryosph. Discuss. 8, 3117–3139. doi:10.5194/tcd-8-3117-2014

Scheuchl, B., Mouginot, J., Rignot, E., Morlighem, M., Khazendar, A., 2016. Grounding line retreat of Pope, Smith, and Kohler Glaciers, West Antarctica, measured with Sentinel-1a radar interferometry data. Geophys. Res. Lett. 43, 8572–8579.

Schlenker, W., Hanemann, W.M., Fisher, A.C., 2007. Water availability, degree days, and the potential impact of climate change on irrigated agriculture in California.

Clim. Change 81, 19–38.

Segawa, T., Miyamoto, K., Ushida, K., Agata, K., Okada, N., Kohshima, S., 2005. Seasonal change in bacterial flora and biomass in mountain snow from the Tateyama Mountains, Japan, analyzed by 16S rRNA gene sequencing and real-time PCR. Appl. Environ. Microbiol. 71, 123–130. doi:10.1128/AEM.71.1.123-130.2005

Serreze, M.C., Clark, M.P., Armstrong, R.L., Mcginnis, A., Pulwarty, R.S., 1999. Characteristics of the western United States snowpack from snowpack telemetry (SNOTEL) data. Water Resour. Res. 35, 2145–2160.

Shepherd, A., Shepherd, A., Ivins, E.R., Geruo, A., Barletta, V.R., Bentley, M.J., Bettadpur, S., Briggs, K.H., Bromwich, D.H., Forsberg, 2012. A Reconciled Estimate of Ice-Sheet Mass Balance Andrew Shepherd. Science (80-.). 338, 1183–1189. doi:10.1126/science.1228102

Singh, P., 2001. Snow and glacier hydrology, 37th ed. Kluwer Academic Publishers.

Singh, T.P., Singh, S., Tiwari, S.C., 2013. Assessment of digital image classification algorithms for forest and land-use classification in the eastern Himalayas using the IRS LISS III sensor. Int. J. Remote Sens. 34, 4105–4126. doi:10.1080/01431161.2013.772675

Sterle, K., McConnell, J., Dozier, J., Edwards, R., Flanner, M., 2013. Retention and radiative forcing of black carbon in eastern Sierra Nevada snow. Cryosphere 7, 365–374. doi:10.5194/tc-7-365-2013

Sterle, K.M., Mcconnell, J.R., Dozier, J., Edwards, R., Flanner, M.G., 2013. The Cryosphere Retention and radiative forcing of black carbon in eastern Sierra Nevada snow. Cryosph. 365–374. doi:10.5194/tc-7-365-2013

Stine, S., 1994. Extreme and persistent drought in California and Patagonia during mediaeval time. Nature 369, 546–549. doi:10.1038/369546a0

Swain, D.L., Tsiang, M., Haugen, M., Singh, D., Charland, A., Rajaratnam, Bala Diffenbaugh, N.S., 2014. The extraordinary California drought of 2013/2014: Character, context, and the role of climate change. Bull. Am. Meteorol. Soc. 95, 53.

Takeuchi, N., Dial, R., Kohshima, S., Segawa, T., Uetake, J., 2006. Spatial distribution and abundance of red snow algae on the Harding Icefield, Alaska derived from a satellite image. Geophys. Res. Lett. 33, 1–6. doi:10.1029/2006GL027819

Taylor, R.G., Scanlon, B., Döll, P., Rodell, M., Van Beek, R., Wada, Y., Longuevergne, L., Leblanc, M., Famiglietti, J.S., Edmunds, M., Others, A., 2013. Ground water and climate change. Nat. Clim. Chang. 3, 322–329. doi:10.1038/NCLIMATE1744

Villalba, R., Lara, A., Boninsegna, J.A., Masiokas, M., Delgado, S., Aravena, J.C., Roig, F.A., Schmelter, A., Wolodarsky, A., Ripalta, A., 2003. Largescale temperature changes across the Southern Andes: 20th -century variations in the context of the past 400 years, in: Climate Variability and Change in High Elevation Regions: Past, Present \& Future. Springer Netherlands, pp. 177–232.

Vuille, M., Bradley, R.S., 2000. Mean annual temperature trends and their vertical structure in the tropical Andes. Geophys. Res. Lett. 27, 3885–3888.

Wada, Y., Beek, L.P.H. Van, Kempen, C.M. Van, Reckman, J.W.T.M., Vasak, S., Bierkens, M.F.P., 2010. Global depletion of groundwater resources 37, 1–5. doi:10.1029/2010GL044571

Warren, C.R., Sudgen, D.E., 1993. Patagonian Icefields: a glaciological review. Arct. Alp. Res. 25, 316–331.

Wechsler, S.P., Kroll, C.N., 2006. Quantifying DEM Uncertainty and its Effect on Topographic Parameters. Photogramm. Eng. Remote Sens. 72, 1081–1090. doi:10.14358/PERS.72.9.1081

White, a., Copland, L., 2013. Spatial and temporal variations of glacier extent across the Southern Patagonian Icefield since the 1970s. Cryosph. Discuss. 7, 1–34. doi:10.5194/tcd-7-1-2013

Williams, R., Ferrigno, J., 1988. Satellite image atlas of glaciers of the world:South America, U.S. Geological Survey Professional Paper. Washington, DC.

Willis, M.J., Melkonian, A.K., Pritchard, M.E., Rivera, A., 2012. Ice loss from the Southern Patagonian Ice Field, South America, between 2000 and 2012. Geophys. Res. Lett. 39, 1–6. doi:10.1029/2012GL053136